# Beamline 8.0.1

# Surface and Materials Science, Imaging Photoelectron Spectroscopy, Soft X-Ray Fluorescence

### Angle-dependent soft x-ray emission spectra of hexagonal boron nitride
Muramatsu, Y., R.C.C. Perera

### Dynamical relativistic effects in photoionization: Spin-orbit-resolved angular distributions of xenon *4d* photoelectrons near the Cooper minimum
Hemmers, O., H. Wang, G. Snell, M.M. Sant' Anna, I. Sellin, N. Berrah, D.W. Lindle, P.C. Deshmukh, N. Haque, S.T. Manson

### Electronic structure of alkali metal-doped $M_8Si_{46}$ (M=Na, K) clathrates
Moewes, A., E.Z. Kurmaev, J.S. Tse, M. Geshi, M.J. Ferguson, V.A. Trofimova, Y.M. Yarmoshenko

### Electronic structure of BeS studied by resonant inelastic x-ray scattering
Fuchs, O., L. Weinhardt, C. Heske, E. Umbach, A. Fleszar, C. Bostedt, L.J. Terminello, R.C.C. Perera

### Electronic structure of CMR compounds investigated by means of XES
Küpper, K., B. Schneider, S.G. Chiuzbaian, M. matteucci, D.D. Sarma

### Electronic structure of graphite fluorides
Kurmaev, E.Z., A. Moewes, D.L. Ederer, H. Ishii, K. Seki, M. Yanagihara, F. Okino, H. Touhara

### Excitation-energy dependence of Cu $L_{2,3}$ x-ray spectra of Cu, $Cu_2O$ and CuO
Kawatsura, K., K. Takahiro, N. Takeshima, T. Morikawa, Y. Muramatsu, R.C.C. Perera

### First separate measurements of the nondipole parameters γ and δ: Showcase neon 2p photoemission
Hemmers, O., M. Blackburn, T. Goddard, P. Glans, H. Wang, S.B. Whitfield, R. Wehlitz, I.A. Sellin, D.W. Lindle

### Layer-structure-distribution in the sample plane of Mo/Si multilayers measured by total-electron-yield x-ray standing wave methods
Muramatsu, Y., H. Takenaka, E.M. Gullikson, R.C.C. Perera

### Magnetic reversal of perpendicularly-biased Co/Pt multilayers
Hellwig, O., S. Maat, J.B. Kortright, E.E. Fullerton

### Multi-atom resonant photoemission effects from solid surfaces and free molecules
Mannella, N., B.S. Mun, S.-H. Yang, A.W. Kay, F.J. Garcia de Abajo, E. Arenholz, A.T. Young, Z. Hussain, H. Wang, O. Hemmers, D.W. Lindle, M.A. Van Hove, C.S. Fadley

### O 1s XAS of $H_2O$ in the solvation shell of monovalent and trivalent ions
Näslund, L.-Å., Ph. Wernet, H. Ogasawara, D. Edwards, S. Myneni, A. Nilsson

### Partial density of states of B-2*p* in $AlB_2$ type compounds
Nakamura, J., K. Kuroki, N. Yamada, T.A. Callcott, D.E. Ederer, J.D. Denlinger, R.C.C. Perera

### Resolving magnetic and chemical correlation lengths in CoPtCr-based recording media
Hellwig, O., D.T. Margulies, B. Lengsfield, E. E. Fullerton, J.B. Kortright

### Soft x-ray emission and absorption spectra in the Si *L* region of polysilanes
Muramatsu, Y., M. Fujino, E.M. Gullikson, R.C.C. Perera

### Soft x-ray emission spectroscopy of the liquid-solid interface between water and a $Cu(In,Ga)(S,Se)_2$ thin film solar cell absorber
Heske, C., U. Groh, O. Fuchs, L. Weinhardt, E. Umbach, Ch.-H. Fischer, Th. Schedel-Niedrig, M.Ch. Lux-Steiner, S. Zweigart, F. Karg, J.D. Denlinger, B. Rude, C. Andrus, F. Powell

### Soft x-ray probe of bulk bandgaps in divalent hexaborides
Denlinger, J.D., J.W. Allen, Z. Fisk

### Soft x-ray spectroscopy of noble gas atoms doped in solid matrices
Muramatsu, Y., R.C.C. Perera

### Spectroscopic observation of polaron-lattice band structure in the conducting polymer polyaniline
Kurmaev, E.Z., M.I. Katsnelson, A. Moewes, M. Magnuson, J.-H. Guo, S.M. Butorin, J. Nordgren, D.L. Ederer, M. Iwami

### X-ray absorption and emission spectroscopy at the nitrogen K-edge in dilute $GaAs_{1-x}N_x$
Adamcyk, M., A. Ballestad, A. Moewes, E. Nodwell, T. Tiedje, S. Tixier

### X-ray emission spectra and electronic structure of charge transfer salts
Kurmaev, E.Z., A. Moewes, U. Schwingerschlögl, R. Claessen, M.I. Katsnelson, H. Kobayashi, S. Kagoshima, Y. Misaki, D.L. Ederer, K. Endo, M. Yanagihara

### X-ray transitions for studying the electronic structure of 5d metals
Kurmaev, E.Z., A. Moewes, Z. Pchelkina, I. Nekrasov, T.A. Callcott, D.L. Ederer

# Angle-Dependent Soft X-Ray Emission Spectra of Hexagonal Boron Nitride

**Y. Muramatsu[1] and R. C. C. Perera[2]**
[1]*Japan Atomic Energy Research Institute, Sayo-gun, Hyogo 679-5148, Japan*
[2]*CXRO, Lawrence Berkeley National Laboratory, Berkeley, California 94720, USA*

Hexagonal boron nitride (*h*-BN) is a basic boron compound, which has been widely used as a reference sample in soft x-ray spectroscopy. It adopts a layered structure similar to graphite. To obtain detailed structural information for *h*-BN using soft x-ray emission spectroscopy, we have measured its angle-dependent soft x-ray emission spectra.

Commercially obtained *h*-BN power pressed on indium sheets and pyrolytic (*p*) BN plate was used for spectroscopic measurements. Soft x-ray emission spectra in the B *K* and N *K* regions were measured using a grating x-ray spectrometer installed in the undulator beamline, BL-8.0.1. The photon energy of the monochromatized incident beam was tuned to about 230 eV (for B *K*) and 430 eV (for N *K*). The incident angle ($\theta$) of the monochromatized beam to the sample surface was adjusted to 15, 45 and 75 degrees. Measured x-ray emission spectra were analyzed using discrete variational (DV)-X$\alpha$ molecular orbital calculations.

Figure 1 shows the angle-dependent B *K* and N *K* x-ray emission spectra of *p*-BN. In the B *K* spectra, intensity of the high-energy shoulder near 184 eV increases as $\theta$ increases. Intensities of the low-energy satellite near 170 eV and the low-energy shoulder near 178 eV both decrease as $\theta$ increases. In the N *K* spectra, intensity of the high-energy peak at 398.5 eV drastically increases as $\theta$ increases, while intensity of the low-energy shoulders near 385 eV and 390 eV decrease as $\theta$ increases. Upper panels of Figure 2 show the calculated density-of-states (DOS) spectra of occupied B2p- and N2p-orbitals in the model cluster of $B_{48}N_{48}H_{24}$. These calculated DOS spectra reproduce the x-ray emission spectra measured with an incident angle of 45 degrees. Lower panels of Figure 2 show the B2p- and N2p-DOS spectra calculated by considering the contributions of $\sigma$- and $\pi$-components in x-ray emission. In the B2p-DOS spectra, intensity of the high-energy shoulder (near -4 eV) increases as $\theta$ increases. Intensities of the low-energy shoulder (-10 eV) and low-energy peak (-18 eV) decrease as $\theta$ increases. In the N2p-DOS spectra, intensity of the high-energy peak (-2 eV) increases as $\theta$ increases, while intensities of the low-energy shoulders (-6 eV and –10 eV) decrease as $\theta$ increases. These calculated spectra well reproduce the measured angle-dependent x-ray emission spectra. Thus, it can be confirmed that angle-dependent x-ray emission measurements will provide detailed structural information on *h*-BN.

We thank Dr. J. Denlinger of the Lawrence Berkeley National Laboratory for his help and support in performing x-ray emission measurements. This work is supported by the Hyogo Science and Technology Association and the US Department of Energy under contract No. DE-AC03-76SF00098.

Principal Investigator: Yasuji Muramatsu, Japan Atomic Energy Research Institute. Email: murama@spring8.or.jp. Telephone: +81-791-58-2601.

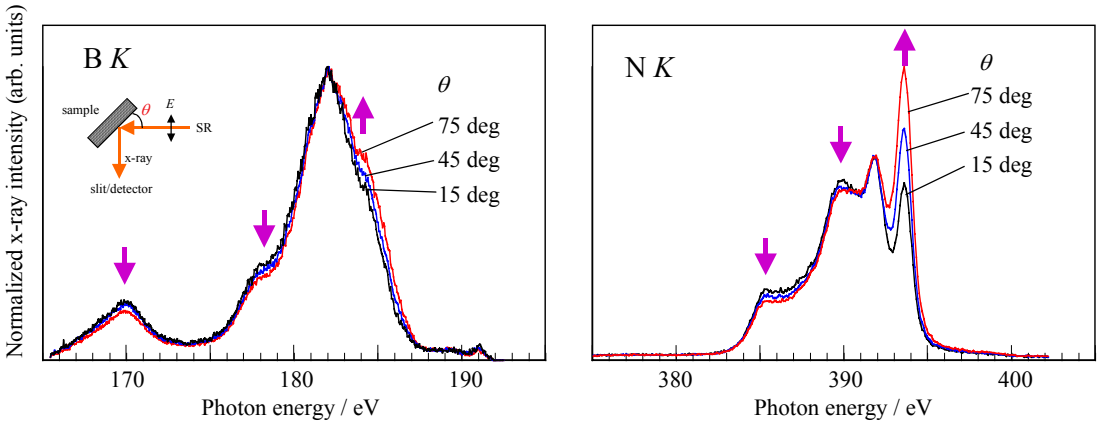


**Figure 1** Angle-dependent x-ray emission spectra in the B *K* (left panel) and N *K* (right panel) regions of *p*-BN.

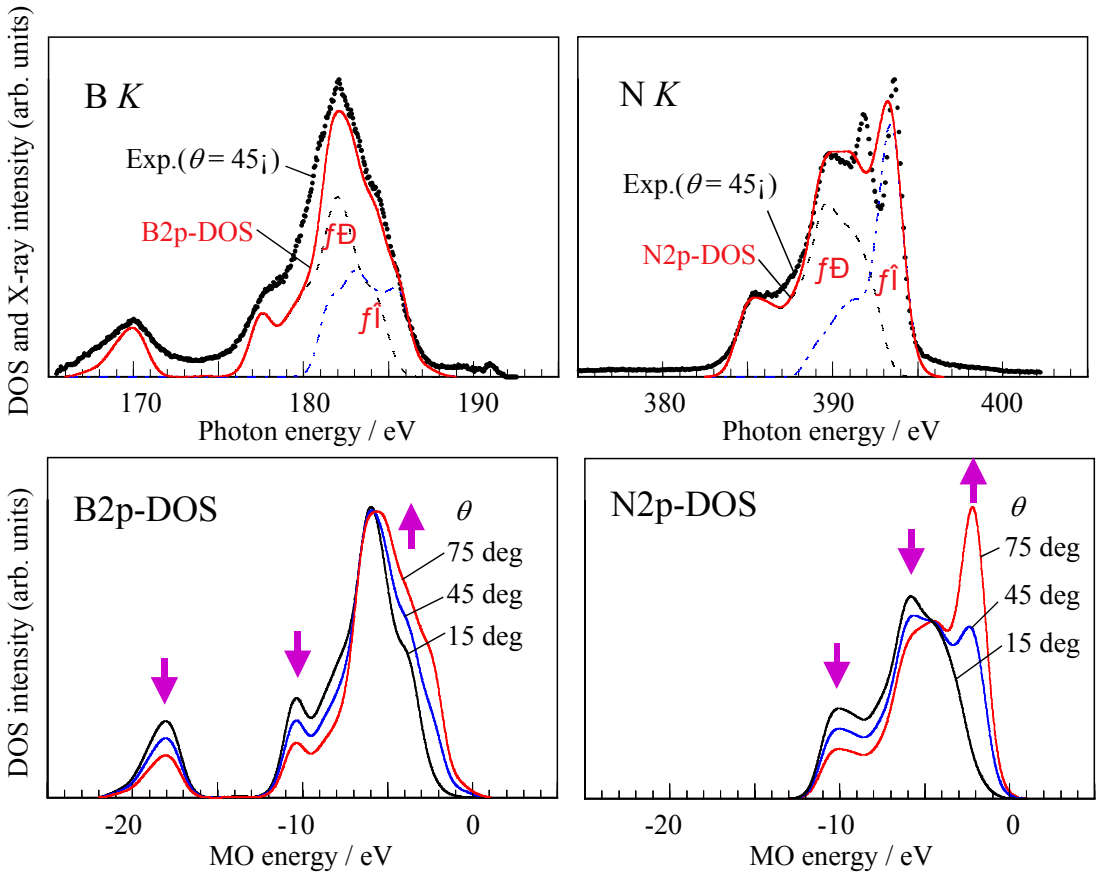


**Figure 2** Upper panels show the occupied B2p- and N2p-DOS spectra of the $B_{48}N_{48}H_{24}$ model cluster. X-ray emission spectra measured with an incident angle of 45 degrees are superimposed on the calculated spectra. Lower panels show the angle-dependent B2p- and N2p-DOS spectra with incident angles of 15, 45 and 75 degrees.

# Dynamical Relativistic Effects in Photoionization: Spin-Orbit-Resolved Angular Distributions of Xenon 4*d* Photoelectrons near the Cooper Minimum

O. Hemmers,[1] H. Wang,[1,2] G. Snell,[3,4] M. M. Sant'Anna,[4] I. Sellin,[5] N. Berrah,[3]
D. W. Lindle,[1] P.C. Deshmukh,[6,7,8] N. Haque,[9] and S. T. Manson[7]
[1]Department of Chemistry, University of Nevada, Las Vegas, NV 89154-4003
[2]Department of Physics, Uppsala University, Box 530, S-751 21 Uppsala, Sweden
[3]Department of Physics, Western Michigan University, Kalamazoo, MI 49008-5151
[4]Advanced Light Source, Lawrence Berkeley National Laboratory, Berkeley, California 94720, USA
[5]Department of Physics, University of Tennessee, Knoxville, TN 37996
[6]Department of Physics, Indian Institute of Technology-Madras, Chennai 600036, India
[7]Department of Physics and Astronomy, Georgia State University, Atlanta, GA 30030
[8]Center for Theoretical Studies of Physical Systems, Clark-Atlanta University, Atlanta, GA 30314
[9]Department of Physics, Morehouse College, Atlanta, GA 30314

## INTRODUCTION

Relativistic effects in atoms have long been known to be important for photoionization dynamics at high **Z** [1,2]. At low and intermediate **Z**, where the predominant effect of relativity has been thought to be spin-orbit splitting of states into $j=l\pm1/2$ with differing threshold energies [1], recent advances in experiment [3] and theory [4] have demonstrated observable consequences of relativistic effects on photoionization dynamics. One of the most sensitive dynamical quantities in photoionization is the energy of a Cooper minimum, where the dipole matrix element for a particular channel goes through (or nearly goes through) zero. Relativistic interactions were predicted to significantly affect Cooper minima two decades ago [2]. Here, we report on a combined experimental and theoretical study of 4*d* photoionization in Xe where the spin-orbit components $4d_{5/2}$ and $4d_{3/2}$ are individually resolved. Experimentally this is difficult in the energy region of the $4d\rightarrow\varepsilon f$ Cooper minima because the dominant $d\rightarrow f$ contribution to the cross section is very small. In the absence of dynamical effects due to relativistic interactions, Cooper minima for $4d_{5/2}$ and $4d_{3/2}$ photoionization will be located at the same *kinetic energy*. Consequently, $\beta_{5/2}$ and $\beta_{3/2}$ would be identical as a function of photoelectron energy. However, the present measurements clearly exhibit differences in the $\beta$ parameters and confirm the long-untested theoretical prediction of Kim *et al.* [2]. Furthermore, $\beta_{5/2}$ and $\beta_{3/2}$ differ not only in the immediate vicinity of the Cooper minima, but over a broad energy region, demonstrating the importance of relativistic effects in the photoionization of intermediate-**Z** atoms over a much larger energy range than previously suspected. The $4d\rightarrow\varepsilon f$ non-relativistic Cooper minimum splits into three minima relativistically; $4d_{5/2}\rightarrow\varepsilon f_{5/2}$, $4d_{5/2}\rightarrow\varepsilon f_{7/2}$ *and* $4d_{3/2}\rightarrow\varepsilon f_{5/2}$. Each would appear at the same photoelectron energy in the absence of dynamical effects resulting from relativistic interactions.

## EXPERIMENTS

To check possible systematic errors related to a particular experimental method, the measurements were done independently with hemispherical and time-of-flight (TOF) electron spectrometers at two different undulator beamlines at the Advanced Light Source (ALS) at Lawrence Berkeley National Laboratory. One experiment was carried out at beamline 10.0.1 using an endstation designed for gas-phase angle-resolved studies based on the Scienta SES-200 hemispherical electron analyzer (HEA) [5]. The analyzer is rotatable in the perpendicular plane,

allowing electron angular-distribution studies. Measurements at the $\theta$ angles of 0°, 54.7° and 90° were performed, and angular-distribution parameters were determined. In the TOF measurements, performed at ALS beamline 8.0, two analyzers are mounted in the perpendicular plane at $\theta$=0° and $\theta$=54.7°, allowing simultaneous measurements for accurate determination of $\beta$ parameters [6]. To determine $\beta$ parameters, the data were calibrated with the Ne-2*s* photoline, which has a fixed $\beta$ value of 2. In both experiments, for most of the data, the photon energy was increased in 2-eV steps, because the energy splitting of the spin-orbit components is 2.0 eV. This approach permitted the measurement of $\beta_{5/2}$ and $\beta_{3/2}$ at the same photoelectron *kinetic energy*, and the difference $\beta_{3/2}$-$\beta_{5/2}$ could be calculated easily. At higher energies, where larger energy steps were used (TOF measurements only), continuous curves were interpolated through the measured values of $\beta$ and used to estimate the difference $\beta_{3/2}$-$\beta_{5/2}$.

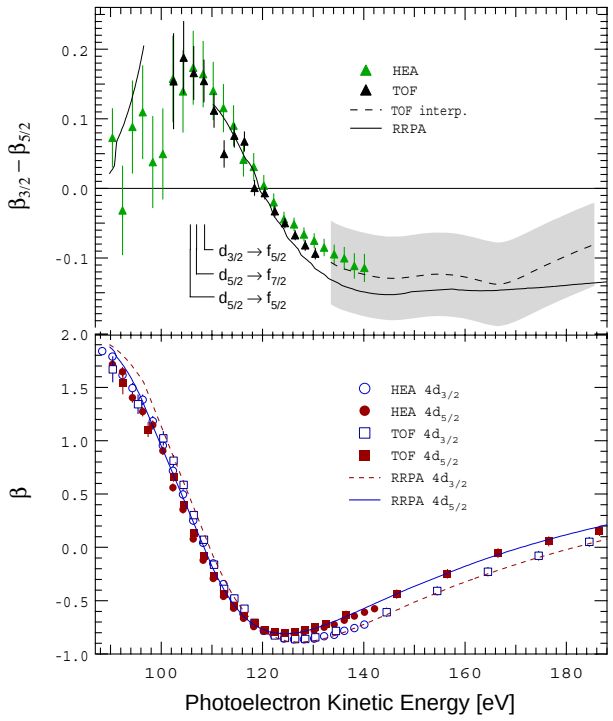


Figure 1. Lower panel: Photoelectron angular-distribution parameters, $\beta_{5/2}$ and $\beta_{3/2}$, for Xe 4*d* ionization as a function of photoelectron energy. The points are the present experiment and the curves are our theoretical results. Upper panel: $\beta_{3/2}$-$\beta_{5/2}$ as a function of photoelectron energy derived from the data in the lower panel. The dashed curve was obtained via interpolation of the TOF data, and the shaded area represents error bars. Omitted from theory is the region of the $4p \rightarrow ns,nd$ resonances. Also shown are theoretical predictions for the locations of the Cooper minima.

## RESULTS

Calculations were performed using the relativistic random-phase approximation (RRPA) [7] based upon the Dirac Equation; relativistic effects are included on an *ab initio* basis. All relativistic single-excitation channels from the 4*s*, 4*p*, 4*d*, 5*s* and 5*p* subshells were included in the calculation, a total of 20 interacting channels. As noted above, in the absence of relativistic effects, $\beta_j$ *must* be independent of $j$ as a function of photoelectron energy. The present results for $\beta_{5/2}$ and $\beta_{3/2}$ as a function of photoelectron energy are shown in the lower panel of Fig. 1, where a clear difference is evident. To focus on this difference more clearly, values of $\beta_{3/2}$-$\beta_{5/2}$ are shown in the upper panel of Fig. 1, where zero corresponds to the nonrelativistic expectation. Also shown in Fig. 1 are the results of our RRPA calculations. The agreement is remarkably good between theory and experiment. The part missing from the theoretical curve is the $4p \rightarrow ns,nd$ resonance region where the theoretical results are affected by autoionization. There is also excellent agreement between the two sets of experimental results, providing confidence in the reliability of the measurements. Note particularly that the $\beta$-parameter curves are not simply shifted, but have different shapes, *e.g.*, $\beta_{3/2}$ goes lower than $\beta_{5/2}$, and the differences persist to higher energy. At still higher energies, recent work has shown that interchannel interactions are pervasive and often dominant for most subshells of most atoms at most energies [8], so much so

that even the asymptotic form of the high-energy nonrelativistic photoionization cross section for non-*s*-states is altered. Thus, as long as 4*d* photoionization does not dominate the total cross section, significant interchannel interactions will modify the 4*d* transition amplitudes. But there is no reason to expect these interchannel interactions will modify each relativistic amplitude in the same way, *i.e.*, interchannel coupling will cause observable differences between $\beta_{3/2}$ and $\beta_{5/2}$ for *all* higher energies. Near threshold, it is also known $\beta_{3/2}$ and $\beta_{5/2}$ differ due to differing exchange interactions among the relativistic channels. Only in the shape-resonance region, 30-80-eV kinetic energy, are there no differences between $\beta_{3/2}$ and $\beta_{5/2}$, because the 4*d* cross section dominates here and the energy is high enough so exchange interactions are no longer important; interchannel interactions are negligible *only* in this narrow region. Thus, except for a small energy region near the 4*d* shape resonance, equality of $\beta_{3/2}$ and $\beta_{5/2}$ is the exception, not the rule.

## CONCLUSIONS

Finally, there is no reason to suspect Xe 4*d* is a special case; the results found in this work should be quite general. We thus expect effects of relativistic interactions on interchannel coupling will be widespread over all intermediate-**Z** atoms. These effects also should be manifest in clusters, molecules, surfaces, and solids.

## ACKNOWLEDGMENTS

The authors thank the staff of ALS for their support during the experiments.

## REFERENCES

1. S. T. Manson, C. J. Lee, R. H. Pratt, I. B. Goldberg, B. R. Tambe, and A. Ron, Phys. Rev. A **28**, 2885 (1983).
2. Y. S. Kim, A. Ron, R. H. Pratt, B. R. Tambe and S. T. Manson, Phys. Rev. Lett. **46**, 1326 (1981).
3. G. S. Canton-Rogan, A. A. Wills, T. W. Gorczyca, M. Wiedenhöft, O. Nayandin, C. N. Liu and N. Berrah, Phys. Rev. Lett. **85**, 3113 (2000).
4. H. S. Chakraborty, A. Gray, J. T. Costello, P. C. Deshmukh, G. N. Haque, E. T. Kennedy, S. T. Manson and J.-P. Mosnier, Phys. Rev. Lett. **83**, 2151 (1999).
5. N. Berrah, B. Langer, A. Wills, E. Kukk, J. D. Bozek, A. Farhat and T. W. Gorczyca, J. Electron Spectrosc. & Relat. Phenom. **101-103**, 1 (1999).
6. O. Hemmers, S. B. Whitfield, P. Glans, H. Wang, D.W. Lindle, R. Wehlitz, and I. A. Sellin, Rev. Sci. Instrum. **69**, 3809 (1998).
7. W. R. Johnson and C. D. Lin, Phys. Rev. A **20**, 964 (1979).
8. D. L. Hansen, O. Hemmers, H. Wang, D. W. Lindle, I. A. Sellin, H. S. Chakraborty, P. C. Deshmukh and S. T. Manson, Phys. Rev. A **60**, R2641 (1999).

This work was supported by the DOE, Office of Science, BES, DOE EPSCoR, NSF, NASA and CNPq, Brazil. The ALS is funded by the DOE, Materials Sciences Division, Basic Energy Sciences, under Contract No. DE-AC03-76SF00098.

Principal investigator: Dennis Lindle, Department of Chemistry, University of Nevada, Las Vegas, NV 89154-4003. Email: lindle@unlv.edu. Telephone: 702-895-4426.

This work has been published in Phys. Rev. Lett. **87**, 123004 (2001).

# Electronic structure of alkali metal-doped $M_8Si_{46}$ (M=Na, K) clathrates

A. Moewes[1], E.Z. Kurmaev[2], J.S. Tse[3], M. Geshi[3], M.J. Ferguson[3], V.A. Trofimova[2], and Y.M. Yarmoshenko[2]

[1]University of Saskatchewan, Dept. of Physics and Engineering Physics, 116 Science Place, Saskatoon, SK S7N 5E2, Canada,

[2]Institute of Metal, Russian Academy of Sciences-Ural Division, 620219 Yekaterinburg, GSP-170, Russia,

[3]Steacie Institute for Molecular Sciences, National Research Council of Canada, Ottawa, Ontario, Canada K1A 0R6

## INTRODUCTION

Silicon clathrates are networks of Si cages and can be considered as the Si-analog to fullerenes ($C_{60}$) with Silicon substituting the Carbon. The Si cages in clathrate structures share faces to satisfy the $sp^3$ bonding. All Si-atoms in clathrates are tetrahedrally coordinated with the Si-atoms occupying the centers of slightly imperfect tetrahedrons. Their indirect bandgap makes silicon clathrates promising candidates for optoelectronical and thermoelectrical devices. It has been shown recently that semiconductor clathrates also have thermoelectric properties [6] and can form three-dimensional arrays of nano-sized clusters [7]. Although pure silicon and germanium clathrates are predicted to be locally stable, experiments have been able to synthesize the metal-doped clathrate compounds only. The interaction between the metallic impurity atoms inside the clathrate and the semiconductor skeleton modifies the electronic structure of the clathrates. A charge-balanced Zintl-phase model has been suggested for these compounds with the guest (alkali metal or alkaline earth) donating its charge to the host frame. This model was confirmed by band structure calculations of $Na_8Si_{46}$ [8], $K_8Ge_{46}$ [9] and $Na_2Ba_6Si_{46}$ [10]. Recent experiments however, have raised the question whether the guest is close to being neutral in some cases [11-12]. In order to estimate the validity of the rigid band model, we have carried out x-ray emission measurements of crystalline Si (c-Si), $K_8Si_{46}$ and $Na_8Si_{46}$ and compare these to our calculations.

## DISCUSSION OF CALCULATIONS AND MEASUREMENTS

The densities of (occupied electronic) states (DOS) of $Si_{46}$, $Na_8Si_{46}$ and $K_8Si_{46}$ obtained from FLAPW calculations are shown in Fig. 1. The main features of total and partial density of states (DOS) are very similar for all three compounds. Differences occur mainly in the degree of filling of the energy bands by valence electrons and the energy position with respect to the Fermi level. For $Si_{46}$ the valence band is completely filled and the conduction band is empty giving rise to its insulating or intrinsic semiconducting behavior. In the cases of $Na_8Si_{46}$ and $K_8Si_{46}$ the additional sodium and potassium electrons fill the next energy band and the Fermi level is overlapping the conduction band providing the metallic properties of this doped clathrate. Similar behavior has been observed in calculated band structures of $Ge_{46}$ and $K_8Ge_{46}$ and $Na_8Si_{46}$ and $Ba_8Si_{46}$. The conduction-band density of states does not show strong modifications upon the inclusion of metal atoms. This is due to weak hybridization between the $Si_{46}$ conduction-band states and Na and K states and indicates that metal-metal and metal-Si interactions are ionic and that Na and K act as electron donors. Therefore alkali metal doping introduces a narrow band labeled as *D* in Fig. 1. This band - directly below the Fermi level - is separated by an energy gap of several eV from the main density of electronic states (features A, B and C) and should give rise to a spectroscopically observable feature. Its origin is in the lowest conduction band in the undoped $Si_{46}$ clathrate. Our calculations also indicate that a significant charge transfer from Na or K to the Si skeleton is

taking place and the rigid band model is a valid model for describing the electronic structure of these clathrates. We define the rigid band as a rigid shift of the Fermi level from the pristine $Si_{46}$ to $Na_8Si_{46}$ when filling empty bands with electrons from the Na atom.

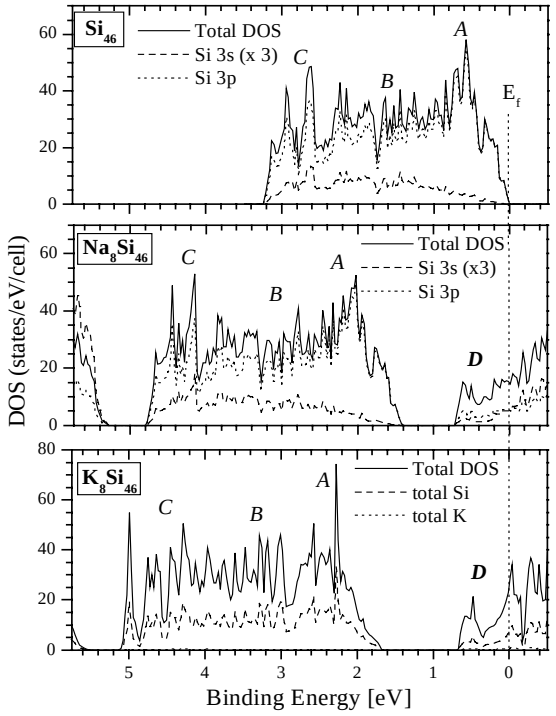


Figure 1. Total and partial density of states (DOS) for $Si_{46}$ and clathrates $Na_8Si_{46}$ and $K_8Si_{46}$.

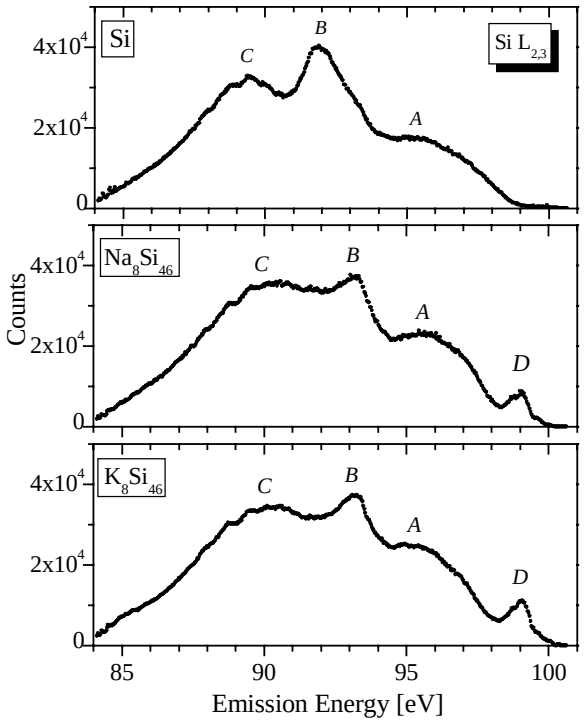


Figure 2. Si $L_{2,3}$ XES of c-Si, $Na_8Si_{46}$ and $K_8Si_{46}$.

Fig. 2 displays the Si $L_{2,3}$ emission spectra of crystalline silicon (c-Si) and Si-clathrates ($Na_8Si_{46}$ and $K_8Si_{46}$) as solid dots. Three main features labeled *A*, *B* and *C* are observed in both, crystalline Si and clathrates and are due to transitions from *s, d* and *sd*-like bands, respectively. The feature *D* discussed above has its spectroscopic counterpart in the additional feature that is present at 99 eV and labeled *D*. Feature D is present only in the spectra clathrates. It results from transitions of the lowest conduction band, introduced due to charge-transfer from the metal atoms and it corresponds to feature *D* in Fig. 1. The spectroscopic presence of this band demonstrates good agreement between experiment and density of state calculations and that the rigid band model is a good description for these materials.

This work was supported by Natural Sciences and Engineering Research Council (NSERC), the Russian Foundation for Basic Research (Projects 00-15-96575) and the NATO Collaborative Linkage Grant.

Principal investigator: Alexander Moewes, University of Saskatchewan, Dept. of Physics and Engineering Physics. Email: moewes@usask.ca. Telephone: 306-966-6431.

# Electronic structure of BeS studied by resonant inelastic x-ray scattering

O. Fuchs[1], L. Weinhardt[1], C. Heske[1], E. Umbach[1], A. Fleszar[2], C. Bostedt[3], L.J. Terminello[3], and R.C.C. Perera[4]

[1]Experimentelle Physik II, [2]Institut für Theoretische Physik, Universität Würzburg, Am Hubland, 97074 Würzburg, Germany
[3]Lawrence Livermore National Laboratory, Livermore, CA 94551, USA
[4]Lawrence Berkeley National Laboratory, Berkeley, CA 94720, USA

## INTRODUCTION

Due to their large energy gap and hardness, beryllium chalcogenides are interesting materials for improving the lifetime of optical devices made of other II-VI-semiconductors by forming multinary alloys [2]. Amongst them, beryllium sulfide (BeS) is an indirect semiconductor with a band gap of 7.4 eV direct and 4.7 eV indirect [1]. BeS, which is presently only available in powder form, is the only sulfur-containing II-VI-compound without any published experimental information about its electronic structure. This is due to the fact that the commonly employed method of choice (photoelectron spectroscopy) cannot be applied to an insulating powder because of charging effects, the lack of a suitable surface preparation method, and the fact that no sufficiently large single crystals are available.

We have therefore performed a combined soft x-ray absorption (NEXAFS) and resonant inelastic X-ray scattering (RIXS) study to investigate the electronic band structure of BeS powder using high brightness synchrotron radiation in the soft x-ray regime. RIXS is a bulk-sensitive photon-in-photon-out-process and therefore unaffected by charging effects as well as, to a large extent, by surface contaminations. Both NEXAFS and RIXS spectra were collected utilizing the high-flux capabilities of beamline 8.0 and the SXF endstation.

## NEXAFS

Figure 1 presents NEXAFS spectra of four differently treated BeS and BeO samples. Due to the insulating properties of BeS, electron-yield detection does not provide a reliable absorption signal. We therefore have recorded the partial fluorescence yield between 98 and 110 eV, covering emission from the complete valence band region and avoiding the contribution of the large elastically scattered peak for excitation energies above 110 eV. The bottom three spectra were taken from a commercial BeS-powder (Alfa Aesar) with a purity of 99% and a grain size smaller than 150 microns, mounted on carbon tape. The powder was shipped under Ar atmosphere, and spectrum a) was taken right after breaking the Ar seal. Spectrum b) was recorded after a 9-month storage in air, and spectrum c) after an additional sputtering step with 2 keV Argon ions (3 hours, 4 $\mu$A

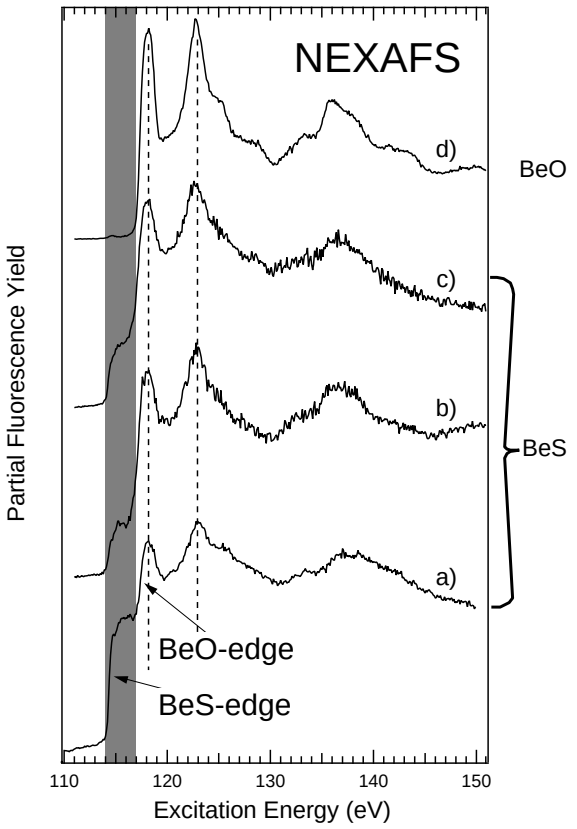


Figure 1: Be 1s NEXAFS-spectra for differently prepared samples.

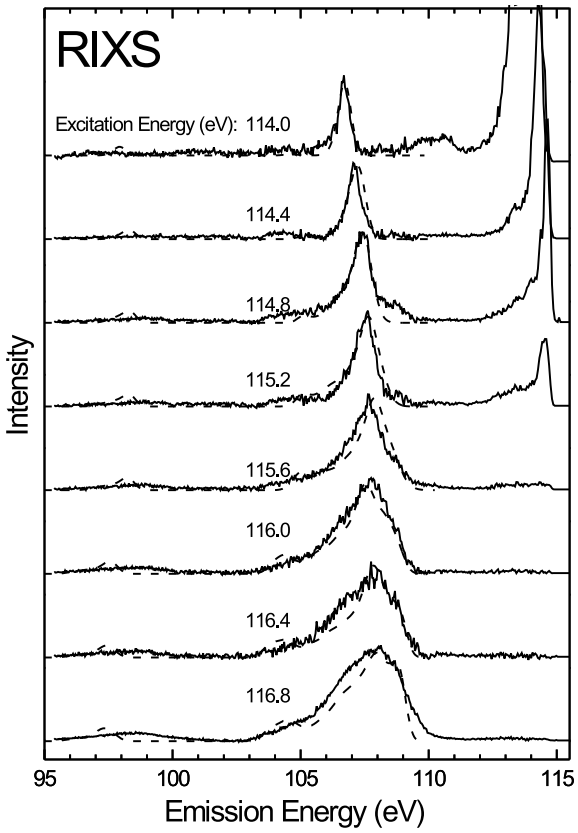


Figure 2: RIXS-spectra of BeS (solid lines) at excitation energies from 114 to 117 eV and simulated spectra based on an LDA-calculation (dashed lines).

sample current). Spectrum d) was taken from a BeO-reference sample, in order to identify the contributions from surface oxidation of the BeS-powder. While a comparison of the BeS- and BeO-spectra reveals a substantial contribution of oxide even for the fresh BeS powder, presumably due to humidity in the Ar atmosphere (BeS + $H_2O \rightarrow$ BeO + $H_2S$), we can nevertheless identify an excitation energy range (114-117 eV), in which only transitions into the conduction band of BeS are possible (gray region in figure 1). This is due to the fact that the band gap of BeO is substantially larger (11 eV direct band gap [3]) than that of BeS.

**RIXS**

Figure 2 shows the RIXS spectra (solid lines) recorded for the energy regime in which a resonant excitation into the BeS conduction band is possible (114-117 eV). The spectral shapes show an obvious dependance on the excitation energy revealing detailed information about the band structure of BeS. The theory for a detailed interpretation of such effects was first developed by Y. Ma [4] and is briefly outlined here. The excitation and de-excitation of the intermediate (undisturbed) state have to be considered as a combined one-step process which preserves crystal momentum, i.e., both the exciting and

the emitted photon interact with the solid state band structure at the same $\vec{k}$-vector of the brillouin zone if one neglects the momentum transfer of the photons [4]. This one-step scattering process can be described by the 'Kramers Heisenberg' formalism. This is generally applied for a description of Raman scattering processes and indicates the visualization of RIXS as an electronic Raman scattering process. In case of a 'disturbing' event during the RIXS process (e.g. phonon scattering), the 'coherence' of the excitation and emission process is lost and the momentum is no longer preserved, i.e. emission appears from almost all regions of the brillouin zone. In consequence, an experimental XES spectrum is always composed of two components: a *coherent* and an *incoherent* fraction. The latter resembles an emission spectrum excited far above the absorption edge where conduction band states are available almost all over the brillouin zone. This fact was used to isolate the coherent fraction of the experimental spectra by subtracting a spectrum at high excitation energy (in this case at 150 eV) from the original data.

The coherent part which is shown in figure 2 (solid lines) can be simulated with the help of a three-dimensional band structure calculation. Such simulated RIXS-spectra were computed based on an LDA band structure calculation of BeS [1]. The calculations simulate the RIXS process by taking the full matrix element into account. Thus, they utilize a three-dimensional $\vec{k}$-space representation of the occupied and unoccupied states as well as the dipole operator , leading to the application of dipole selection rules. Also, the band gap of the LDA band structure was corrected by suitable GW-calculations. The LDA-based results are presented as dashed lines and show good agreement with the experimental data. The broadening of the emission spectrum to lower as well as to higher emission energies with rising excitation energy indicates the dispersion of the valence states typical for a material with indirect band gap. In the present case, the broadening is due to probing the states between the conduction band minimum at the X-point and other high symmetry points (Γ- and W-point). At energies above 117 eV one should be able to excite electrons into unoccupied states at high symmetry points other than the X-point. This should result in strong resonances in the RIXS-spectra. For examinations at these energies, a BeS sample with very low surface oxidation is needed.

**CONCLUSIONS**

RIXS is a uniquely suited tool for studying the electronic structure of *insulating* BeS *powder*. By exciting within the band gap of BeO-surface contaminations, it is possible to probe the occupied and unoccupied states of the BeS bulk. A comparison with calculated spectra based on three-dimensional LDA gives very good agreement with the coherent part of the experimental RIXS spectrum.

# References


[1] A. Fleszar and W. Hanke, *Phys. Rev. B* **62**, 2466 (2000)
[2] Th. Litz et al., *J. Crystal Growth* **185**, 1 (1998)
[3] Landolt-Börnstein online (http://www.landolt-boernstein.com)
[4] Y. Ma, *Phys. Rev. B* **49**, 5799 (1994)



This work was funded by the German DFG through SFB 410, TP B3.


Principal Investigator: C. Heske, E. Umbach, Experimentelle Physik II, University of Würzburg, Germany. Email: heske@physik.uni-wuerzburg.de. Telephone: ++49-931-888-5127.

# Electronic structure of CMR compounds investigated by means of XES

K. Küpper[1], B. Schneider[1], S. G. Chiuzbaian[1], M. Matteucci[2] and D. D. Sarma[3]

[1]University of Osnabrück, Department of Physics, Barbarastr. 7, D-49069 Osnabrück, Germany
[2]Institute of Condensed Matter, National Research Council c/o Sincrotone Trieste, Padriciano 99, 1-34012 Trieste, Italy
[3]Solid State and Structural Chemistry Unit, Indian Institute of Science, Bangalore 560012, India

## INTRODUCTION

In the last few years the manganese perovskites $La_{1-x}A_xMn_{1-y}TM_yO_3$ (A = Ca, Ba, Sr, TM = Co, Ni, Fe) have been subject to intense experimental and theoretical studies due to the colossal magnetoresistance effect (CMR) [1, 2, 3]. The mother compound $LaMnO_3$ is an A-type antiferromagnetic insulator with orthorhombic crystal structure. We present results of Resonant X-ray emission spectroscopy (RXES) of $LaMnO_3$ performed at at Beamline 8.0.1 equipped with SXF endstation.

Recently the CMR effect in a double perovskite system, $Sr_2FeMoO_6$, has been discovered [4]. This material shows a strong effect at low magnetic fields and a high ferromagnetic transition temperature ($T_c \approx 420$K) and a half metallic behaviour as predicted on the basis of band structure calculations. In contrast $Sr_2FeWO_6$ is an antiferromagnetic insulator [5]. Because of the different transport properties of these two materials, it is predicted that an alloy $Sr_2FeMo_xW_{1-x}O_6$ will show a metal-insulator transition (MIT) as a function of x. While in an earlier work the critical concentration was reported to be between $0.4 < x_c < 0.5$ [6], Ray *et. al.* found $x_c \approx 0.25$ [7]. The aim of this work is to investigate the influence of the predicted MIT to the partial density if states. Therefore we recorded RXES data at the L edge of Fe, the M edge of Mo, and the K edge of O of $Sr_2FeMoO_6$ and $Sr_2FeMo_xW_{1-x}O_6$, respectively.

## RESULTS AND DISCUSSION

### $Sr_2FeMoO_6$ and $Sr_2FeMo_{0.6}W_{0.4}O_6$

Figure 1 shows the Fe L-emission spectra taken at indicated excitation energies, for both samples.

We recognise that these spectra for both materials look very similar. One can investigate additionally to the NXES-peak a rather weak elastic peak. At $E_{exc} \approx 720$ eV

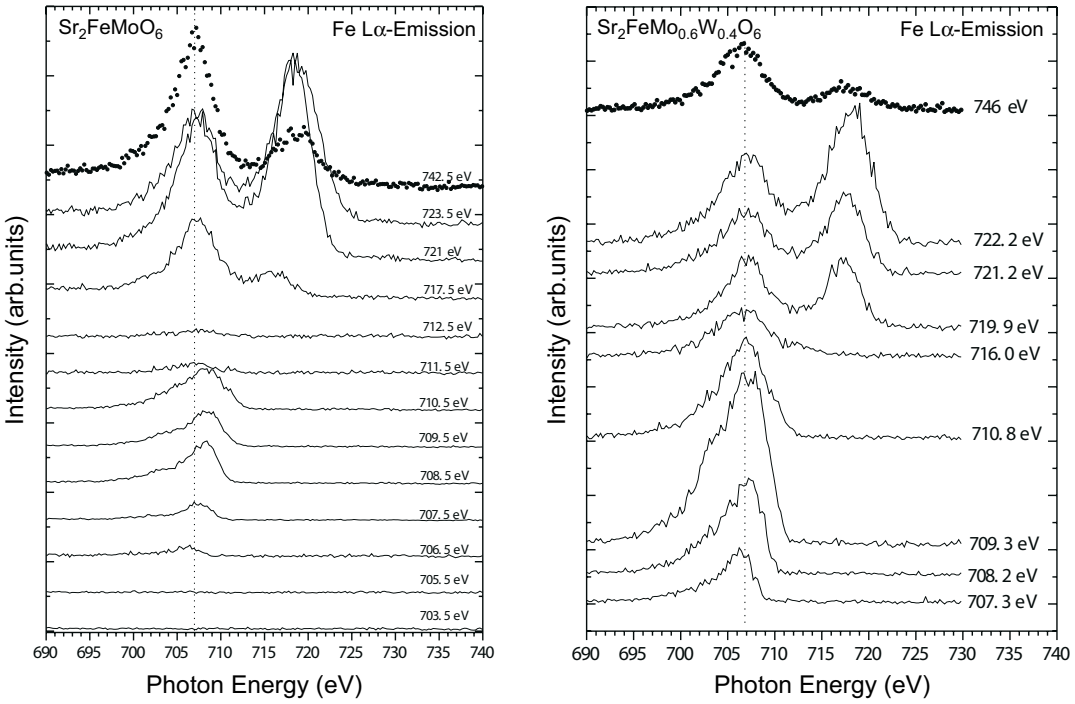


Figure 1: Fe L$\alpha$ emission spectra of $Sr_2FeMoO_6$ and $Sr_2FeMo_{0.6}W_{0.4}O_6$

a strong resonance for both samples can be observed. At $E_{exc}$ = 738 eV one observes an emission from the 3d level not only into the $2p_{3/2}$ level but also into the $2p_{1/2}$ level. The intensity ratio of both components is slightly below the expected value of 2. This indicates the presence of Coster-Kronig-transitions. The O K$\alpha$-emission spectra (not shown here) show for both materials only a weak energy dependence. The main emission features can be observed at 525.5 eV for both samples. This results are in good agreement with the relusts of Ray *et. al.* [7], the measurements of Fe L-emission of $Sr_2FeMo_{0.6}W_{0.4}O_6$ show no significant difference compared to the recorded spectra of $Sr_2FeMoO_6$, thus $Sr_2FeMo_{0.6}W_{0.4}O_6$ shows halfmetallic behaviour, although doped with 40 % tungsten on Mo lattice site.

## $LaMnO_3$

In figure 2 we present Mn L-emission spectra of $LaMnO_3$. The Mn $L_{2,3}$ emission features are strongly dependent on the excitation energy. At $E_{exc}$ = 642.7 eV a maximum in intensity of three emission peaks around 640 eV is observed. With increasing excitation energy, the intensity of the $L_2$ emission peaks drops to almost zero when the $L_3$ emission peak reaches a maximum of intensity around 650 eV. At higher excitation energy the normal x-ray emission takes place. These results are in in further evaluation in order to prepare further measurements on $La_{1-x}A_xMn_{1-y}TM_yO_3$ (A = Ca, Ba, Sr, TM = Co, Ni, Fe)-compounds. These measurements are necessary for a deeper understanding of hybridization in presence of different dopants in different concentrations.

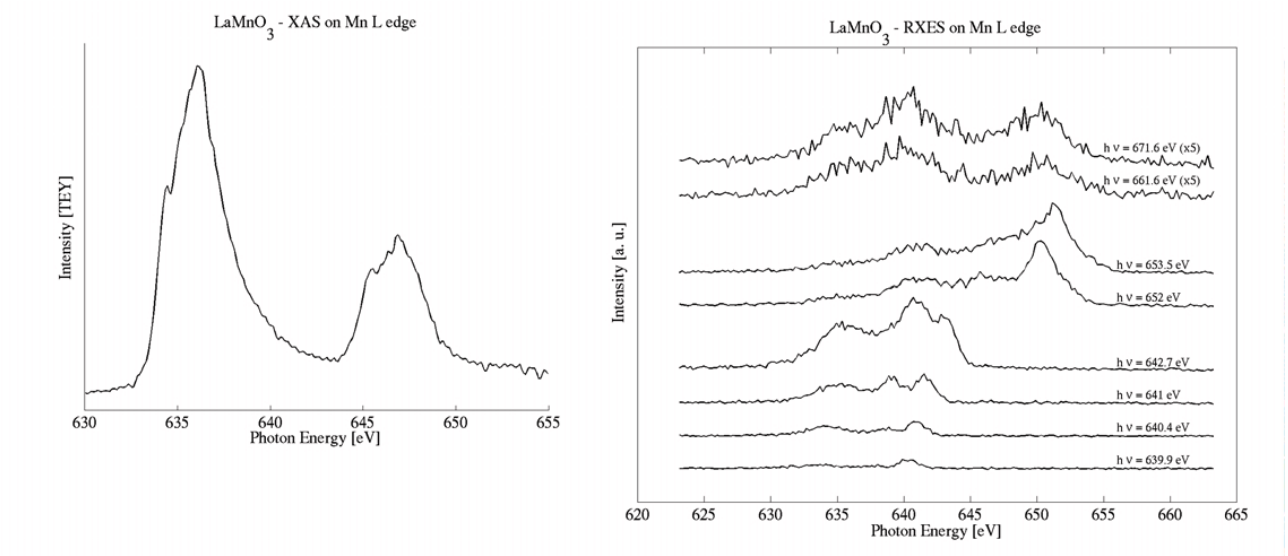


Figure 2: Mn L absorption and emission spectra of $LaMnO_3$

# References

[1] A. Millis, Nature, 1998, **392**, 147

[2] M. B. Salamon and M. Jaime, Rev. Mod. Phys., 2001, **73**, 583

[3] I. O. Troyanchuk, M. V. Bushynski, N. V. Pushkarev, H. Szymczak, and K. Bärner, J. Mag. mag. Mat., 2001, **225**, 331

[4] K.-I. Kobayashi, T. Kimura, H. Sawada, K. Tekura, and Y. Tokura, Nature, 1998, **395**, 677

[5] H. Kawanaka, I. Hase, S. Toyama, and Y. Nishihara, Physica B, 2000, **281+282**, 518

[6] T. Nakagawa, K. Yoshikawa, and S. Nomura, J. Phys. Japan, 1969, **27**, 880

[7] S. Ray, A. Kumar, S. Majumdar, E. V. Sampathkumaran, and D. D. Sarma, J. Phys. Cond. Mat., 2001, **13**, 607

This work was partly supported by BMBF (project 05SF8MPA/0)

Principal investigator: apl. Prof. Dr. M. Neumann, University of Osnabrück, Barbarastr. 7, D-49069 Osnabrück, Germany, Email: mneumann@uos.de, Telephone: +49541 969 2668

# Electronic structure of graphite fluorides

E.Z. Kurmaev[1], A. Moewes[2], D.L. Ederer[3], H. Ishii[4], K. Seki[4], M. Yanagihara[5], F.Okino[6], and H. Touhara[6]

[1]Institute of Metal Physics, Russian Academy of Sciences-Ural Division, 620219 Yekaterinburg GSP-170, Russia
[2] Department of Physics and Engineering Physics, University of Saskatchewan, 116 Science Place, Saskatoon, Saskatchewan S7N 5E2, Canada
[3]Department of Physics, Tulane University, New Orleans, LA 70118, USA
[4]Research Center for Materials Science and Department of Chemistry, Graduate School of Science, Nagoya University, Furocho, Chikusa-ku, Nagoya 464-8602, Japan
[5]Research Institute for Scientific Measurements, Tohoku University, Sendai 980-77, Japan
[6]Department of Chemistry, Faculty of Textile Science and Technology, Shinshu University, Ueda 386-8567, Japan

Fluorination of graphite leads to the formation of polycarbon monofluoride $(CF)_n$ and polydicarbon monofluoride $(C_2F)_n$. These compounds are exceptional lubricants under high temperature and high vacuum and quite successful cathodic depolarizers in a high-energy density battery. It is supposed that their structure is layered and altered from graphite by inserting covalently bonded fluorine atoms above and below every hexagon in each layer. According to Ref. 1 the structure of graphite fluorides is an infinite array of *trans*-linked cyclohexane chairs. It also has been suggested that it might be an infinite array of *cis-trans*-linked cyclohexane boats [2]. First principle calculations of the stability of these two configurations have shown that the energetic difference between these two structures is 0.0725 eV/atom in favour of the chair conformation, which is considered now the optimal structure for graphite fluorides [3]. Based on these recently performed *ab-initio* band structure calculations for $(CF)_n$ it has been concluded that carbon atoms have completely lost their aromatic nature [3]. In order to experimentally verify these conclusions regarding the chemical bonding, we have measured carbon and graphite X-ray emission spectra (XES) of $(CF)_n$ and $(C_2F)_n$.

The measurements were performed at Beamline 8.0 using the soft X-ray fluorescence endstation [4]. The samples were excited non-resonantly at 310 eV and 720 eV. Fig. 1 a shows X-ray fluorescence measurements of $(CF)_n$ and $(C_2F)_n$ [5]. Carbon Kα XES of $(CF)_n$ and $(C_2F)_n$ display features labelled *1-5* that are more similar to those of diamond where carbon atom has $sp^3$ bonding configuration than to graphite (configuration $sp^2$). Our findings confirm that in $(CF)_n$ and $(C_2F)_n$ all carbon atoms are of $sp^3$ type and covalently bonding to fluorine. This is in good agreement with results of nuclear magnetic measurements [6] according to which a resonance line is observed in the $^{13}C$ NMR spectrum of graphite fluoride and attributed to the $sp^3$ carbon atoms. Fig. 1 b presents fluorine Kα emission measurements of $(CF)_n$ and $(C_2F)_n$. A chemical shift in the F Kα emission spectra of about 0.7 eV takes place with respect to the spectrum of the ionic compound LiF. On the other hand, an increase in line width is observed for F Kα XES of $(CF)_n$ (~3.1 eV) and $(C_2F)_n$ (~3.6 eV) with respect to that of LiF (~2.8 eV). Both effects could be due to an increase in covalency in the chemical bonding. The fluorine spectra therefore also show that fluorine atoms are covalently bonding to carbon atoms.

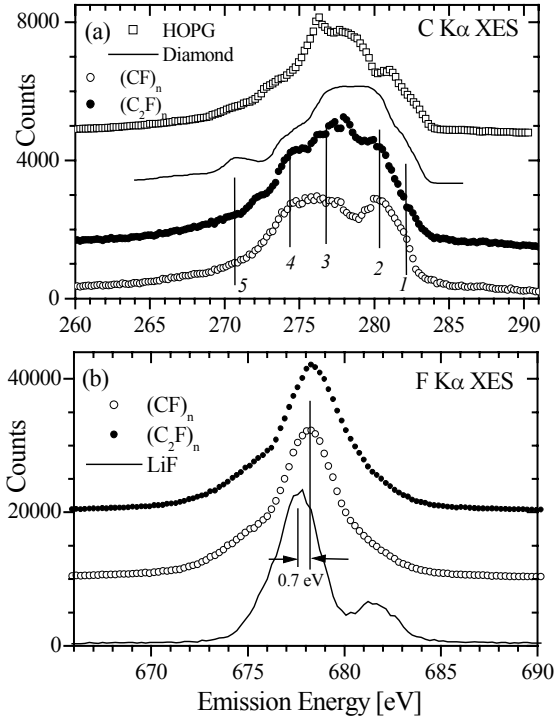


**Fig. 1 Carbon (a) and fluorine (b) XES of $(CF)_n$, $(C_2F)_n$ and reference compounds.**

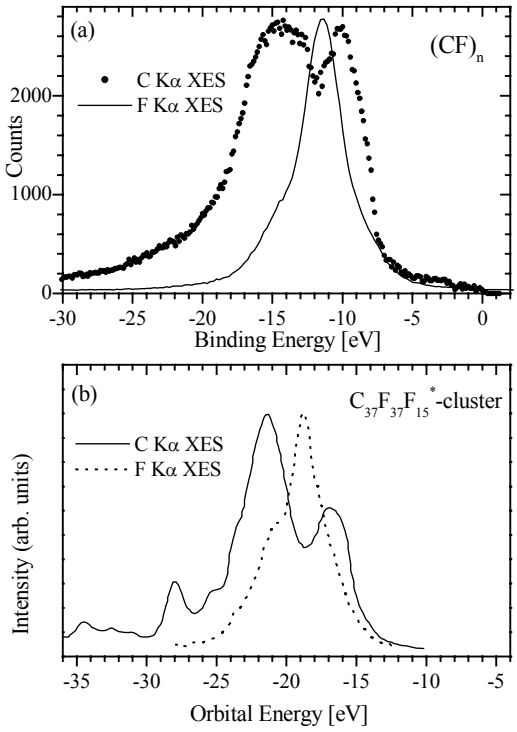


**Fig. 2 (a) Experimental carbon and fluorine Kα XES of $(CF)_n$. (b) Theoretical C and F Kα XES of $C_{37}F_{37}F^*_{15}$ cluster.**

Fig. 2 shows carbon and fluorine spectra of $(CF)_n$ in the binding energy scale. The emission energies are converted to binding energies using XPS C 1s and F 1s measurements of $(CF)_n$ [$E_{b.e.}$ (C 1s) = 290.4 eV and $E_{b.e.}$ (F 1s) = 689.6 eV. These emission spectra are caused by $2p \rightarrow 1s$ dipole transitions and therefore give a possibility to study the occupied carbon and fluorine 2p-states. Both spectra show a negligible intensity in the vicinity of the Fermi level, which is in agreement with electrical measurements of $(CF)_n$ according to which this material is an insulator. The intensity maximum of fluorine Kα XES occupy some intermediate position between two main peaks of carbon Kα XES of $(CF)_n$. According to the band structure calculations [3], F 2p-states are located at the bottom of the valence band: the F σ band is separated from the bottom of the C σ band by a gap of 8.4 eV at Γ and the F π-bands span a 6.8 eV range below the Fermi level interacting with lower π and upper σ carbon bands. The experiment shows (see Fig. 2) that F 2p-states are located at the middle of the valence band pushing up and down the carbon 2p-subbands. Our findings are more close to results of semi-empirical MO LCAO calculation of electronic structure of $(CF)_n$ [7]. According to these MO LCAO calculations, carbon 2p-states form two subbands originating from σ(C-C), τ*(C-F) and σ(C-C), τ(C-F) orbitals, respectively, divided by ~4.7 eV (Fig. 2b). Fluorine 2p-states are formed by the F 2p lone pair and occupy energy range between carbon 2p-subbands (Fig. 2b). The tails of fluorine 2p-states overlap with carbon 2p-states forming τ*(C-F) and τ(C-F) bonds. This MO LCAO structure is in an agreement with carbon and fluorine Kα XES (see Fig. 2a). The splitting of C Kα XES of $(CF)_n$ is found to be about 4.6 eV and F Kα XES is located exactly in minimum between two peaks of carbon spectrum.

To conclude, we have studied X-ray emission spectra of constituents of $(CF)_n$ and $(C_2F)_n$. We found that carbon atoms are of the $sp^3$ type and covalently bound to fluorine. Our measurements show that results of band structure calculations based on chair-type structure of $(CF)_n$ are not confirmed. Therefore the crystal structure of graphite fluorides is still not solved and must be refined.

## REFERENCES


1. W. Rudorff and G. Rudorff, Z. Anorg. Allg. Chem. 253 (1947) 281.
2. L.B. Ebert, J.I. Brauman, and R.A. Huggins, J. Am. Chem. Soc. 96 (1974) 7841.
3. J.-C. Charlier, X. Gonze and J.-P. Michenaud, Phys. Rev. B 47 (1993) 16162.
4. J.J. Jia, T.A. Callcott, J. Yurkas, A. W.Ellis, F.J. Himpsel , M.G. Samant, J. Stöhr, D.L. Ederer, J.A. Carlisle, E.A. Hudson, L.J. Terminello, D.K. Shuh, and R.C.C. Perera, Rev. Sci. Instrum. 66 (1995) 1394.
5. E.Z. Kurmaev, A. Moewes, D.L. Ederer, H. Ishii, Seki, M. Yanagihara, F.Okino and H. Touhara, Phys. Lett. A 288 (2001) 340.
6. C.A. Wilkie, G.Y. Lin, D.T. Haworth, J. Solid State Chem. 30 (1979) 197.
7. L.G. Bulusheva, A.V. Okotrub, V.N. Mit'kin, V.V. Murakhtanov, L.N. Mazalov, Zh. Struct. Khim. 36 (1995) 630; L.G. Bulusheva and A.V. Okotrub, Rev. Inorg. Chem., 19 (1999) 79.



The Russian Foundation for Basic Research (Project 00-15-96575) and NATO Collaborative Linkage Grant supported this work. Funding by the Natural Sciences and Engineering Research Council (NSERC) is gratefully acknowledged. The Deutsche Forschungsgemeinschaft (Schwerpunktprogramm 1073) funded the work in Augsburg. The Advanced Light Source at Lawrence Berkeley National Laboratory is supported by U.S. Department of Energy (Contract No. DE-AC03-76SF00098).



Principal investigator: Ernst Kurmaev, Institute of Metal Physics, Russian Academy of Sciences-Ural Division, 620219 Yekaterinburg GSP-170, Russia. Email: kurmaev@ifmlrs.uran.ru. Telephone: +7-3432-744183.

# Excitation-Energy Dependence of Cu $L_{2,3}$ X-Ray Emission Spectra of Cu, $Cu_2O$ and CuO

K. Kawatsura[1], K. Takahiro[1], N. Takeshima[1], T. Morikawa[1], Y. Muramatsu[2] and R.C.C. Perera[3]

[1] Department of Chemistry and Materials Technology, Kyoto Institute of Technology, Sakyo-ku, Kyoto 606-8585, Japan

[2] Synchrotron Radiation Center, Kansai Research Establishment, Japan Atomic Energy Research Institute, 1-1-1 Kouto, Mikazuki, Hyogo 679-5148, Japan

[3] Center for X-Ray Optics, Lawrence Berkeley National Laboratory, 1 Cyclotron Road, Berkeley, California 94720, USA

## INTRODUCTION

Cu metal and its oxides have recently attracted considerable attention for the study of the electronic structure of copper oxides based on the superconducting matters. The Cu *L* X-ray emission spectra of Cu metal and its oxides have been measured by many laboratories for studying the electronic structure of the valence bands and the effect of chemical bonding on the satellites structure of the main peak of Cu $L\alpha_{1,2}$ X-ray emission using usual X-ray source [1,2] and synchrotron radiation [3-5]. The incident photon energy dependence was measured for Cu $L_{2,3}$ satellites using synchrotron radiation [3-5]. Changes in the Cu $L_{2,3}$ X-ray emission spectra with Cu metal and its oxides have been measured using electron excitation by Fischer [6]. He found that relative intensity $L\beta_1/L\alpha_{1,2}$ significantly depends on the incident electron energy and the target. The relative intensity $L\beta_1/_{L\alpha 1,2}$ decreases with increase of excitation energy and it increases considerably for the oxides as compared to the metals.

In the present experiment, we have measured excitation-energy-dependence of Cu $L_{2,3}$ X-ray emission spectra of Cu, $Cu_2O$ and CuO using synchrotron radiation in order to study the effect of chemical bonding in the excitation and deexcitation processes of inner-shell electrons of Cu metal and its oxides.

## EXPERIMENT

The Cu (99.99 %) foil sample and sintered $Cu_2O$ (99.9 %) and CuO (99.9 %) samples were commercially obtained. The spectral measurements in the Cu *L* region of these samples were performed at the beamline BL-8.0.1 for X-ray emission and fluorescence yield (FY) X-ray absorption measurements and at BL-6.3.1 for total-electron yield (TEY) X-ray absorption measurements.

In order to determine the excitation energies, XA spectra were measured by total electron-yields measurements. The incident photon current was continuously monitored using a gold mesh in

front on the sample to normalize the XE spectra.

## RESULTS AND DISCUSSION

Cu $L_{2,3}$ X-ray emission (XE) spectra of Cu, $Cu_2O$ and CuO spectra were measured at ten different excitation energies from 930~934 eV, at the $L_3$ threshold energy, up to energies as high as 990 eV, above the $L_2$ threshold energy. Figure 1 shows Cu $L_{2,3}$ XE spectra normalized to the integrated photon flux, excited at specific energies. The spectra were measured at 930~934 eV ($L_3$ threshold), at 950~952 eV ($L_2$ threshold), and at 990 eV (above the $L_2$ threshold). The relative intensity $L\beta_1/L\alpha_{1,2}$ significantly depends on the incident photon energy and the target. The intensity ratio for the Cu target is constant at any incident photon energy. On the other hand, those for the $Cu_2O$ and CuO targets are the highest at the $L_2$ threshold energy, decrease abruptly just after the $L_2$ threshold energy, and then increase with the incident photon energy. This tendency is of interest from the view of the chemical effects on the excitation and deexcitation processes for inner-shell electrons.

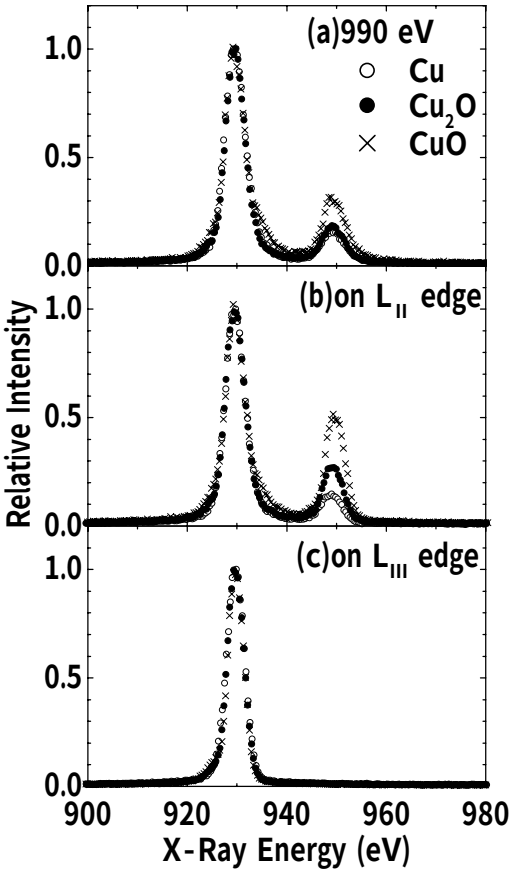


Figure 1. Comparison in the Cu L x-ray emission spectra of Cu, $Cu_2O$ and CuO. Excitation energies are tuned at 990eV (a), $L_2$ (b) and $L_3$ (c) thresholds.

## ACKNOWLEDGMENTS

We thank Dr. Jonathan Denlinger and Dr. Ponnusamy Nachimuthu for their helpful supports in performing X-ray emission and absorption measurements in BL-8.0.1 and BL-6.3.1, respectively. This work has been supported by the Hyogo Science and Technology Association and the US Department of Energy under Contract No. DE-AC03-76SF00098.

## REFERENCES

1. V. Barnole, J.M. Mariot, C.F. Hague, C. Michel and B. Raveau, Phys. Rev. B **41**, 4262 (1990).
2. C. Sugiura, J. Phys. Soc. Jpn. **63**, 1835 (1994)
3. N. Wassdahl, J.-E. Rubensson, G. Bray, P. Glans, P. Bleckert, R. Nyholm, S. Cramm, N. Martensson and J. Nordgren, Phys. Rev. Lett. **64**, 2807 (1990).

4. K. Ichikawa, K. Jouda, S. Tanaka, K. Soda, M. Matsumoto, Y. Taguchi, T. Katsumi, O. Aita, H. Maezawa, Y. Azuma and H. Kitazawa, J. Electr. Spectr. Relat. Phenom. **78**, 183 (1996).
5. M. Magnuson, N. Wassdahl and J. Nordgren, Phys. Rev. B **56**, 12238 (1997).
6. D.W. Fischer, J. Appl. Phys. **36**, 2048 (1965).

This work was supported by the Hyogo Science and Technology Association and the US Department of Energy under Contract No. DE-AC03-76SF00098.

Principal investigator: Yasuji Muramatsu, Synchrotron Radiation Center, Kansai Research Establishment, Japan Atomic Energy Research Institute, 1-1-1 Kouto, Mikazuki, Hyogo 679-5148, Japan. E-mail: murama@spring8.or.jp. Telephone: +81-791-58-2601.

# First Separate Measurements of the Nondipole Parameters γ and δ: Showcase Neon 2p Photoemission

O. Hemmers,[1] M. Blackburn,[2] T. Goddard,[2] P. Glans,[3] H. Wang,[4] S. B. Whitfield,[5]
R. Wehlitz,[6] I. A. Sellin,[7] and D. W. Lindle[1]

[1]Department of Chemistry, University of Nevada, Las Vegas, NV 89154-4003
[2]Advanced Light Source, Lawrence Berkeley National Laboratory, Berkeley, CA 94720, USA
[3]Department of Physics, Mid-Sweden University, Sundsvall S-85170, Sweden
[4]Department of Physics, Uppsala University, Box 530, S-751 21 Uppsala, Sweden
[5]Department of Physics and Astronomy, University of Wisconsin, Eau Claire, WI 54702-4004, USA
[6]Synchroton Radiation Center, University of Wisconsin, Stoughton, WI 53589, USA
[7]Department of Physics and Astronomy, University of Tennessee, Knoxville, TN 37996-1200, USA

## INTRODUCTION

The familiar dipole approximation [i.e., exp(ik·r)≈1] limits photon interactions to purely electric-dipole (*E1*) effects. For photoemission processes, this approximation leads to the well-known expression for the differential photoionization cross section,

$$\frac{d\sigma(h\nu)}{d\Omega} = \frac{\sigma(h\nu)}{4\pi}\left[1+\frac{\beta(h\nu)}{2}\left(3\cos^2\theta-1\right)\right] \qquad (1)$$

which describes the angular distribution of photoelectrons ejected from a randomly oriented sample by 100 % linearly polarized light. Here, $\sigma(h\nu)$ is the partial photoionization cross section, and θ is defined as the angle between the outgoing electron and the photon polarization vector of the incoming, linear polarized light. In the dipole approximation, the parameter $\beta(h\nu)$ completely describes the angular distribution of photoelectrons, and all higher-order interactions, such as electric-quadrupole (*E2*) and magnetic-dipole (*M1*), are neglected. Over the past few decades, the dipole approximation has facilitated a basic understanding of the photoionization process in atoms and molecules, as well as the application of photoelectron spectroscopy to a wide variety of condensed-phase systems.

Beyond the dipole approximation, predictions and observations of high-photon-energy ($h\nu \geq 5$ keV) deviations from dipolar photoelectron angular distributions have enjoyed a successful history dating from the 1930's. Small deviations from expected dipolar angular distributions at photon energies between 1 and 2 keV were attributed qualitatively to the effects of higher-order photon interactions. These so-called *nondipole* effects in the angular distributions of photoelectrons, which are primarily due to first-order (*E2* and *M1*) corrections [*O(k)*] to the dipole approximation [i.e., exp(ik·r) ≈1 + ik·r], were later shown to lead to the expression

$$\frac{d\sigma(h\nu)}{d\Omega} = \frac{\sigma(h\nu)}{4\pi}\left[1+\frac{\beta(h\nu)}{2}\left(3\cos^2\theta-1\right)+\left(\delta(h\nu)+\gamma(h\nu)\cos^2\theta\right)\sin\theta\cos\phi\right] \qquad (2)$$

for 100 % linearly polarized light. The angle θ is defined above and φ is the angle between the photon propagation vector and the projection of the electron momentum vector into the plane perpendicular to the photon polarization vector. $\gamma(h\nu)$ and $\delta(h\nu)$ are the nondipole angular-distribution parameters attributable to first-order interactions only. Values of the first-order

nondipole parameters are determined by the strength of electric-quadrupole (E2) and magnetic-dipole (M1) photoionization amplitudes relative to the corresponding electric-dipole (E1) amplitudes. Expressions for $\gamma$ and $\delta$ include *only* cross terms of the E2 and M1 amplitudes with the E1 amplitudes; "pure" quadrupole or magnetic-dipole interactions are not present in the first-order correction. Because the pure transitions are not included, the only manifestation of the first-order breakdown in the dipole approximation will be a change in the angular distribution of photoelectrons, specifically a forward/backward asymmetry relative to the photon propagation direction. The initial experiments motivated theoretical work, and more recent publications include quantitative predictions for a variety of atomic subshells. To date, all published experimental nondipole data did not separate the $\gamma$ and $\delta$ parameters, except for the special case of n*s* photolines, where $\delta$=0. The sum of $\gamma$ and $\delta$ parameters is commonly expressed using the $\zeta$ parameter ($\zeta = \gamma + 3\delta$), which has been used for most of the experimental and recent theoretical work. The present work concentrates on the separate determination of $\gamma$ and $\delta$ parameters for Ne 2*s* and 2*p* valence photoemission between 150 and 1200 eV and comparison to theoretical data.

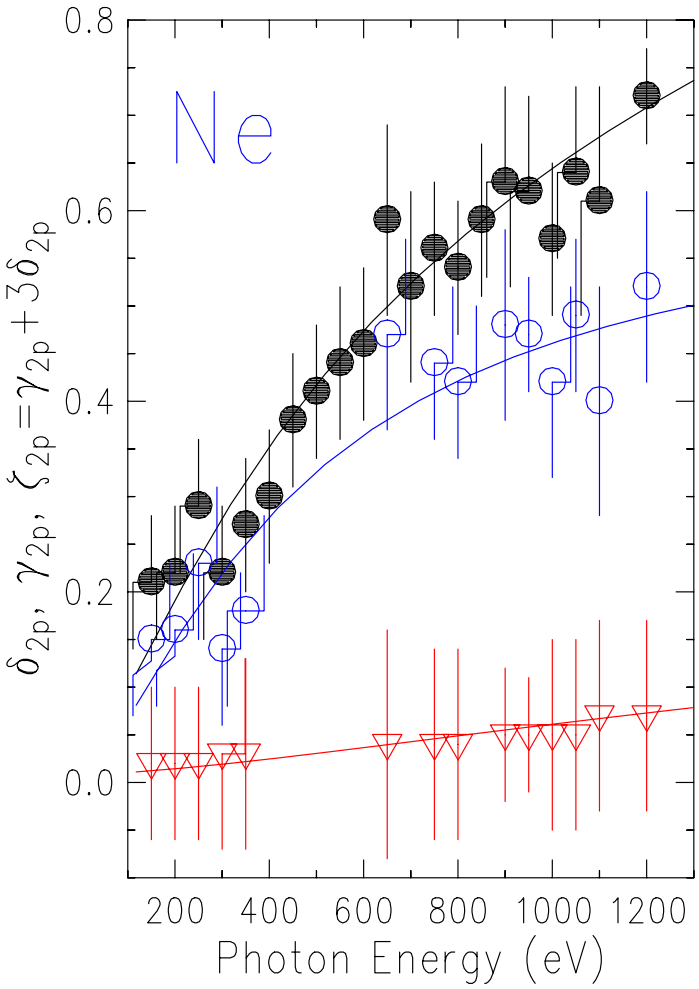


Figure 1. Photoelectron angular-distribution anisotropy parameter, $\delta$ (open triangles), $\gamma$ (open circles), and $\zeta$ (filled circles), for Ne 2*p*. The theoretical data (solid line) are independent-particle calculations.

## EXPERIMENTS

The present experiments were performed at the Advanced Light Source (ALS) of the Lawrence Berkeley National Laboratory on undulator beamline 8.0, which covers the 80-1300 eV photon-energy range. During the measurements the ALS operated at 1.9 GeV in two-bunch mode with a photon pulse every 328 ns. Four time-of-flight (TOF) electron analyzers, equipped with microchannel-plate detectors, collected spectra simultaneously at different angles. The interaction region was formed by an effusive gas jet intersecting the 0.4-mm-diameter photon beam. Energy resolution of the TOF analyzers with a focus size of 0.4 mm is about 1% of the final electron kinetic energy. A retarding voltage was used to slow the high-kinetic-energy electrons to a final kinetic energy of about 200 eV, thus maintaining the analyzer resolution at about 2 eV.

## RESULTS

Figure 1 shows the experimental and theoretical data for the $\gamma$, $\delta$, and $\zeta$ parameters for Ne 2*p* photoionization. All data agrees very well with theory but for certain energies it was not possible to satisfactorily separate the two parameters $\gamma$ and $\delta$ and therefore the separated nondipole components $\gamma$ and $\delta$ show less data than there are shown for $\zeta$. Even though $\delta$ is very small for the Ne 2*p* photoionization it is not zero and clearly shows a trend to increase with photon energy. The relatively large error bars reflect a possible systematic uncertainty and not the statistical error of each point.

## CONCLUSIONS

In summary, this is the first comprehensive study of dipole and nondipole angular-distribution parameters for atomic valence photoionization, in this case covering the photon-energy region from 150 eV to 1200 eV. For the first time the individual nondipole parameters $\gamma$ and $\delta$ have been separately determined for a non-*s*-subshell photoline. The measured nondipole contributions to the photoelectron angular distributions agree very well with existing calculations. It is important to appreciate the fact that doing gas-phase and solid-state angle-resolved photoemission experiments can show sizeable nondipole effects below 1 keV; this work clearly demonstrates nondipole effects may need to be considered in photoemission measurements, *even* for $h\nu<1$ keV.

## ACKNOWLEDGMENTS

The authors thank the staff of the ALS for their support, the IBM, LBNL, LLNL, University of Tennessee, and Tulane University collaboration for beam time at beamline 8.0. This work was supported by the National Science Foundation under Award No. PHY-9876996 and the Department of Energy. Work at the Advanced Light Source is supported by the Director, Office of Energy Research, Office of Basic Energy Sciences, Materials Sciences Division, of the U. S. Department of Energy under Contract No. DE-AC03-76SF00098.

Principal investigator: Dennis Lindle, Department of Chemistry, University of Nevada, Las Vegas, NV 89154-4003. Email: lindle@unlv.edu. Telephone: 702-895-4426.

This work has been accepted for publication in J. Electron Spectrosc. Relat. Phenom. (2002)

# Layer-Structure-Distribution in the Sample Plane of Mo/Si Multilayers Measured by Total-Electron-Yield X-Ray Standing Wave Methods

**Y. Muramatsu[1], H. Takenaka[2], E. M. Gullikson[3], and R. C. C. Perera[3]**

[1]*Japan Atomic Energy Research Institute, Sayo-gun, Hyogo 679-5148, Japan*

[2]*NTT Advanced Technology Corporation, Musashino-shi, Tokyo 180-8585, Japan*

[3]*Center for X-Ray Optics, Lawrence Berkeley National Laboratory, Berkeley, California 94720, USA*

Total-electron-yield (TEY) x-ray standing-wave measurements of multilayer x-ray mirrors have been performed, by monitoring sample photocurrents in BL-6.3.2 to obtain information on their layer/interface structure. Specifically, we have measured mapping spectra of x-ray standing-wave signals in a Mo/Si multilayer at normal incidence, which visibly illustrates the spatial distribution of layer structure in the sample plane.

The Mo/Si multilayer x-ray mirror, deposited on a 4-inch silicon wafer, consists of 50 periods of 19.6-Å Mo and 45.2-Å Si layers. The multilayer x-ray mirror sample is mounted on a sample holder in the reflectometer and a wire is connected to monitor the sample photocurrent. In total electron yield (TEY) x-ray absorption spectral measurements, x-ray standing-wave structure is observed when the photon-energy/wavelength of incident x-rays and the incident angle satisfy the Bragg reflection condition of the multilayer sample.

Figure 1 shows the TEY x-ray standing-wave spectra of a Mo/Si multilayer mirror measured along the 4-inch-wafer-size sample plane at the center (denoted by A in the Figure), middle (Bx, By) and periphery (Cx, Cy) positions. In the center position spectrum, standing-wave structures are observed near 96 eV and the standing-wave peak is observed at 97.68 eV. In the spectra of the middle and periphery positions, standing-wave structures are clearly shifted to higher-energy regions. Figure 2 shows the mapping spectrum of TEY x-ray standing-wave signals over the quarter of the 4-inch-wafer-size Mo/Si multilayer mirror measured with an incident angle of 90°. The photon energy of incident x-rays is fixed at 97.68 eV, identical to the peak energy of the center position x-ray standing-wave. The spot size of incident x-rays on samples is estimated to be less than 0.5 $mm^{\phi}$, and spectra are obtained using a 1-mm step scan along the x- and y-axes. This figure depicts periodic-length-changes of Mo/Si layers in the sample plane; the Mo/Si layers gradually become shorter from the center toward the periphery. The contour line also reveals a distribution of layer structure that is slightly wider along the y-axis than along the x-axis. This implies the sputtering source gas used in the deposition process of the multilayers is distributed slightly offset from the y-axis. These results indicate that TEY x-ray standing-wave measurements are useful for evaluating the layer/interface structure of multilayer x-ray mirrors.

We express thanks to Dr. H. Ito and Dr. K. Nagai of the NTT Advanced Technology Corporation for the preparation of multilayer samples. This work is supported by the Hyogo Science and Technology Association and the US Department of Energy under contract No. DE-AC03-76SF00098.

Principal investigator: Yasuji Muramatsu, Japan Atomic Energy Research Institute. Email: murama@spring8.or.jp. Telephone: +81-791-58-2601.

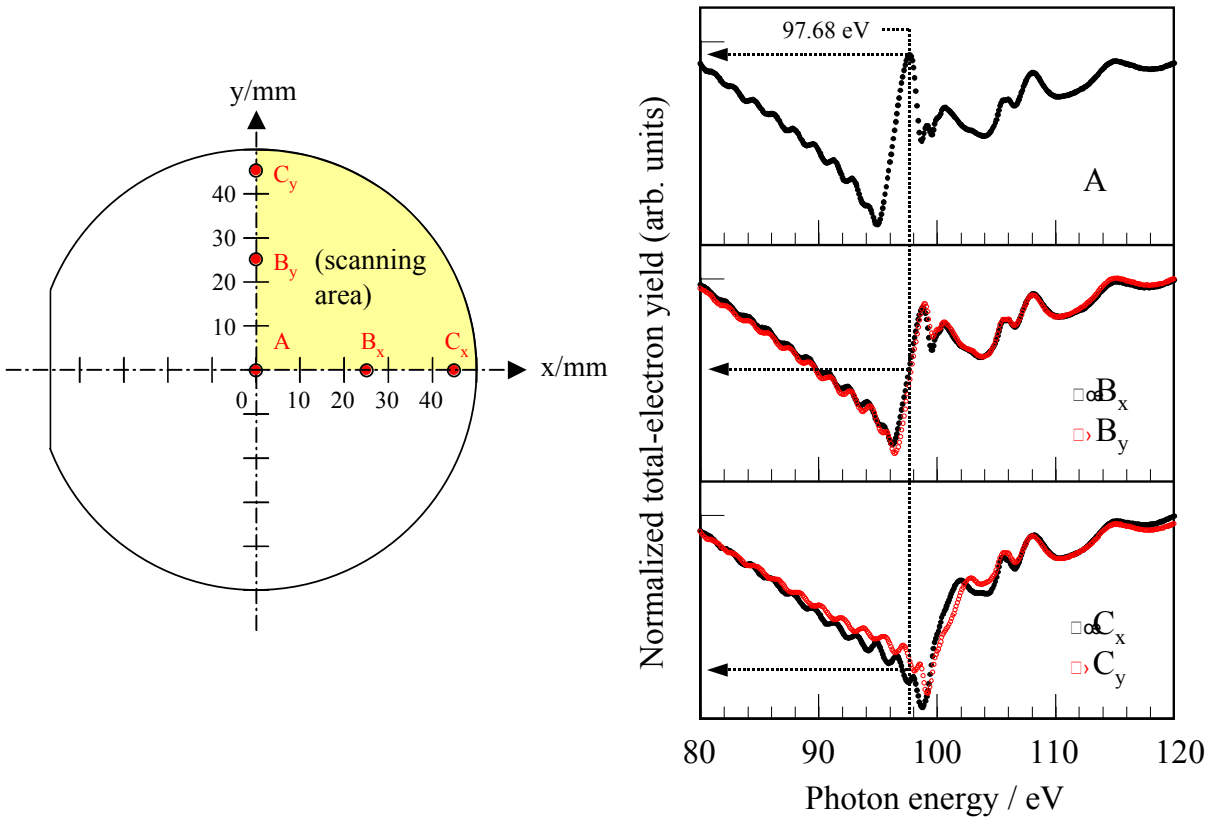


**Figure 1** TEY x-ray standing-wave spectra of the Mo/Si multilayer measured at the center (denoted by A), middle (Bx, By), and edge (Cx, Cy) positions along the 4-inch sample plane.

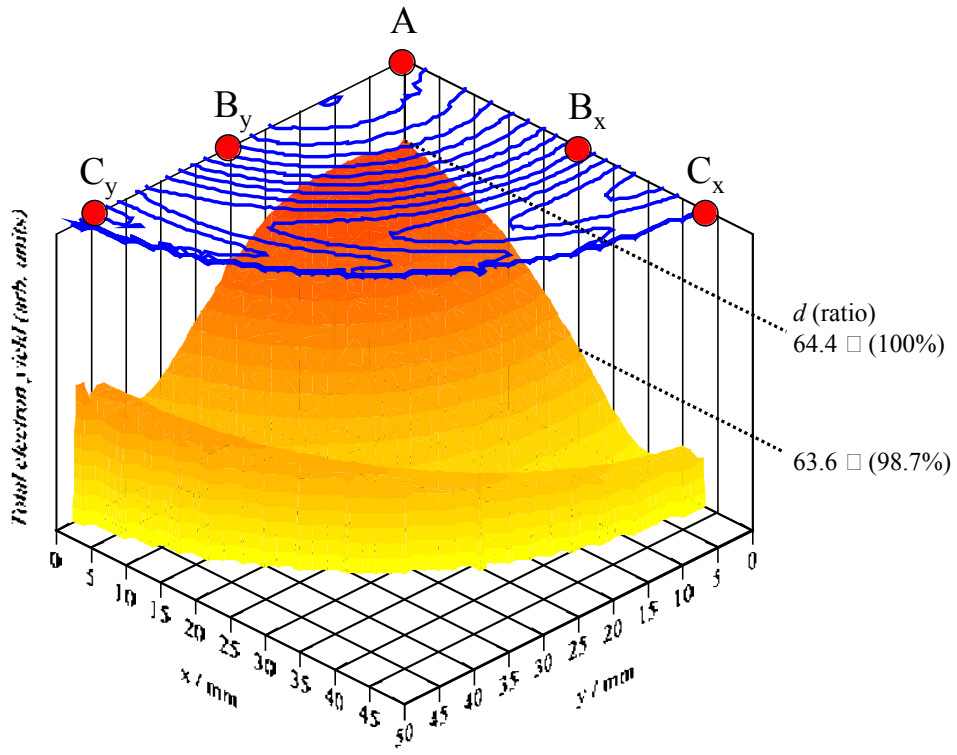


**Figure 2** Mapping spectrum of the TEY x-ray standing-wave signals in the quarter of the 4-inch-wafer-size Mo/Si multilayer measured with an incident angle of 90°. The photon energy of incident x-rays is fixed at 97.68 eV.

# Magnetic reversal of perpendicularly biased Co/Pt multilayers

O. Hellwig[1], S. Maat[1], J. B. Kortright[2], and Eric E. Fullerton[1]
[1]IBM Almaden Research Center, San Jose, California 95120, USA
[2]Materials Sciences Division, Ernest Orlando Lawrence Berkeley National Laboratory,
University of California, Berkeley, California 94720, USA

## IN-PLANE AND PERPENDICULAR EXCHANGE BIAS

Exchange-bias (EB) is a phenomena in which suitably prepared systems consisting of a ferromagnetic (F) phase in contact with an antiferromagnetic (AF) phase produces in an offset of the hysteresis loop of the F phase and an enhancement of its coercivity [1,2]. Although well established, a convincing microscopic description that explains experimental details of exchange bias has remained elusive [3,4]. A recent focus of experimental attention has been the interaction of EB with the details of the magnetization reversal of the F layer in thin film systems [5-7]. A common finding in thin film systems having in-plane anisotropy is that exchange bias produces an asymmetrical shape in the F layer hysteresis loop that is related to differences in its magnetic reversal mode on the ascending and descending branch [5-7].

A new class of EB film systems involves F layers having perpendicular, not in-plane, magnetic anisotropy (PMA) [8]. We are studying perpendicularly biased Co/Pt multilayers using laboratory measurements and resonant soft x-ray magnetic small-angle scattering (SAS) [9]. Hysteresis loops measured using SQUID magnetometry reveal the expected coercivity enhancement and loop shift, but do not show asymmetric loop shapes [9]. Our goal in ALS experiments was thus to use resonant SAS to study the distribution of magnetic domains around exchange biased hysteresis loops to determine if EB systems having PMA show differences in these properties compared to EB systems with in-plane anisotropy.

## SCATTERING FROM MAGNETIC STRUCTURE THROUGH REVERSAL

Resonant magnetic SAS has been shown to be extremely sensitive to the presence and spatial distribution of magnetic domains in F Co/Pt multilayers [10]. This high sensitivity results because the predominant scattered intensity originates precisely from the magnetic heterogeneity associated with the ferromagnetic domains, and this scattering is orders of magnitude stronger than the scattering when the F films are saturated.

The sample studied here consists of a compound multilayer structure as indicated in Fig. 1, and can be described as a $\{[Co(4\ Å)/Pt(7\ Å)]_4Co(6\ Å)/CoO(10\ Å)\}_{10}$ superlattice. There are ten F sublayer regions each consisting of a Co/Pt multilayer of 4.5 periods. Each of these F sublayer stacks has PMA and is sandwiched between AF CoO layers just 1 nm thick. This sample thus has 20 F/AF exchange bias interfaces distributed in depth through its structure, and was grown onto a $SiN_x$ membrane for transmission x-ray scattering measurements.

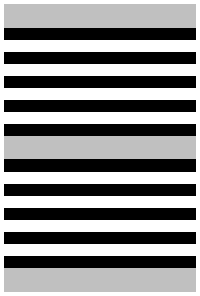

Figure 1. Schematic of part of the compound $\{[Co(4\ Å)/Pt(7\ Å)]_4Co(6\ Å)/CoO(10\ Å)\}_{10}$ structure forming the perpendicularly biased Co/Pt multilayer structure studied here. The 4.5 bilayer thick Co/Pt regions form ferromagnetic sublayers having perpendicular magnetic anisotropy. Each of these is sandwiched between two layers of antiferromagnetic CoO, producing a perpendicularly biased structure in which the bias is distributed in depth through the structure. In this schematic CoO layers are grey, Co layers are black, and Pt layers are white.

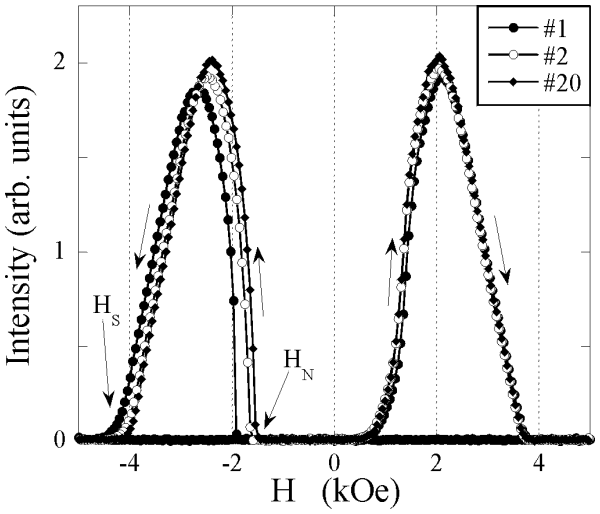


Figure 2. Field-dependent small-angle scattering measurements of a perpendicular {[Co(4 Å)/Pt(7 Å)]$_4$Co(6 Å)/CoO(10 Å)}$_{10}$ superlattice structure. The sample was positive field cooled to 85 K where the first, second, and twentieth field cycles are shown. $H_N$ and $H_S$ indicate the nucleation and saturation fields, respectively, for the descending branch of the hysteresis loop. The arrows indicate the field-sweep direction.

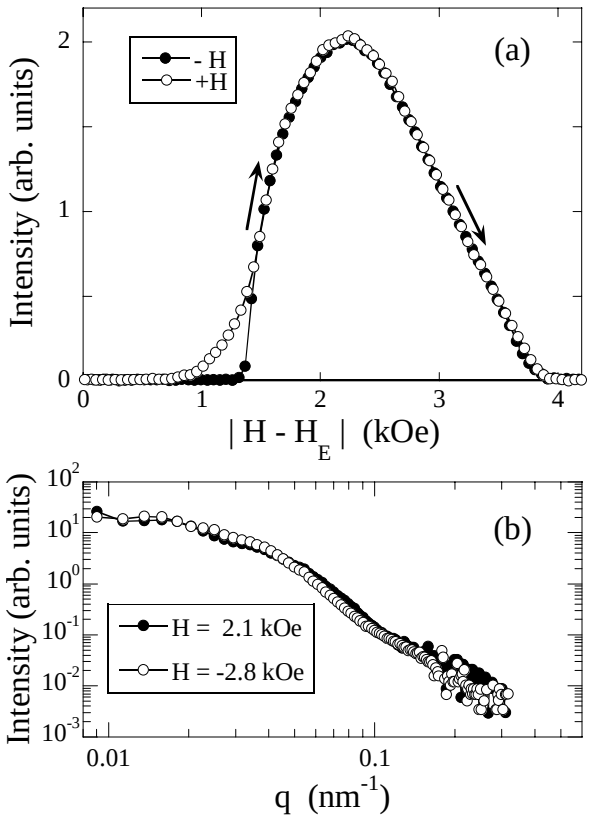


Figure 3. (a) Field-dependent small-angle scattering measurement of the perpendicular superlattice structure after field cycling 20 times. The data are corrected for the average bias field $H_E$ and then plotted vs. absolute field tom compare the intensity distributions for decreasing (filled circles) and increasing (open circles) field sweeps. (b) $q$ scans measured in an applied field of $H$ = -2.8 kOe after positive saturation (descending branch) and $H$ = 2.1 kOe after negative saturation (ascending branch).

Resonant SAS measurements tuned to the Co $L_3$ scattering peak can be made as a function of in-plane scattering vector $q$, applied perpendicular magnetic field $H$, and temperature. Measurements reported here were made after positive field cooling to 85 K to set the bias direction. The sample was thus saturated with no domains present during this cooling.

Shown in Figure 2 are several SAS hysteresis scans measured at 85 K and $q$ = 0.027 Å$^{-1}$ corresponding to an in-plane spatial frequency of $2\pi/q$ = 235 nm matching the periodicity of the labyrinth domains observed at room temperature. The scans show the first, second, and twentieth field cycles, each exhibiting expected strong scattering peaks resulting from the domains formed on reversal, and a negative bias field. Two effects are evident on repeated field cycling. First, there is a systematic shift of the nucleation fields $H_N$ and saturation fields $H_S$ toward the origin. Second is an increase in peak intensities on cycling. Both effects are more pronounced for the descending than the ascending branch of the loops, and can be understood as training effects (*i.e.*, relaxation of AF CoO grains) often observed in polycrystalline EB structures.

Scans of $H$ and $q$ after the 20$^{th}$ cycle, beyond which training effects were negligible, are shown in Figure 3. The $H$ scans show the ascending and descending peaks overlaid after correcting for the bias field $H_E$. While there are differences in the initial reverse domain nucleation processes (i.e., the shapes of the curves as the peak starts to grow from low $|H - H_E|$, once nucleated the reversal behavior of the sample after training appears identical in both field directions.

The *q* scans in Fig. 3b are obtained at $H$ = -2.8 and 2.1 kOe corresponding roughly to the peak intensities in Fig. 3a. The lack of a strong peak in these *q* scans is consistent with a relatively disordered domain structure during reversal. Because the *q* scans measure the spatial frequency spectrum of the magnetic domains, their near equivalence on ascending and descending branches confirms that on average the domain distribution is nearly identical on reversal in both directions in the biased state. We note that the *q* scans for this sample when it is demagnetized, either at room temperature or after zero-field cooling, do show pronounced peaks similar to that in Ref. 10, indicating that exchange bias does alter the spatial distribution of energies that determine the domain distributions during reversal.

## CONCLUSIONS

This work further demonstrates the high sensitivity of resonant soft x-ray scattering to magnetic domain structure present during the reversal of ferromagnetic films. We find that there are clear differences in the initial nucleation properties of reverse domains on the ascending and descending branches of the hysteresis loops, in agreement with studies of in-plane EB systems. Once nucleated, however, the evolution of these reverse domains is quite symmetric with respect to positive and negative field sweeps for this and similar samples studied. This behavior for perpendicular EB films is in contrast to many experiments from in-plane biased systems. We can understand the differences to result from the collinear uniaxial magnetic anisotropy and unidirectional exchange bias axis in the perpendicular bias samples studied here, whereas samples having in-plane anisotropy rarely have a single, unique anisotropy axis. These results thus suggest that asymmetric reversal is not an inherent property of exchange bias systems but rather depends on the anisotropy and microstructure of the constituent layers.

## REFERENCES


[1] J. Nogués and I. K. Schuller, J. Magn. Magn. Mat. **192**, 203 (1999).
[2] A. E. Berkowitz and K. Takano, J. Magn. Magn. Mat. **200**, 552 (1999).
[3] R. L. Stamps, J. Phys. D: Appl. Phys. **33**, R247 (2000).
[4] M. Kiwi, J. Magn. Magn. Mater. **234**, 584 (2001).
[5] C. Leighton, M. R. Fitzsimmons, P. Yashar, A. Hoffman, J. Nogués, J. Dura, C. F. Majkrzak, and I. K. Schuller, Phys. Rev. Lett. **86**, 4394 (2001).
[6] V. I. Nikitenko, V. S. Gornakov, A. J. Shapiro, R. D. Shull, K. Liu, S. M. Zhou, and C. L. Chien, Phys. Rev. Lett. **84**, 765 (2000).
[7] H. D. Chopra, D. X. Yang, P. J. Chen, H. J. Brown, L. J. Swartzendruber, and W. F. Egelhoff, Phys. Rev. B **61**, 15312 (2000).
[8] S. Maat, K. Takano, S. S. P. Parkin, and Eric E. Fullerton, Phys. Rev. Lett. **87**, 087202 (2001).
[9] O. Hellwig, S. Maat, J. B. Kortright, and E. E. Fullerton, "Magnetic reversal of perpendicularly-biased Co/Pt multilayers," Phys. Rev. B, **65** (in press).
[10] J. B. Kortright, S.-K. Kim, G. P. Denbeaux, G. Zeltzer, K. Takano, and Eric E. Fullerton, Phys. Rev. B **64**, 092401 (2001).



Work at the ALS and JBK were supported by the Director, Office of Energy Research, Office of Basic Energy Sciences, Materials Science Division, of the U.S. Department of Energy under Contract No. DE-AC03-76SF00098.



Principal investigator: Eric Fullerton, IBM Almaden Research Center. Email: eef@almaden.ibm.com. Telephone: (408) 927-2430.

# Multi-Atom Resonant Photoemission Effects from Solid Surfaces and Free Molecules

N. Mannella[1,2], B.S. Mun[1,2], S.-H. Yang[2], A.W. Kay[1,2,#],F.J. Garcia de Abajo[1,3], E. Arenholz[4], A.T. Young[4], Z. Hussain[4], H. Wang[5], O. Hemmers[5], D.W. Lindle[5], M.A. Van Hove[1,2], and C.S. Fadley[1,2]

[1]Dept. of Physics, University of California-Davis, Davis, CA 95616
[2]Materials Sciences Division, Lawrence Berkeley National Laboratory, Berkeley, CA 94720
[3] Centro Mixto CSIC-UPV/EHU, San Sebastian, Spain
[4]Advanced Light Source, Lawrence Berkeley National Laboratory, Berkeley, CA 94720
[5]Dept. of Chemistry, University of Nevada, Las Vegas, NV 89154
[#]Present address: Intel Corporation, Portland, OR

## INTRODUCTION

In prior work at the ALS, it has been pointed out that a new type of interatomic resonant photoemission effect exists, and that this effect furthermore has the potential of providing a useful probe of near-neighbor atomic identities, bonding, and magnetism [1-5]. The phenomenon has been termed multi-atom resonant photoemission (MARPE). In measuring this effect, the photoelectron intensity of a given core level from atom "A" (e.g. O 1s from MnO) is monitored while the photon energy is tuned through a strong absorption edge for a core level on another atom "B" in the sample (e.g. the Mn 2p edges in MnO). Initial observations on MnO and other metal oxides appeared to show significant entirely-positive interatomic resonant effects in photoemission of up to 100% [1]. Additional measurements in Auger emission and soft x-ray emission from MnO seemed to confirm that such effects were also present in secondary decay processes as a result of resonant enhancement of the initial O 1s core hole formation [2]. A theoretical model for these effects based on the extension of intraatomic resonant photoemission ideas to the interatomic case was also developed and compared favorably with experiment [3]. Other measurements on transition-metal compounds [6] and an adsorbate-substrate system [7a] seemed to confirm these measurements and analysis.

Subsequently, it has been realized that such experimental measurements require very careful allowance for potential detector non-linearities [4,5,7b], since the observed electron intensities (particularly inelastically scattered backgrounds) change dramatically in going over any core resonance. In particular, the detector used for several of the first MARPE studies [1,2,4-7a], the standard microchannel plate-plus-phosphor-plus-CCD camera incorporated in the Gammadata-Scienta series of electron spectrometers, exhibits not only a typical saturation effect for high countrates, but also a strong quadratic component of counting that goes above linear for low countrates. Thus, spectra obtained in this low-countrate regime, while not exhibiting any kind of saturation effect, can be artificially enhanced in intensity in passing over a core-level resonance. Methods of accurately correcting spectra for these non-linearities have been discussed [4,5,7b, and abstract by Mannella et al. in this 2001 Compendium]. When these effects are allowed for, the magnitude of the effect is reduced and the form is found to change, with the shape usually involving a negative-then-positive swing in intensity reminscent of a Fano profile in form [4,5,7b,8].

We here report more recent experimental results providing further evidence of such interatomic resonant effects in photoemission, for two very different limiting-case types of systems: a cleaved single-crystal oxide-NiO and a free molecule-$SF_6$. These data are discussed in terms of existing theoretical models for such MARPE effects [3,5], in particular, an x-ray optical (dielectric) approach that well describes the NiO data and a microscopic quantum mechanical model that should be useful in describing the $SF_6$ data.

## EXPERIMENTAL PROCEDURE

The NiO measurements were performed on beamline 4.0.2 and made use of the Advanced Photoelectron Spectrometer/Diffractometer located there. Detector non-linearities were corrected for in all data presented here, using methods described elsewhere [4,5, and abstract in the 2001 Compendium]. A NiO single crystal was cleaved just before insertion into ultrahigh vacuum via a loadlock, then ion bombardment and annealing in oxygen to remove minor surface contaminant levels and assure correct stoichiometry before measurement. The incidence angle of the radiation was varied from grazing values of 5° to much higher values up to 40° (cf. experimental geometry in Figure 1(a)).

The $SF_6$ measurements were performed on beamline 8.0.1 and made use of a time-of-flight spectrometer described in detail elsewhere [9]. The detectors in this spectrometer are positioned in angle with respect to the incoming radiation and polarization vector such that non-dipole contributions to the angular distributions can be readily measured with high accuracy. For reference, the angular distributions of photoelectrons from a randomly oriented ensemble of free molecules is given by $d\sigma / d\Omega = (\sigma / 4\pi)\{ 1 + \beta P_2(\cos\Theta_e) + [\delta + \gamma \cos^2\Theta_e] \sin\Theta_e \cos\Phi_e \}$, with $\beta$ the dipole asymmetry parameter and $\delta$ and $\gamma$ the first-order non-dipole parameters (cf. geometry in Figure 2(a), with $\Phi_e$ being the azimuthal angle around the polarization vector $\boldsymbol{\varepsilon}$) [9].

## EXPERIMENTAL RESULTS AND DISCUSSION

**NiO(001):** In Figure 1, we show experimental O 1s intensities from NiO as a function of photon energy and for five different x-ray incidence angles. For the lowest incidence angle of 5°, the effect of crossing the Ni 2p absorption resonances is dramatic, yielding a negative-then-positive excursion on crossing $2p_{3/2}$ whose amplitude is 75% of the intensity below the resonance. The magnitudes of these effects decreases as the incidence angle is increased, falling off to about 5% for an incidence angle of 40°.

Also shown in Figure 1 are theoretical curves based on an x-ray optical model of such effects, as discussed previously [5]. The optical constants that are key inputs for this model have been derived from concomitant partial-yield x-ray absorption measurements, with corrections for x-ray incidence angle and secondary electron takeoff angle [4], and subsequent Kramers-Kronig analysis [5]. The resulting theoretical curves are in excellent agreement with experiment for the lowest angle, and the agreement is very good for all other angles as well, although with some overprediction of the amplitudes at the higher angles. Non-zero effects are observed and predicted over the full angle range, in qualitative agreement with prior data for MnO [5]. These data thus disagree with one aspect of an earlier study of NiO by Finazzi et al. [8], in which they did not observe any sort of MARPE effect in O 1s emission from NiO; this lack of any effect appears to be due to measuring with too high an incidence angle and having insufficient statistical accuracy to resolve the small remaining effects seen, e.g. in Figures 2(e)-2(f).

We thus expect such MARPE effects to be observable in photoemission from any solid surface, with strength depending on the relative intensities of the absorption resonances. Furthermore, for homogeneous systems with flat surfaces, the x-ray optical model should provide a reasonably quantitative picture of the observed phenomena. Effects following an x-ray optical analysis have also recently been observed for photoemission from an adsorbate on a metal-$N_2$/Ni(001) [10]. For more complex cases with, e.g., three-dimensional nanometer-scale heterogeneity, the use of a microscopic model will be more appropriate.

**$SF_6$:** In Figure 2, experimental results for $SF_6$ are summarized. The x-ray absorption coefficient is shown in Figure 2(b), and the S 2p photoemission intensity and its asymmetry parameters were measured as photon energy was scanned across the "A" absorption resonance (corresponding to a F

$1s\ t_{1u}$-to-$a^*_{1g}$ excitation). Although the total S 2p intensity (proportional to $\sigma$) does not show a significant change in crossing the resonance (≤few %), the dipole asymmetry parameter $\beta$ (as shown in Figure 2(b)) exhibits about a 15% excursion in magnitude that is also of the same general form as those in Figure 1. Similar effects are also seen in the parameters $\delta$ and $\gamma$ [11].

Thus, interatomic resonant effects are also seen in this free molecule, and although they are too small to be observed as yet in the total intensity, they are clearly observed in the various asymmetry parameters. No theoretical calculations have as yet been performed for this case, but the x-ray optical model would clearly be inappropriate, and a microscopic approach such as that discussed previously [3,5] is the logical starting point for understanding these effects.

## CONCLUSIONS

Multi-atom resonant photoemission effects are found in both the total intensities from homogeneous solid surfaces and adsorbates on such surfaces, for which an x-ray optical model is found to well describe the data, and in the angular distribution asymmetry parameters of a free molecule, for which a microscopic theoretical approach will be necessary. Similar effects in nanoscale structures will lie somewhere between these two cases.

## REFERENCES


1. A. Kay, E. Arenholz, B.S. Mun, F.J. Garcia de Abajo, C.S. Fadley, R. Denecke, Z. Hussain, and M.A. Van Hove, *Science* **281**, 679(1998).
2. (a) E. Arenholz, A.W. Kay, C.S. Fadley, M.M. Grush, T.A. Callcott, D.L. Ederer, C. Heske, and Z. Hussain, *Phys. Rev. B* **61**, 7183 (2000); (b) E. Arenholz, A.W. Kay, unpublished results.
3. F.J. Garcia de Abajo, C.S. Fadley, and M.A. Van Hove, *Phys. Rev. Lett*. **82**, 4126 (1999).
4. A.W. Kay, Ph.D. dissertation (University of California-Davis, September, 2000), Chapters 4 and 5.
5. A.W. Kay, F.J. Garcia de Abajo, S.H. Yang, E. Arenholz, B.S. Mun, M.A. Van Hove, Z. Hussain, and C.S. Fadley, Physical Review B **63**, 5119 (2001).
6. A. Kikas, E. Nommiste, R. Ruus, A. Saar, and I. Martinson, Sol. St. Commun. **115**, 275 (2000).
7. (a) M.G. Garnier, N. Witkowski, R. Denecke, D. Nordlund, A. Nilsson, M. Nagasono, and N. Mårtensson, and A. Föhlisch, Maxlab Annual Report for 1999 and private communication correcting this data; (b) D. Nordlund, M. G. Garnier, N. Witowsky, R. Denecke, A. Nilsson, M. Nagasono, N. Mårtensson and A. Föhlisch, Phys. Rev. B **63**, 121402 (2001).
8. M. Finazzi, G. Ghiringhelli, O. Tjernberg, L. Duo, A. Tagliaferri, P. Ohresser, and N. B. Brookes, Phys. Rev. B **62**, R16215 (2000).
9. (a) O. Hemmers et al., Rev. Sci. Instrum. **69**, 3809 (1998); (b) O. Hemmers et al., Phys. Rev. Lett. **87**, 273003 (2001).
10. D. Menzel, W. Wurth, A. Föhlisch, P. Fuelner, S.-H. Yang, and C.S. Fadley, private communication.
11. H. Wang, O. Hemmers, P. Focke, M. M. Sant'Anna, D. Lukic, C. Heske, R. C. C. Perera, I. Sellin, and D. Lindle, to be published.



This work was supported by the U.S. Department of Energy, Office of Science, Office of Basic Energy Sciences, Materials Sciences Division, under Contract No. DE-AC03-76SF00098, and the National Science Foundation.



Principal investigator: N. Mannella, Department of Physics UC Davis, and Materials Sciences Division, Lawrence Berkeley National Laboratory. Email: norman@electron.lbl.gov. Telephone: 510-486-4581


Figure 1. (a) Experimental geometry for measurements on Ni(001). (b)-(f) O 1s intensity as photon energy is scanned through the Ni $2p_{1/2\text{-}3/2}$ absorption resonances. Both experimental data (blue points) and theoretical calculations based on an x-ray optical model (red curves) are shown.

Figure 2. (a) Experimental geometry for measurements on gas-phase $SF_6$. (b) The x-ray absorption coefficient in the F 1s region as measured by partial electron yield. (c) The dipole asymmetry parameter β as photon energy is scanned through the "A" resonance in (b).

**Figure 1.**

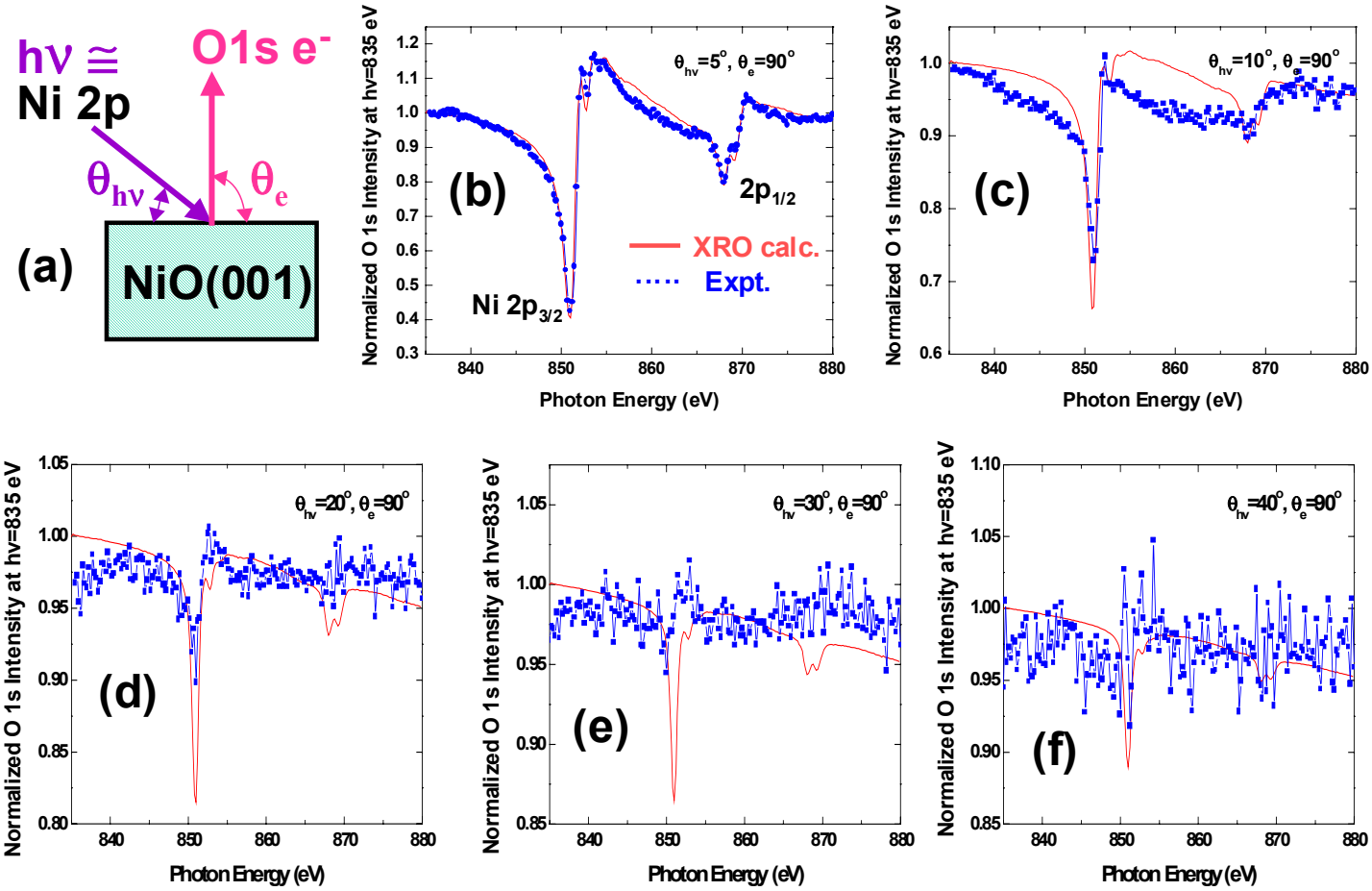


**Figure 2.**

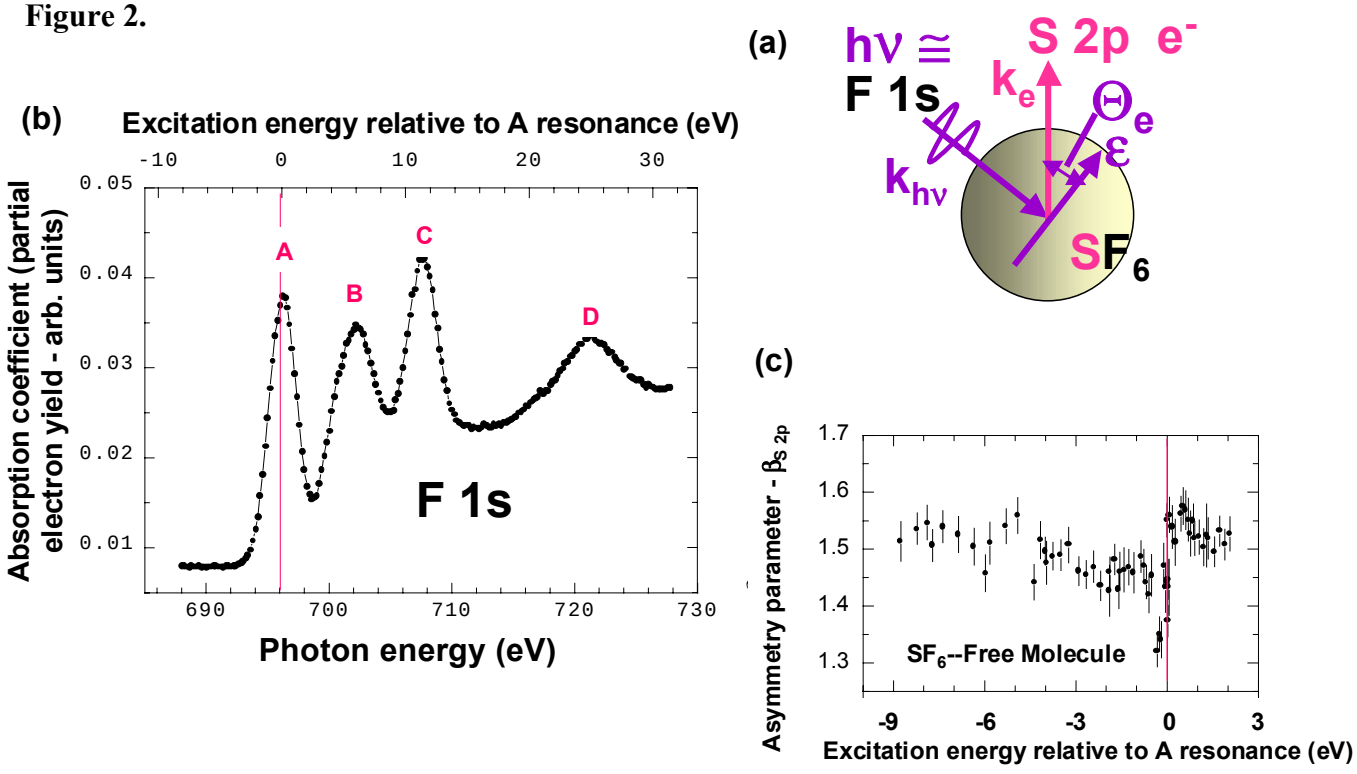

# O 1s XAS of $H_2O$ in the solvation shell of monovalent and trivalent ions

L.Å. Näslund[1], Ph. Wernet[2], H. Ogasawara[1], D. Edwards[3], S. Myneni[3] and A. Nilsson[1,2]

[1]Stockholm University, SCFAB, Fysikum, S-106 91 Stockholm, Sweden
[2]SSRL, 2575 Sand Hill Road, MS 69, Menlo Park, CA94025, USA
[3]Department of Geosciences, Princeton University, Princeton, NJ 08544, USA

## INTRODUCTION

Earlier experiments with the Soft X-ray Endstation for Environmental Research (SXEER) have shown that pure liquid water consists of three different species of water molecules - symmetric (SYM), acceptor asymmetric (A-ASYM), and donator asymmetric (D-ASYM) [1]. By dissolving Potassium Chloride or Aluminum Chloride we introduce a fourth type of water species - water molecules in the solvation shell of the dissolved ions. X-ray Absorption Spectroscopy at the oxygen K-edge (O 1s XAS) gives the information of Oxygen p-character and hence the local geometric arrangement around the probed oxygen atom. In this report we will show some of the XAS spectra we have obtained at beamline 8.0.

## O 1s XAS OF WATER WITH DISSOLVED KCl AND $AlCl_3$

If we dissolve Potassium Chloride (KCl) into water, the water molecules will form a solvation shell around each Potassium- and Chloride ion. These water molecules will have a different electronic structure than a water molecule in the bulk water. We can actual say that we have a fourth water species. Figure 1 is showing a XAS spectrum at the oxygen edge of water with dissolved KCl. We can see changes in two energy ranges. The pre-edge at 535 eV has higher intensity and has a shoulder at 534.3 eV. This is probably due to changes in the distribution of D-ASYM water species in the bulk water. The higher intensity at 537.0 eV can be explained by water molecules in the solvation shell of $K^+$ ion. Preliminary calculations are supporting the experimental data.

Comparing water dissolved KCl with water dissolved Aluminum Chloride ($AlCl_3$) can give some input to the interpretation. An O 1s XAS spectrum of water with dissolved $AlCl_3$ is shown in figure 2. As in dissolved KCl there is a shoulder at 534.3 eV. For water with dissolved $AlCl_3$ the shoulder is more distinct and indicates that the feature at 535 eV is a double peak. However, the interpretation is the same as in the case of dissolved KCl - there are changes in the distribution of D-ASYM water species in the bulk. At higher energy the O 1s XAS spectrum of water with dissolved $AlCl_3$ is showing higher intensity than pure water. If we compare the spectrum of water dissolved $AlCl_3$ with water dissolved KCl we can see that water dissolved $AlCl_3$ have lower intensity at 537.0 eV and higher intensity at 540.5 eV. This can be explained by differences in the electronic structure of water molecules in the solvation shell of trivalent ions from that of monovalent ions. Preliminary calculations show that the fourth water species, water molecules in the solvation shell of the $Al^{3+}$ ion, is giving higher intensity in a different energy range than the water molecules in the solvation shell of the $K^+$ ion.

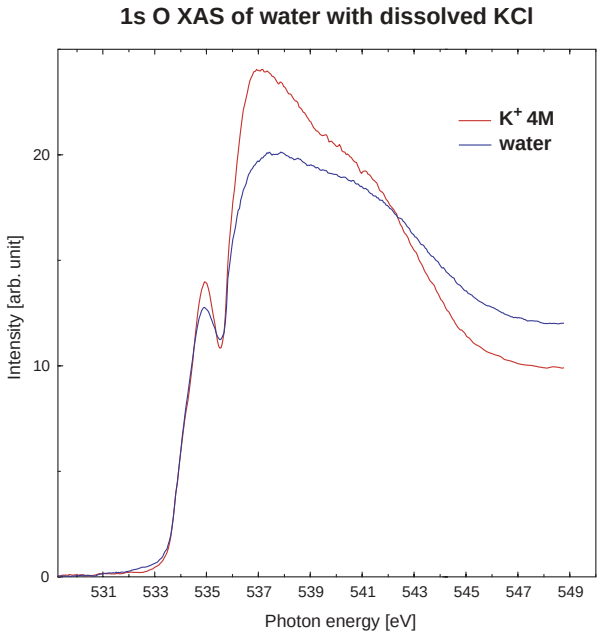


Figure 1. Oxygen 1s XAS of water with dissolved Potassium Chloride (KCl) compared to pure water. The spectrum of water with dissolved KCl has a shoulder at 534.3 eV. It is easier seen in figure 2.

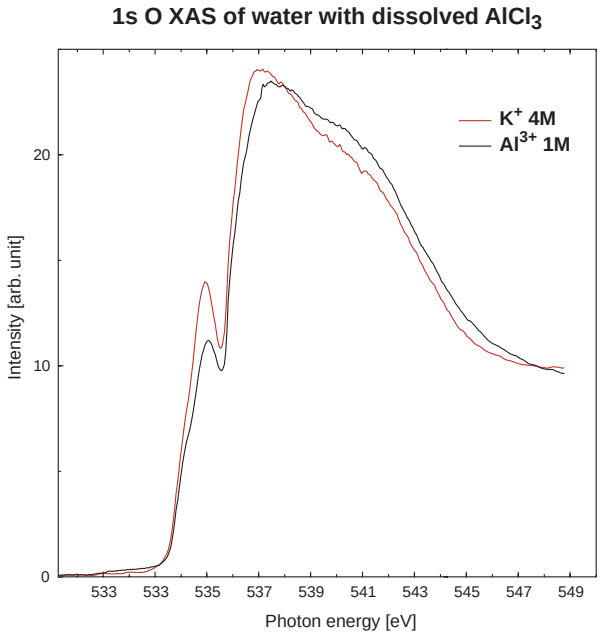


Figure 2. Oxygen 1s XAS of water with dissolved Aluminum Chloride ($AlCl_3$) compared to water with dissolved Potassium Chloride (KCl).

## CONCLUSION

We have shown that O 1s XAS is sensitive enough to resolve the electronic structure of water molecules in a solvation shell of an ion. As an example we have presented differences in the O 1s XAS spectrum between pure liquid water, water with dissolved KCl and water with dissolved $AlCl_3$. The distribution of the D-ASYM water species in bulk water is changing when KCl or $AlCl_3$ is dissolved in the water. Further investigation will tell how the distribution is changed.

## ACKNOWLEDGMENTS

M. Cavalleri and L.G.M Pettersson at Fysikum, University of Stockholm have done the preliminary calculations and are involved in the analyzing of the data collected at Beamline 8.0.

## REFERENCES

*1.* S. Myneni, Y. Luo, L.Å. Näslund, M. Cavalleri, L. Ojamäe, H. Ogasawara, A. Pelmenschikov, Ph. Wernet, P. Väterlein, C. Heske, Z. Hussain, L.G.M. Pettersson, and A. Nilsson, *Journal of Physics: Condensed Matter, In press*

This work is supported by the Basic Energy Sciences (Geosciences, Department of Energy, USA), the Swedish Royal Academy of Science (KVA), and the Göran Gustafssons Foundation for Research in Natural Science and Medicine.

Principal investigator: S. Myneni, Department of Geosciences, Princeton University, Princeton, NJ 08544, USA. Email: smyneni@Princeton.EDU. Telephone: 609-258 5848.

# Partial Density of States of B-2*p* in $AlB_2$ type Compounds

J. Nakamura,[1] K. Kuroki,[1] N. Yamada,[1] T.A. Callcott,[2] D.E. Ederer,[3]
J.D. Denlinger[4] and R.C.C. Perera[5]

[1]Department of Applied Physics and Chemistry, The University of Electro-Communications, Chofu, Tokyo 182-8585, Japan

[2]Department of Physics, University of Tennessee, Knoxville, TN 37996

[3]Department of Physics, Tulane University, New Orleans, LA 70118

[4]Advanced Light Source, Ernest Orlando Lawrence Berkeley National Laboratory, University of California, Berkeley, CA 94720

[5]Center for X-ray Optics, Ernest Orlando Lawrence Berkeley National Laboratory, University of California, Berkeley, CA 94720

Since the discovery of superconductivity in $MgB_2$ with a transition temperature, $T_c$, of 39 K by Nagamatsu *et al.*,[1] large number of researches from experimental[2-5] and theoretical point[6-12] of view have been performed on this compound and on a series of isostructural diborides. Although there are many experimental results that suggest holes in B-2*p*σ band with a strong electron-phonon coupling play important roles in the superconductivity of $MgB_2$, the reason for the high value of $T_c$ is not clear.

In order to clarify the mechanism of high $T_c$ superconductivity in $MgB_2$, it is important to investigate the difference in the electronic states between $MgB_2$ and other isostructural diborides. In the present study, we present X-ray emission (XES) and absorption spectra (XAS) near the boron (B) *K* edge in $MB_2$ (*M*=Mg, Al, Ta and Nb). $AlB_2$ and $TaB_2$ are not superconductors and a superconductivity in $NbB_2$ is controversial now. XAS was measured by both the total fluorescence yield (TFY) and the total electron yield (TEY) measurements at the same time. The reason we choose boron is because the band calculations for $MgB_2$ indicate that the bands near the Fermi energy are mainly composed from boron 2*p* orbitals.

The commercial specimens from Rare-Metallic Co. characterized by powder X-ray diffraction and dc-magnetization measurements, were used as samples of $MB_2$ (*M*=Mg, Al, Ta and Nb). The dc magnetization measurements indicate that the superconducting transition temperature of about 38 K for $MgB_2$ sample, and no superconducting transition for $TaB_2$, $NbB_2$ and $AlB_2$ above 1.8 K. The soft X-ray emission and absorption spectroscopies were performed at BL-8.0.1 of Advanced Light Source (ALS) in LBNL. In order to calibrate energy, XAS by TEY were also measured at the well calibrated beam line BL- 6.3.2 of the ALS.

Figure 1(a) shows XES ( ○ ) and XAS ( ● ) of $MgB_2$. The sharp decrease of XES and XAS at about 186.3 eV is attributed to the Fermi energy measured from 1*s* core level. The solid line in Fig. 1(b) is the boron PDOS obtained from a band structure calculation[10], where we have taken into account the effect of the instrumental resolution by gaussian broadening. The intensities of experimental XES and XAS in Fig. 1(a) are scaled to the theoretical PDOS in the energy region, $E \leq 182$ eV for XES and $187 \text{ eV} \leq E \leq 191$ eV for XAS. The sum of the experimental XES and XAS are also plotted in Fig. 1(b). It can be seen that the overall feature of both XES and XAS, including the existence of a large PDOS around the Fermi energy, are remarkably well reproduced by the band structure calculation, enabling us to attribute each observed structure to *p*π and/or *p*σ states. Namely, the existence of peaks A and B, which is consistent with recent studies[3], are characteristic of bonding *p*σ states. The region C in the energy range from 187 to 191 eV is attributed to the *p*π states. A sharp peak D at about 192 eV in XAS is reported to be a resonance peak of *p*π* state[3], and also corresponds to antibonding

$p\sigma^*$ state predicted by a band calculation. Thus peak D contains both the $p\sigma^*$ and resonance state of $p\pi^*$ states.

Figure 1(c) shows XES and XAS of $AlB_2$. The intensity of XES is normalized so that the area intensity coincides with that for $MgB_2$ below $E_F$, while the intensity of XAS is scaled so that the intensity in the high energy region, $E \geq 198$ eV, coincides with that for $MgB_2$. In the high energy region, XAS shows no strong characteristic peaks. A broad tail of XES below 183 eV is similar to that of $MgB_2$, but the value of $E_F$ shifts to be 187.5 eV. The form of XES of $AlB_2$ is broad compared to that of $MgB_2$. Figure 1(d) shows experimental PDOS derived from the sum of XES and XAS. A dip is observed at about 188 eV near the Fermi energy, indicating that the B-2*p* PDOS around the Fermi energy is drastically reduced compared to that in $MgB_2$. This is the major difference between $MgB_2$ and $AlB_2$.

This difference can be understood from results of the band calculation for $AlB_2$.[12] Namely, there are several factors that make the boron 2*p* PDOS around the Fermi level in $AlB_2$ much smaller than in $MgB_2$. First of all, the bonding $\sigma$ bands, whose tops are located above the Fermi level in $MgB_2$, are fully filled in $AlB_2$. Secondly, the Fermi level is located at a point where the top of the bonding and bottom of the antibonding $\pi$ bands touch with each other at the *K* point. If the system were purely two-dimensional, this would be a point where the DOS vanishes linearly as a function of energy. Although the $\pi$ band is three dimensional, the above two-dimensional property remains because the system is anisotropic.

The difference between $MgB_2$ and $AlB_2$ can qualitatively be understood within a simple rigid band model, namely by simply shifting the Fermi energy as mentioned above. To be more precise, there are some quantitative differences, whose origin seems to lie beyond a rigid band picture. Namely, in $AlB_2$, the intensity of XAS just above the dip is larger than that in $MgB_2$, while the intensity of peaks A and D is suppressed. Looking again into the band calculation results, these features may be attributed to the increase of three dimensionality in $AlB_2$.

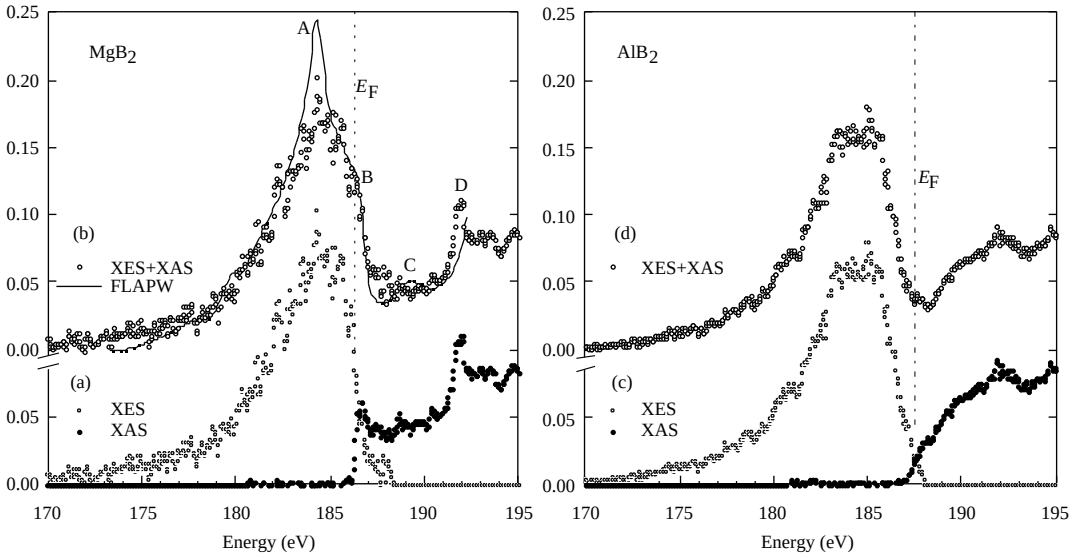


Fig.1 (a) The observed XES ( ○ ) and XAS ( ● ) spectra of $MgB_2$. (b) The sum of XES and XAS ( □ ) and the theoretical PDOS (solid line) derived from FLAPW method broadened with experimental resolution. (c) The observed XES ( ○ ) and XAS ( ● ) spectra of $AlB_2$. (d) The sum of XES and XAS ( □ ).

The XES and XAS of $TaB_2$ and $NbB_2$ are similar to those for $AlB_2$ except for a shift in

the Fermi energy up to 188.6 eV, owing to a larger band filling compared with $AlB_2$. The B-2*p* PDOS at the Fermi energy of $TaB_2$ is similar to that for $AlB_2$, so if $TaB_2$ is indeed superconducting, the difference between these two compounds should lie elsewhere. In $NbB_2$ compound, the Fermi energy is almost the same as that of $TaB_2$, but a considerable amount of DOS below the Fermi energy is observed. In both compounds, $TaB_2$ and $NbB_2$, band calculation suggests a strong hybridization between B-2$p\pi$ and Ta-5*d* or Nb-4*d* electrons. The characters of the states near the Fermi energy in $TaB_2$ and $NbB_2$ cannot be identified from the present results.

To summarize, the most characteristic feature in $MgB_2$ as compared to other related materials is the large B-2*p* PDOS around the Fermi level. Since this is partially attributed to the existence of the $p\sigma$ bonding band at the Fermi level, one may be tempted to consider that the $p\sigma$ band plays a crucial role in the occurrence of superconductivity in $MgB_2$.[8] This is indeed probable, but is not necessarily the case because the $p\pi$ band filling is also different between $MgB_2$ and other materials as mentioned above, which should result in a large difference in the shape of the $p\pi$ band Fermi surfaces. Let us note that the shape of the Fermi surfaces can play an essential role in the occurrence of superconductivity. For example, in those mechanisms that exploit nesting between the Fermi surfaces of bonding and antibonding $\pi$ bands, the shape of the Fermi surfaces (namely the $\pi$ band filling) is crucial. We believe that further studies are necessary to clarify this point.

This work was supported by a Grant in Aid for Science Research from the Ministry of Education, Scinece, and Culture, Japan, and published in Phys. Rev. B.[18]

## REFERENCES

[1] J. Nagamatsu et al.: Nature (London) **410**, (2001) 63.
[2] Z. Kurmaev et al.: cond-mat/0103487.
[3] T.A. Callcott et al.: Phys. Rev. B**64**, 132504 (2001)
[4] S.L. Bud'ko et al.: Phys. Rev. Lett. **86**, 1877 (2001).
[5] H. Schmidt et al.: Phys. Rev. B **63**, 220504 (2001).
[6] J. Kortus et al.: Phys. Rev. Lett. **86**, 4656 (2001).
[7] M. Imada, J. Phys. Soc. Jpn. **70**, 1218 (2001).
[8] K. Yamaji, J. Phys. Soc. Jpn. **70**, 1476 (2001).
[9] K. D. Belashchenko et al.: Phys. Rev. B **64**, 092503 (2001)
[10] G. Satta et al.: Phys. Rev. B **64**, 104507 (2001)
[11] J.M. An and W. E. Pickett, Phys. Rev. Lett. **86**, 4366 (2001).
[12] S. Suzuki et al.: J. Phys. Soc. Jpn. **70**, 1206 (2001).
[13] D. Kaczorowski et al.: cond-mat/0103571.
[14] V.A. Gasparov et al.: cond-mat/0104323.
[15] A.S. Cooper et al.: Proc. Nat. Acad. Sci. **67**, 313 (1970).
[16] J. Akimitsu et al., Abstract for 2001 Annual meeting of Physical Society of Japan, Vol 3. p.533.
[17] L. Leyarovskaya and E. Leyarovski, J. Less Common Met. **67**, 249 (1979).
[18] J. Nakamura et al., Phys. Rev. B **64**, 174504 (2001).

Email: jin@pc.uec.ac.jp.

# Resolving magnetic and chemical correlation lengths in CoPtCr-based recording media

O. Hellwig,[1] J. B. Kortright,[2] D. T. Margulies,[1] B. Lengsfield,[1] and E. E. Fullerton[1]
[1]IBM Almaden Research Center, San Jose, California 95120, USA
[2]Materials Sciences Division, Ernest Orlando Lawrence Berkeley National Laboratory, University of California, Berkeley, California 94720, USA

## GRANULAR RECORDING MEDIA

Current magnetic recording media consists of chemically segregated, polycrystalline grains whose grain-centers are ferromagnetic with in-plane anisotropy and whose grain boundaries are nominally non-magnetic [1]. This chemically and magnetically heterogeneous microstructure has evolved through several generations of recording media via an increasingly complex set of alloys from CoCr to CoPtCr to CoPtCrB. The additives Cr and later B are known to segregate to and produce nonmagnetic grain boundary phases that were believed to reduce exchange coupling between adjacent grains, thereby enabling sharper bit transitions and higher recording density [2]. Chemical heterogeneity associated with these films is resolved using high-resolution TEM and micro-EELS [3]. It has remained difficult, however, to directly measure the magnetic correlation lengths giving the distance over which grain-to-grain magnetism is correlated.

We have found that both magnetic and chemical heterogeneity in recording media films are strong scattering sources when tuned to specific soft x-ray core resonances to enhance contrast [4,5]. This transmission small-angle scattering (SAS) measurement positions the scattering vector $q$ in the film plane to optimize coupling to in-plane structure (Fig. 1b, inset) [6]. Although soft x-ray wavelengths limit the maximum $q$, spatial resolution to 1 nm is available.

## Q-RESOLVED RESONANT SCATTERING

SAS $q$ scans measured at the resonant intensity peaks at the Co and Cr $L_3$ lines are shown in Fig. 1. Scans of the common underlayer structure (without any media layer) reveal the contributions from the underlayer and the SiN membrane. These scans are almost featureless, with enhanced low $q$ scattering that is also observed in scattering from the substrate alone, and with a weak, broad peak at $q \cong 0.015$ Å$^{-1}$ observed at the Cr resonance. For the samples with media layers there is additional, strong SAS at both the Cr and Co edges arising from the media layer. This scattering is strongly resonantly enhanced, as is illustrated in Fig. 1b by the 10-fold decrease in scattering just 10 eV below the Co $L_3$ peak (dashed line) compared to that measured at the peak (open circles). Similarly strong and sharp resonant enhancements are observed near the Cr $L_3$ line.

The SAS scans from the different media samples show similar features. The Cr-edge data has a peak at $q \cong 0.07$ Å$^{-1}$ for all samples. This peak results from interference between neighboring scattering centers separated by $2\pi/q \cong 100$ Å, typical of grain diameters observed in TEM images of media grown on similar underlayers [2]. We attribute this Cr resonant peak to the average grain diameter of the media. It is well established that chemical segregation during the growth of CoCr alloys involves Cr diffusion to the grain boundaries resulting in a magnetic Co-rich core of the grain with non-magnetic or weakly magnetic Cr-rich grain boundaries [6,7], as shown schematically in Fig. 1b. Thus, by tuning to the Cr edge, we enhance the chemical contrast between the magnetic grain core and the Cr-rich grain boundaries.

The Co-edge scattering is expected to arise from both magnetic and chemical correlations (and their interference). These data show the same interference peak at $q \cong 0.07$Å$^{-1}$ that was observed in the

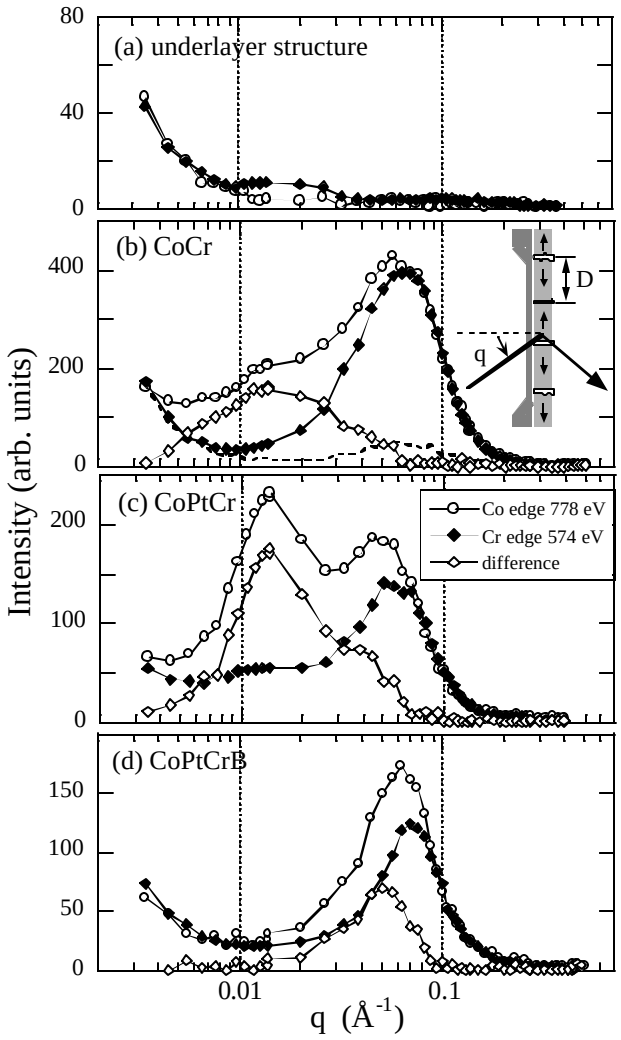


Figure 1. Resonant SAS from the underlayer structure without media layer (a) and from CoCr (b), CoPtCr(c), and CoPtCrB (d) media measured at the Co and Cr L3 lines as indicated. The inset shows the scattering geometry and media layer with magnetic grains (diameter D) with the in-plane magnetization direction represented by the arrows and nonmagnetic grain boundaries. The open diamonds are the difference between the Co- and Cr-edge data. The dashed line in (b) is the nonresonant scattering measured 10 eV below the Co edge.

Cr-edge data, as well as additional scattering at significantly lower $q$ values. The observation of high-$q$ resonant scattering from the grain structure at both the Co and Cr edges confirms that this scattering arises from in-plane compositional variations of Co and Cr. The additional lower-$q$ scattering arises predominantly from correlated magnetic regions larger than the grain size. For the CoPtCr film (Fig. 1c), this additional scattering is clearly resolved as a peak at $q \cong 0.015$ Å$^{-1}$ corresponding to a real space distance of ≅ 400 Å. The difference of the Co and Cr resonant scans (scaled to match at high $q$) results from Co magnetic-magnetic correlations and magnetic-charge interference, with the former dominating the low-$q$ peak and the latter contributing progressively to increasing $q$. The low-$q$ peak is thus a measure of the magnetic correlation length in these media films.

Boron additions are seen to reduce the magnetic correlation length from 4-5 times the chemical grain size to closely approach the grain size, consistent with improved recording performance and inferred magnetic correlation lengths from recording signal to noise measurements.

**MODELING ENERGY SPECTRA**

The above interpretation of magnetic and chemical peaks is qualitative. One approach to independent, quantitative determination of the scattering sources contributing to the peaks is to model the energy spectra of the scattering at each peak [5]. Measured Co $L_3$ energy spectra at these two peaks for the CoPtCr sample are shown as symbols in Fig. 2, and clearly have very different shape. Modeling these resonant shapes requires measured values of charge and magnetic atomic scattering factors $f$ for Co. These were obtained from transmission absorption measurements of the saturated media film with linear and circular polarization, followed by Kramers-Kronig transformation of the imaginary part of these quantities to obtain their real parts. Non-resonant $f$ values for Cr and Pt were taken from tabulated values [9].

Following standard SAS formalisms, the amplitude for different scattering sources is given by the difference of amplitudes of the two phases defining the heterogeneity. The simplest model for pure magnetic scattering yields amplitude proportional to the magnetic part of $f$ for Co [5, 6]. The corresponding intensity is scaled and plotted in Fig. 2, with a small non-resonant background added.

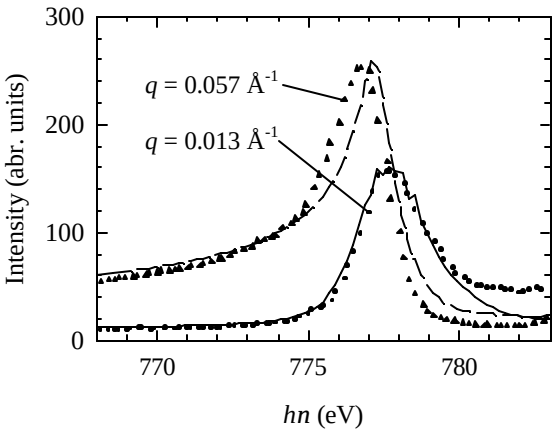


Figure 2. SAS energy spectra across the Co $L_3$ line of the CoPtCr media at the high- and low-$q$ peaks (symbols). Model spectra based on measured Co resonant scattering factors (lines) confirm the magnetic and chemical origin of the two peaks.

The good agreement of model and measured spectra confirms the magnetic origin of the low-$q$ peak and thus that magnetic correlation lengths in this sample are several times the chemical grain size. Modeling the high-$q$ spectrum requires postulating compositions of the segregated phases at the grain boundaries and centers, forming the appropriate scattering amplitudes of these two phases as linear combinations of elemental scattering factors, and squaring the difference of these amplitudes to obtain the intensity spectrum. A model spectrum is scaled and plotted with the high-$q$ data in Fig. 2, confirming that the high-$q$ peak is consistently modeled assuming chemical origin. Details showing that this model is sensitive to the composition of segregated phases are in ref. [5].

## CONCLUSIONS

Resonant SAS contrast at Co and Cr $L_{2,3}$ lines strongly enhances both magnetic and chemical scattering in recording media films. Since Co and Cr enhancements have different sensitivity to chemical and magnetic heterogeneity, their relative behavior allows clear separation of chemical and magnetic length scales and a very direct measurement of magnetic correlation lengths in granular recording media. The addition of B to the media alloys significantly reduces the magnetic correlation lengths [4]. Modeling of resonant energy spectra at the Co $L_3$ edge using measured resonant Co scattering factors quantitatively confirms magnetic and chemical scattering sources and provides an estimate of the composition of segregated phases yielding the chemical scattering [5].

## REFERENCES

1. H. N. Bertram, Theory of Magnetic Recording (Cambridge University Press, Cambridge, U.K.) 1994.
2. M. Doerner, *et al*., IEEE Trans. Magn. 37 (2001) 1052.
3. M. Doerner, *et al*., IEEE Trans. Magn. 36 (2000) 43.
4. O. Hellwig, D. T. Marguiles, B. Lengsfield, E. E. Fullerton, J. B. Kortright, Appl. Phys. Lett. 80 (2002) 1234.
5. J. B. Kortright, O. Hellwig, D. T. Marguiles, E. E. Fullerton, J. Magn. and Magn. Mater. 240 (2002) 325.
6. J. B. Kortright, *et al.*, Phys. Rev. B 64 (2001) 092401.
7. J. E. Wittig, *et al*., IEEE Trans. Magn. 34 (1998) 1564.
8. N. Inaba, Y. Uesaka, and M. Futamoto, IEEE Trans. Magn. 36 (2000) 54.
9. B. L. Henke, E. M. Gullikson, J. C. Davis, At. Data Nucl. Data Tables 54 (1993) 181; and at http:/www-cxro.lbl.gov/optical_constants/.

This work and JBK were supported by the Director, Office of Energy Research, Office of Basic Energy Sciences, Materials Science Division, of the U.S. Department of Energy under Contract No. DE-AC03-76SF00098.

Principal investigator: Eric Fullerton, IBM Almaden Research Center. Email: eef@almaden.ibm.com. Telephone: (408) 927-2430.

# Soft X-Ray Emission and Absorption Spectra in the Si *L* Region of Polysilanes

**Y. Muramatsu[1], M. Fujino[2], E. M. Gullikson[3] and R. C. C. Perera[3]**
[1]*Japan Atomic Energy Research Institute, Sayo-gun, Hyogo 679-5148, Japan*
[2]*NTT Basic Research Laboratories, Atsugi, Kanagawa 243-0198, Japan*
[3]*CXRO, Lawrence Berkeley National Laboratory, Berkeley, California 94720, USA*

Substituted polysilanes, (SiRR')n, have attracted significant attention because of their unique electronic properties. Their characteristic electronic nature arises from band edge structures which are composed of valence and conduction bands from σ and σ* bands, respectively, which differ from the electronic structure of polyacetylene. To further understand their electronic properties, we have measured the Si *L* x-ray emission spectra of a number of polysilanes with alkyl and phenyl substituents. In addition, their x-ray absorption spectra have also been measured to obtain information regarding unoccupied electronic orbitals.

Chemically synthesized polysilanes, $(SiR_2)n$, where R indicates substitution with a methyl (Me; $CH_3$), ethyl (Et; $C_2H_5$), propyl (Pr; n-$C_3H_7$), butyl (Bu; n-$C_4H_9$), pentyl (Pe; n-$C_5H_{11}$) or phenyl (Ph; $C_6H_5$) group, were used for spectroscopic measurements. Soft x-ray emission spectra in the Si *L* region were measured using a grating x-ray spectrometer installed in the undulator beamline, BL-8.0.1. The photon energy of the monochromatized incident beam was tuned to about 130 eV to effectively excite Si2p-electrons while preventing multiple ionizations. Total-electron-yield (TEY) x-ray absorption spectra were obtained by monitoring sample photocurrent in BL-6.3.2. Measured x-ray emission and absorption spectra were analyzed using discrete variational (DV)-Xα molecular orbital calculations.

Figure 1 shows soft x-ray emission and absorption spectra in the Si *L* region of both the polysilanes and the reference compounds, Si and $SiO_2$. In the emission spectra, polysilane spectral features exhibited similar structures; a main peak near 90 eV, and high-energy and low-energy shoulders clearly differ from those of the Si and $SiO_2$ references. In absorption spectra, alkyl-substituted polysilanes exhibit a threshold energy of 101 eV, while the Ph-substituted polysilane exhibits a slightly lower threshold energy. In the fine-structure at the thresholds of polysilanes, a pre-edge peak is observed near 101 eV and an intense peak is seen at 102 eV for the Ph-substituted polysilane. No such pre-edge or intense peaks, however, are observed in the spectra of alkyl-substituted samples. From spectral analysis using DV-Xα molecular orbital calculations Si *L* x-ray emission spectra, which include a main peak with high- and low-energy shoulders, are explained by the summed DOS spectra of occupied Si3s and Si3d orbitals hybridized with Si3p, C2s and C2p orbitals. X-ray absorption spectra are also qualitatively explained by the summed DOS spectra of unoccupied Si3s and Si3d orbitals. In both x-ray emission and absorption spectra, little difference is observed among alkyl-substituted polysilanes. It is therefore confirmed that the length of alkyl substituents has little effect on the electronic structure of the Si backbone. X-ray spectral features of the Ph-substituted polysilane, however, slightly differ from alkyl-substituted features. This is explained by the difference in hybridization of Si and C orbitals between $sp^2$-C atoms in phenyl substituents and $sp^3$-C atoms in alkyl ones.

We thank Dr. J. Denlinger of the Lawrence Berkeley National Laboratory for his help and support in performing x-ray emission measurements. This work has been supported by the Hyogo Science and Technology Association and the US Department of Energy under contract No. DE-AC03-76SF00098.

Principal Investigator: Yasuji Muramatsu, Japan Atomic Energy Research Institute. Email: murama@spring8.or.jp. Telephone: +81-791-58-2601.

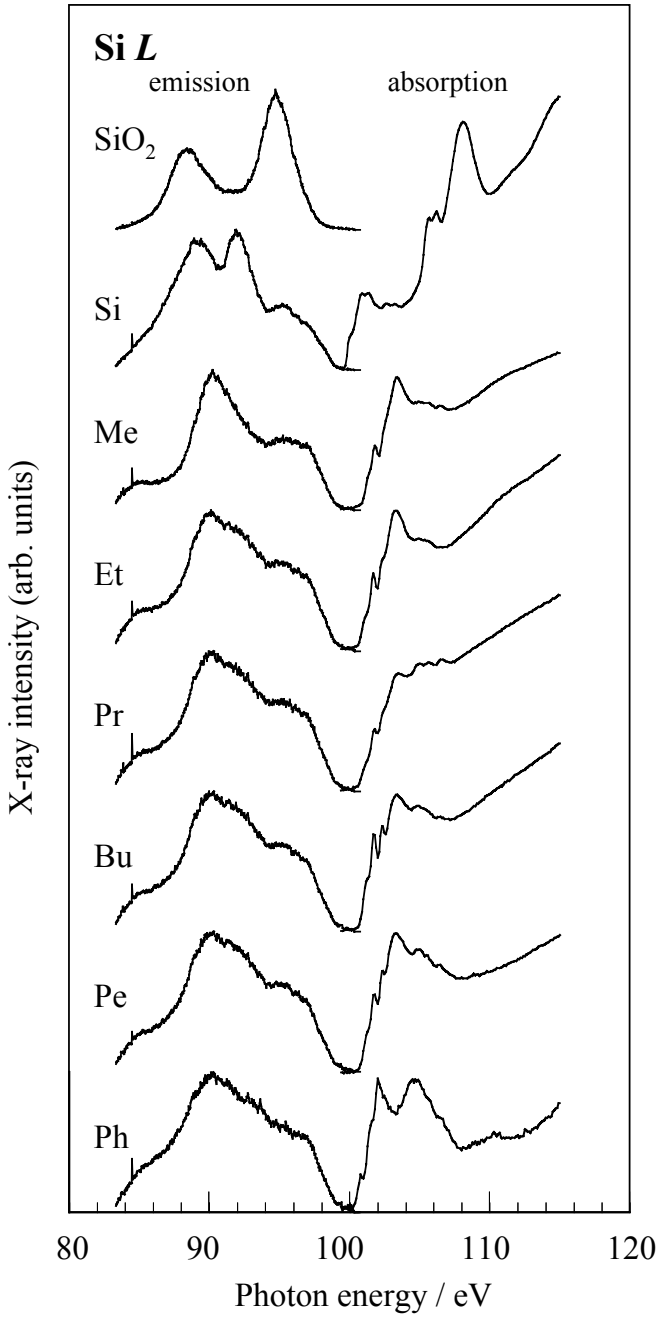


**Figure 1** Soft x-ray emission and TEY x-ray absorption spectra in the Si *L* region of the polysilanes, $(SiR_2)n$, and Si and $SiO_2$ reference compounds. Substituents in the polysilanes, R, are denoted by Me ($CH_3$), Et ($C_2H_5$), Pr (n-$C_3H_7$), Bu (n-$C_4H_9$), Pe (n-$C_5H_{11}$), and Ph ($C_6H_5$).

# Soft X-ray emission spectroscopy of the liquid-solid interface between water and a $Cu(In,Ga)(S,Se)_2$ thin film solar cell absorber

C. Heske[1], U. Groh[1], O. Fuchs[1], L. Weinhardt[1], E. Umbach[1], Ch.-H. Fischer[2], Th. Schedel-Niedrig[2], M.Ch. Lux-Steiner[2], S. Zweigart[3], F. Karg[3], J.D. Denlinger[4], B. Rude[4], C. Andrus[5], and F. Powell[5]

[1]Experimentelle Physik II, Universität Würzburg, Am Hubland, D-97074 Würzburg, Germany
[2]Hahn-Meitner-Institut, Glienicker Str. 100, D-14109 Berlin, Germany
[3]Siemens & Shell Solar GmbH, SSSG T, Otto-Hahn-Ring 6, D-81739 München, Germany
[4]Advanced Light Source, 1 Cyclotron Rd., Berkeley, CA 94720
[5]Luxel Corp., 515 Tucker Ave., Friday Harbor, WA 98250

## INTRODUCTION

The development of experimental methods to probe the properties of liquid-solid interfaces is one of the fundamental issues for understanding a multitude of natural and technological processes involving liquids. Up to date, however, very few experiments have been performed to learn about the electronic structure, particularly if an atom-specific point of view is desired. While in surface science such information can easily be derived from photoelectron spectroscopy, this approach is not viable for the study of liquid-solid interfaces due to the limited information depth of PES. Thus, the necessity to probe "through" a liquid (or solid) layer calls for photon-in-photon-out experiments. The soft X-ray regime, however, which is the most suitable to study core and valence states of light elements, has not yet been explored, mostly due to the high attenuation of soft X-rays in matter. In this report we demonstrate that soft X-ray emission spectroscopy (XES) can be used to investigate the chemical and electronic properties of particular atoms at liquid-solid interfaces, in this case the water–$Cu(In,Ga)(S,Se)_2$ interface. Furthermore, we will show that, with XES, it is possible to monitor interfacial chemical reactions with high spectral resolution *in-situ*.

## MATERIAL SYSTEM

$Cu(In,Ga)(S,Se)_2$ (CISSe) is widely used as an absorber material in thin film solar cells, and conversion efficiencies up to 18.8 % have been achieved [1]. Apart from being a model system for the present investigation, the water–CISSe interface is of large importance for two reasons. First, a complete CISSe solar cell is comprised of several thin film layers, including the CISSe absorber layer and a thin (approx. 20 nm) CdS buffer deposited in a chemical *bath* deposition process. The CdS/CISSe interface plays one of the central roles in understanding the electronic structure of the devices. Hence, the possibility to study liquid-solid interfaces *in-situ* allows the monitoring of the substrate, the growing film, and the interface formation process from a spectroscopic point of view. Secondly, one of the main issues on the way to a complete industrial product is the control of humidity impact on the electronic cell properties. The investigation of the relevant water–solid interfaces is expected to shed light on the chemical and electronic changes induced by the humidity on an accelerated time scale.

## EXPERIMENTAL

High-resolution soft X-ray emission spectroscopy was performed at beamline 8.0 utilizing the SXF endstation. Beamline 8.0 allows experiments with an excitation photon flux of about 4 x

$10^{15}$ photons/sec near the sulfur $L_{2,3}$ edge. Thin films of CISSe were prepared in a rapid thermal process of elemental precursor layers on Mo-coated soda-lime glass in a sulfur-containing environment. The experiments were performed in ultra-high vacuum (UHV) utilizing suitably designed stainless steel liquid cells, which were glued to the CISSe sample surface with a UHV-compatible epoxy. In the design of the liquid cells, a channel of 1.3 μm of liquid water was created between the CISSe surface and a 1 μm-thick polyimide (PI) window. After hardening of the epoxy (approx. 24 hours), the complete assembly was transferred into UHV for experiments. Reference experiments were also conducted on "bare" CISSe films as well as on PI/Vacuum/CISSe sandwich structures.

**RESULTS**

Fig. 1 presents a set of sulfur $L_{2,3}$ emission spectra obtained by excitation well above the absorption edge ($h\nu$ = 200 eV). The bottom spectrum was obtained from the "bare" CISSe film surface, i.e., taken directly from the solar cell production line. Peak (1) stems from the emission of sulfur atoms bound in a sulfide environment, and is due to photons emitted by filling S 2p core holes with S 3s electrons [2]. Peaks (2) are associated with the same electronic transition, but for sulfur atoms bound to oxygen. In the present case, the absence of an additional peak around 161.1 eV indicates that at most two oxygen atoms are bound to each probed sulfur atom. The broad peak (3) is due to Cu 3d states in the upper valence band of CISSe and, because of the local nature of the excitation, is indicative of sulfur-copper bonds. In short, the spectral features of the sulfur XES spectrum give a wealth of detailed information about the local chemical bond of the sulfur atoms, which can now be used to monitor interfacial processes.

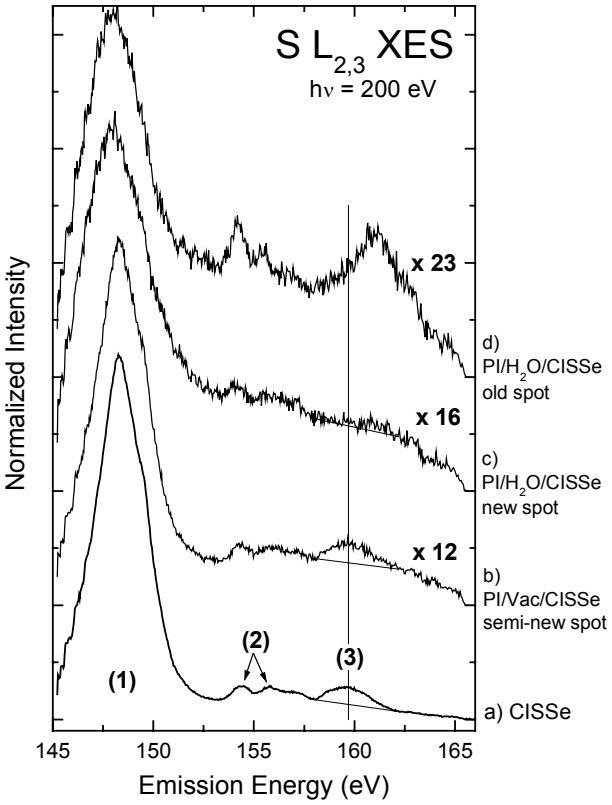


Figure 1. S $L_{2,3}$ X-ray emission spectra of a $Cu(In,Ga)(S,Se)_2$ (CISSe) thin film solar cell absorber film (a) taken from the production process, (b) seen through a 1 μm polyimide (PI) window, and under an additional 1.3 μm water layer (c: new sample spot, d: old sample spot). Samples "under water" show a reduced intensity of the S-Cu-bond and, after X-ray exposure, a sulfate formation.

As indicated in Fig. 1 by the magnification factors at the right hand side, the observed signal intensity is reduced by both the PI window as well as the liquid water layer. These attenuation factors indicate the necessity to use high-flux excitation from a third generation synchrotron source. Note that the PI window is damaged by extended exposure to X-rays. Thus, the transmission decreases as a function of exposure within the probed area, and hence the "age" of the spot also factors into the signal attenuation. The "age" of the different spectra is given on the right-hand side of Fig. 1. A closer inspection of spectra a) and b) reveals that no changes are observed for the PI/Vacuum/CISSe sample (as expected). However, we find a reduction of the intensity associated with sulfur-copper

bonds (peak 3) due to the 24 hour storage "under water" (spectrum c). An even more pronounced spectral change is observed after exposure to X-rays (30 min, spectrum d). Based on the strong S 3d-related emission at 161.1 eV, this spectral change is interpreted as a sulfate formation at the water/CISSe interface.

Apart from a detailed look at the chemical and electronic environment of sulfur atoms, also the Na $K_\alpha$ emission line proves to be a helpful tool to monitor the interfacial reaction at the water/CISSe interface. Na-assisted growth has been shown to substantially improve the efficiency of the CISSe solar cells. Until today, the impact of the Na has not been fully clarified, mostly because several enhancing mechanisms have been proposed and because, due to the complexity of the system, these different mechanisms are not easily separable. An established model by Kronik et al. [3] suggests an interaction of sodium and oxygen at the CISe surface. Nevertheless, apart from a co-adsorption study in ultra-high vacuum [4], no direct experimental evidence of a chemical interaction between sodium and oxygen has yet been reported. Such a direct correlation can now be derived from a simultaneous recording of Cu $L_\alpha$ and Na $K_\alpha$ XES spectra. As expected, we find a small Na signal on the CISSe surface, which does not change in intensity for the PI/Vacuum/CISSe sample. Also, the 24-hour storage under water only leads to a small increase. In contrast, when exposing the sample to the soft X-ray beam, we find a dramatic increase of the Na content at the interface in the course of time, in parallel with the above-discussed surface oxidation (sulfate formation). Apparently, the possibility to form a sulfate species attracts Na atoms from the CISSe film towards the surface. Here, the original driving force could be the X-ray-induced creation of $O^{2-}$ and/or $OH^-$ ions, which then react with the CISSe surface and alter the free energy, such that Na atoms diffuse to the water/CISSe interface. Also the opposite process, namely that the X-ray excitation attracts Na atoms to the surface (e.g., by sample heating), which then act as a catalyst for the surface oxidation, appears possible. Future studies utilizing mini-cells with integrated thermocouples will have to clarify which one of the two scenarios holds true.

In summary, we have presented an experimental investigation of a sulfate formation at the water/CISSe interface. The findings demonstrate that there is a direct correlation between oxidation and sodium enrichment at the interface. The demonstrated general approach of utilizing X-ray emission spectroscopy to study chemical reactions in-situ can be extended to many other liquid-solid interfaces and also lends itself to the study of liquids and solutions as well.

## REFERENCES


1. M. A. Green, K. Emery, D. L. King, S. Igari, and W. Warta, Solar Cell Efficiency Tables (Version 17); Progr. Photovolt. Res. Appl. **9**, 49 (2001).
2. C. Heske, U. Groh, O. Fuchs, E. Umbach, N. Franco, C. Bostedt, L.J. Terminello, R.C.C. Perera, K.H. Hallmeier, A. Preobrajenski, R. Szargan, S. Zweigart, W. Riedl, and F. Karg, phys.stat.sol. (a) **187**, 13 (2001).
3. L. Kronik, D. Cahen, and H.W. Schock, Adv. Materials **10**, 31 (1998).
4. C. Heske, G. Richter, Zhonghui Chen, R. Fink, E. Umbach, W. Riedl, and F. Karg, J. Appl. Phys. **82**, 2411 (1997).



This work was supported by the german ministries BMBF (FKZ 01SF007) and BMWI (FKZ 0329889, FKZ 0329218C), as well as the DFG through SFB 410, TP B3.



Principal investigator: Clemens Heske, Eberhard Umbach, Experimentelle Physik II, University of Würzburg, Germany. Email: heske@physik.uni-wuerzburg.de. Telephone: ++49-931-888-5127.

# Soft X-ray Probe of Bulk Bandgaps in Divalent Hexaborides

J. D. Denlinger[1], J. W. Allen[2] and Z. Fisk[3]
[1]Advanced Light Source, Lawrence Berkeley National Lab, Berkeley, California 94720, USA
[2]Department of Physics, University of Michigan, Ann Arbor, Michigan 48109, USA
[3]NHMFL, Florida State University, Tallahassee, Florida 32306, USA

## INTRODUCTION

The discovery of weak itinerant ferromagnetism in certain divalent hexaborides [1] provides strong motivation to determine the underlying electronic structure giving rise to the metallic carriers. One possibility predicted by LDA band calculations [2] and supported by the interpretation given to magneto-oscillatory studies [3] is a semi-metallic band overlap at the X-point of the cubic Brillouin zone, the absence of which would render stoichiometric material to be insulating. Several theoretical discussions of excitonic insulator origins of the novel ferromagnetism [4] presume the existence of such an overlap. However, a recent quasiparticle band calculation [5] that includes a GW self energy correction, instead predicts $CaB_6$ to be a semiconductor with a 0.8 eV band gap at the X-point.

Such an X-point band gap (>1 eV) is observed in angle resolved photoemission (ARPES) of $CaB_6$, $SrB_6$ and $EuB_6$ [6] providing strong experimental proof of this new semiconducting model for the divalent hexaborides. Reported here are bulk sensitive soft x-ray emission and absorption data (SXE and XAS, respectively) that provide additional proof of the existence of this semiconducting bandgap complementary to the k-dependent band structure information revealed by ARPES. Also consistent with ARPES, the SXE/XAS measurements imply that the chemical potential is at the bottom of the conduction band indicating the presence of excess electrons arising from nonstoichiometric defects. This situation would be consistent with a picture in which the novel magnetic moments in divalent hexaborides are carried by boron vacancies [7]

## EXPERIMENT

Single crystal hexaboride samples were grown from an aluminum flux using powders prepared by boro-thermally reducing cation oxides. Soft x-ray emission and absorption experiments were performed at the ALS Beamline 8.0.1 using the Tennessee/Tulane grating spectrometer. The experimental emission and absorption spectral resolutions were ≈0.35 eV and ≈0.1 eV, respectively. SXE at and above the B K-edge threshold, is used as a probe of the occupied boron 2p partial density of states. X-ray absorption, a probe of the unoccupied states, was measured both with total electron yield (TEY) as a function of photon energy and also with partial fluorescence yield (PFY) with the detection window covering the entire valence band emission. Differences between TEY and PFY signals arise from differing attenuation lengths and the experimental geometry which was set to 60° incidence excitation and 30° grazing emission relative to the sample surface. Absolute PFY energies were calibrated to published TEY spectra of the hexaborides [8] and SXE spectra were calibrated to the excitation energy using an elastic scattering peak in the emission spectra.

## RESULTS

Fig. 1 shows a representative data set of soft x-ray emission and absorption at the boron K-edge for the divalent hexaborides. Data very similar to that shown here for $CaB_6$ was also obtained for $SrB_6$, $EuB_6$, and $YbB_6$. Fig. 1(a) compares the two methods of measuring x-ray absorption, TEY and PFY. TEY, a measurement of the sample current, exhibits a sharp peak at ≈194 eV corresponding to a well-known B 1s→2p $\pi^*$ transition [8] which in part arises from surface layer

oxidation of the air-cleaved sample. Also the absolute TEY signal exhibits a high background (removed in Fig. 1(a)) with declining slope due to the presence of lower energy absorption edges. In contrast, the PFY signal, a measure of valence emission intensities integrated over the energy window shown in Fig. 1(b), does not exhibit the sharp TEY absorption peak due to a greater bulk emission sensitivity. Also the valence band PFY signal inherently has zero pre-threshold intensity and hence is preferred over TEY for careful measurement of the threshold region. The PFY spectrum for $CaB_6$ shows a weak step-like threshold onset at 188.0 eV (highlighted in the logarithmic scale inset to Fig. 1(a)). We interpret the half-step intensity of this threshold onset in the PFY spectrum as the energy position of the chemical potential in the conduction band.

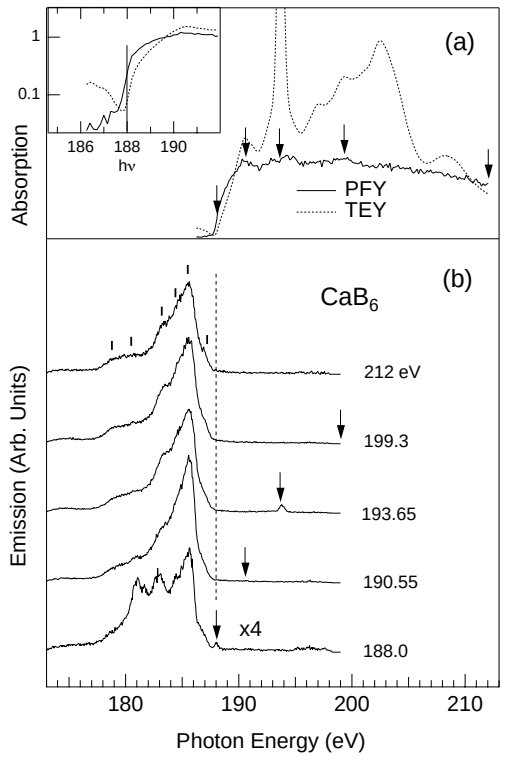


Figure 1. Soft x-ray absorption (TEY, PFY) and emission (SXE) boron K-edge data set for $CaB_6$. Arrows and values indicate the excitation energies. The logarithmic intensity scale of the inset highlights the step intensity onset of the PFY signal with comparison to the TEY threshold.

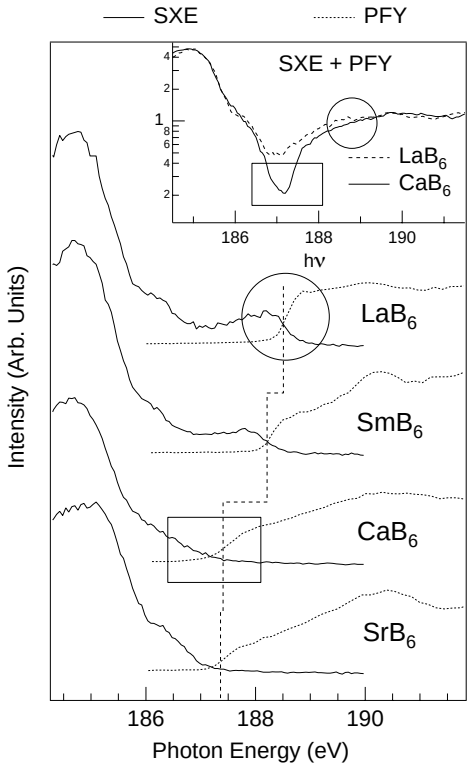


Figure 2. B K-edge SXE and PFY spectra for various hexaborides. The dashed line indicates the half-height energy position of the PFY threshold. Inset: Logarithmic intensity scale comparison of the total DOS, i.e. sum of emission and absorption, for $CaB_6$ and $LaB_6$ with the valence band edge of the DOS aligned.

Valence band emission spectra, shown in Fig. 1(b) were acquired at selected photon energies indicated by arrows in Fig. 1. An elastic peak present in the emission spectra is resonantly enhanced at the B 1s→2p absorption peak and is used for calibration of the SXE energy scale to that of TEY and PFY spectra. Excitation at the selected peaks in the PFY/TEY spectra and far above threshold show similar valence band emission profiles with small variations in the relative intensities of at least six discernable peaks and shoulders. Threshold excitation on the other hand produces much larger variation in the relative intensities (and energies) of the different valence emission peaks (discussed in the next section). The elastic peak is also observed to be enhanced at threshold, thus providing a distinct marker for the location of $E_F$. The non-threshold SXE spectra, on the other hand, exhibit a strong non-metallic decay of intensity approaching $E_F$ and no distinct onset, in contrast to the PFY spectrum.

Fig. 2 shows a comparison of SXE/PFY spectra for two divalent hexaborides $SrB_6$ and $CaB_6$, and for mixed-valent $SmB_6$ and trivalent $LaB_6$, which contain 0.6 and 1 conduction electrons/formula unit, respectively. The PFY spectra have been normalized to have the same intensity far above threshold, while the SXE spectra have been normalized to have the same maximum amplitude. The overall PFY intensities were then scaled so that the SXE and PFY intensities for $LaB_6$ match at threshold. Within experimental resolution, a common SXE/PFY threshold occurs for $SmB_6$ and for $LaB_6$, as expected for simple metals. The increases in photon energy and intensity of the thresholds of $SmB_6$ and $LaB_6$ relative to the divalent systems and to each other are consistent with their differing conduction band fillings. In great contrast, for the divalent hexaborides, the strong decay of SXE intensity to its threshold and the weak PFY intensity at its threshold preclude the two spectra having a common onset.

The inset to Fig. 2 presents a more detailed comparison of $CaB_6$ and $LaB_6$ in which the SXE and PFY spectra have been summed and can be discussed as the boron partial DOS. In addition the $LaB_6$ spectrum has been shifted +0.3 eV, after summing, to align its valence band (185-186.5 eV) to that of $CaB_6$. The key motivation for this comparison is that apart from band filling, LDA calculations predict nearly identical total DOS for the divalent and trivalent systems. For $LaB_6$ the emission and absorption spectra meet smoothly so that the crossover place entirely disappears upon summing (see circles), whereas for $CaB_6$ a distinct dip remains over $\approx$1 eV around 187 eV (see rectangles). This distinct discrepancy immediately tells us that the band structures in the vicinity of the boron valence band maximum for $CaB_6$ and $LaB_6$ are different. The interpretation of this bulk-sensitive measurement as a band gap in the divalent hexaborides is strongly supported by the k-dependent view from ARPES which shows a >1 eV band gap in $CaB_6$ at the X-point in contrast to a 0.2 eV *overlap* of the same two bands in $LaB_6$ [9]. Additional analyses of the overall boron DOS bandwidth and energy centroid, and of threshold-excited SXE spectra provide complementary evidence of the bulk divalent band gap [10].

## REFERENCES


1. D. P. Young *et al*, Nature **397**, 412 (1999); P. Vonlanthen *et al*, Phys. Rev. B **62**, 10076 (2000); H. R. Ott *et al*, Physica B **281-2**, 423 (2000); T. Terashima *et al*, J. Phys. Soc. Jpn. **69**, 2423 (2000).
2. A. Hasegawa and A. Yanase, J. Phys. C, Solid State Phys. **12**, 5431 (1979); S. Massidda, A. Continenza, T. M. D. Pascale, and R. Monnier, Z. Phys. B **102**, 83 (1997).
3. R. G. Goodrich *et al*., Phys. Rev. B **58**, 14896 (1998); M. C. Aronson *et al*., Phys. Rev. B **59**, 4720 (1999).
4. M. E. Zhitomirsky, T. M. Rice, and V. I. Anisimov, Nature **402**, 251(1999); L. Balents and C. M. Varma, Phys. Rev. Lett. **84**, 1264 (2000); V. Barzykin and L. P. Gor'kov, Phys. Rev. Lett. **84**, 2207 (2000).
5. H. J. Tromp *et al*., Phys. Rev. Lett. **87**, 016401 (2001).
6. J. D. Denlinger *et al*., cond-mat/0107429; and ALS Compendium, 2001.
7. R. Monnier and B. Delley, Phys. Rev. Lett. **87**, 157204 (2001).
8. J. J. Jia *et al*., J. Electron Spectrosc. Related Phenom. **80**, 509 (1996).
9. S.-K. Mo *et al*., cond-mat/0107203.
10. J. D. Denlinger, G.-H. Gweon, J. W. Allen, A. D. Bianchi and Z. Fisk, cond-mat/0107426; Surf. Rev. and Lett., in press.



This work was supported at U. of Michigan by the U.S. Dept. of Energy (DoE) under contract No. DE-FG02-90ER45416 and by the U.S. NSF under grant No. DMR-99-71611.



Principal investigator: Jonathan Denlinger, Advanced Light Source, LBNL. Email: JDDenlinger@lbl.gov. Telephone: 510-486-5648.

# Soft X-Ray Spectroscopy of Noble Gas Atoms Doped in Solid Matrices

**Y. Muramatsu[1], and R. C. C. Perera[2]**

[1]*Japan Atomic Energy Research Institute, Sayo-gun, Hyogo 679-5148, Japan*

[2]*CXRO, Lawrence Berkeley National Laboratory, Berkeley, California 94720, USA*

We have measured the soft x-ray emission and absorption spectra of noble-gas atoms doped in carbon, silicon and metal substrates, to investigate their chemical states in solid matrices. Argon or neon ion beams were directed into the solid matrices of highly oriented pyrolytic graphite (HOPG), Si(111), $SiO_2$, Ti, Cr, Ni and Cu with an acceleration voltage of 5 kV. Soft x-ray emission and absorption spectra in the Ar *L* and Ne *K* regions of Ar- and Ne-doped samples were measured using a grating x-ray spectrometer installed in the undulator beamline, BL-8.0.1. Figure 1 shows the Ar *L* x-ray emission spectra of Ar-doped Si(111) measured with excitation energies of (a) 399.6 eV and (b) 256.6 eV. The subtracted spectrum of (a) – (b), clearly indicates that peak structures are observed on the higher-energy sides of both $L\alpha$ and $L\beta$ peaks arising from 399.6-eV excitation. These peak structures may be due to multiple ionizations. Figure 2 shows the Ar *L* x-ray emission spectra of Ar-doped Si(111), HOPG, Ti and Cu measured with 256.6-eV excitation. Peak widths of $L\alpha$ and $L\beta$ peaks in the Ar *L* x-ray emission spectra from Ti and Cu matrices are broader than that of the Si(111) and HOPG matrices. A similar peak broadness was also observed in the Ne *K* x-ray emission spectra of Ne-doped metal matrices. Such peak broadness may be explained by the formation of noble gas bubbles in the metals. To further explain peak broadness in the spectra, molecular orbital calculations are currently in progress. We thank Dr. J. Denlinger of the Lawrence Berkeley National Laboratory for his help and support in performing x-ray emission measurements. This work has been supported by the Hyogo Science and Technology Association and the US Department of Energy under contract No. DE-AC03-76SF00098. Principal Investigator: Yasuji Muramatsu, Japan Atomic Energy Research Institute. Email: murama@spring8.or.jp. Telephone: +81-791-58-2601.

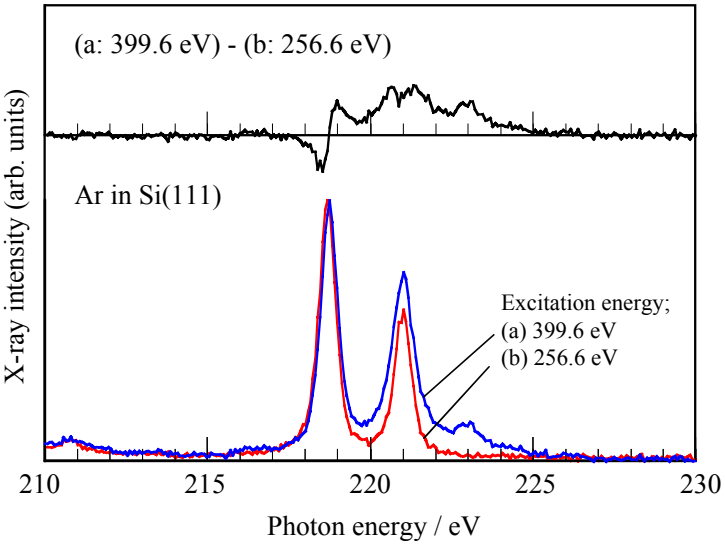


**Figure 1** Ar *L* x-ray emission spectra of Ar-doped Si(111) with excitation energies of (a) 399.6 eV and (b) 256.6 eV. Upper panel shows the subtracted spectrum, (a) – (b).

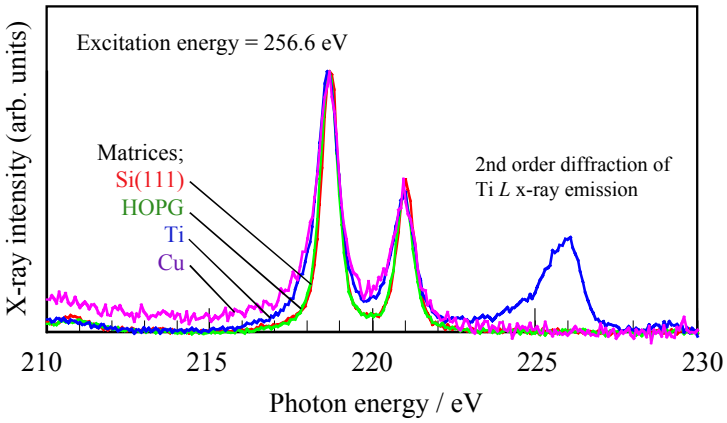


**Figure 2** Ar *L* x-ray emission spectra of Ar-doped Si(111), HOPG, Ti, and Cu matrices. Excitation energy was tuned to 256.6 eV.

# Spectroscopic observation of polaron-lattice band structure in the conducting polymer polyaniline

E.Z. Kurmaev[1], M.I. Katsnelson[1], A. Moewes[2], M. Magnuson[3], J.-H. Guo[3], S.M. Butorin[3], J. Nordgren[3], D.L. Ederer[4], and M. Iwami[5]

[1]Institute of Metal Physics, Russian Academy of Sciences-Ural Division, 620219 Yekaterinburg GSP-170, Russia
[2]University of Saskatchewan, Department of Physics and Engineering Physics, Saskatoon, SK S7N 5E2, Canada
[3]Department of Physics, Uppsala University, Uppsala, P.O. Box 530, S-75 121, Sweden
[4]Department of Physics, Tulane University, New Orleans, LA 70118, USA
[5]Research Laboratory for Surface Science, Okayama University, Okayama 700-8530, Japan

Interest in polyanilines has been reinforced by the discovery of their high electrical conductivity observed in doped phases, giving rise to a new class of conducting polymers. Polyaniline can be prepared in three major forms that differ in the degree of oxidation *y* (the ratio of amine nitrogens over the total number of nitrogen atoms). For the fully reduced leucoemeraldine base (LEB) *y* is one, the half-oxidized emeraldine base (EB) *y* is 0.5 and for fully oxidized pernigraniline base (PNB) *y* is 0. Polyaniline is an insulator in each of these forms with a band gap of 3.6 eV for LEB and EB and about 1.4 eV for PNB. The polymers can also exist in the corresponding protonated (salt) forms but only emeraldine salt (ES) is highly electrically conductive in this case. The largest conductivity reported to date is about 400 S/cm [1], which is 14 orders of magnitude higher than for the insulating emeraldine base form. Protonation does not change the electronic concentration and a local distortion of the chemical bonds is giving rise to conductivity of the polymer. These distortions are commonly referred to as either a polaron (storing the extra positive charge when only one nitrogen is protonated) or a bipolaron (in the case that both imine nitrogens are protonated). In order to explain the conductive state of ES two models have been proposed. A regular distribution of polarons leaves the electronic band half-filled or the random bipolaron structure leads to the formation of extended electronic states at the Fermi energy. There is no direct spectroscopic evidence to date regarding the electronic structure of ES, which is essential for selecting the adequate picture.

We have studied the differences in the electronic structure of protonated and undoped polyemeraldine by means of soft x-ray emission spectroscopy (XES). Our findings support the application of the polaronic-metal model for highly conducting polymers.

The experiments were carried out at Beamlines 7.0 and 8.0.1 at the Advanced Light Source at the Lawrence Berkeley National Laboratory employing the Uppsala University [3] and University of Tennessee at Knoxville [4] endstations. Photons with energies well above the carbon K-edge (300 eV) and well above the nitrogen K-edge (412-430 eV) were delivered to the sample. The X-ray fluorescence spectrometer provides an energy resolution of 0.30 eV and 0.65 eV for the carbon and nitrogen measurements, respectively. For our measurements we have chosen the basic form of undoped and protonated polyemeraldine. The doped samples were prepared by protonation with 60% camphorsulphonic acid (CSA). The protonation with $H^+$ adds holes to the imine groups around the quinoid ring.

Figure 1 shows carbon Kα emission spectra (2p→1s transition) of undoped and protonated emeraldine converted to the binding energy scale [5]. The spectra are normalized to the same peak height in the intensity maximum. The intensity of the C Kα emission in the vicinity of the Fermi level $E_F$ is clearly increased for the protonated emeraldine compared to the undoped sample. This finite density of states at the Fermi level evidences the metallicity of the doped phase. The same tendency of higher spectral intensity in the vicinity of the Fermi level for protonated polyemeraldine with respect to the undoped phase is observed in N Kα XES though these measurements have been performed with less energy resolution (due to the higher emission energy) and lower count rate than the carbon data, the latter being due to the smaller content of nitrogen atoms in polyaniline. Protonating increases the finite density of states near the Fermi level and the origin of the increase is the formation of the polaron band. In the case of the bipolaron band structure no finite density of states is expected near $E_F$. Recently, an extremely small finite density of states for protonated emeraldine has been observed in photoemission measurements [6]. The authors do not indicate the level of protonation and in a protonation of too low concentration could lead to such effect.

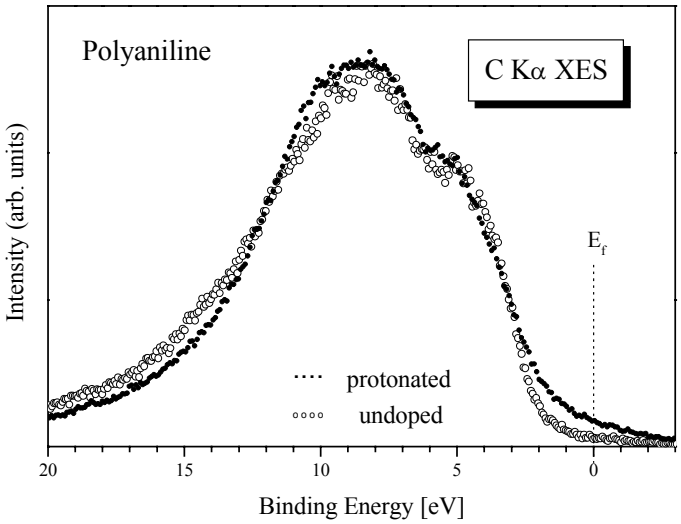


**Figure 1 Carbon Kα XES of undoped and protonated polyemeraldine displayed on the binding energy scale.**

To summarize, we have observed a finite density of states in protonated emeraldine in the vicinity of the Fermi level using soft X-ray emission measurements. This direct observation is in a full agreement with band structure calculations for the polaron lattice and therefore supports a polaronic-metal model for conducting polymers.

## REFERENCES


1. M. Reghu, Y. Cao, D. Moses, and A.J. Heeger, Phys. Rev. B **47**, 1758 (1993).
2. S. Stafström, J.L. Bredas, A.J. Epstein, H.S. Woo, D.B. Tanner, W.S. Huang, and A.G. MacDiarmid, Phys. Rev. Lett. **59**, 1464 (1987).
3. J. Nordgren, G. Bray, S. Gramm, R. Nyholm, J.-E. Rubensson, and N. Wassdahl, Rev. Sci. Instrum. **60**, 1690 (1989).
4. J.J. Jia, T.A. Callcott, J. Yurkas, A. W.Ellis, F.J. Himpsel , M.G. Samant, J. Stöhr, D.L. Ederer, J.A. Carlisle, E.A. Hudson, L.J. Terminello, D.K. Shuh, and R.C.C. Perera, Rev. Sci. Instrum. 66 (1995) 1394.
5. E.Z. Kurmaev, M.I. Katsnelson, A. Moewes, M. Magnuson, J.-H. Guo, S.M. Butorin, J. Nordgren, D.L. Ederer and M. Iwami, J. Phys: Condens. Matter 13 (2001) 3907.
6. H.Sakamoto, M. Itow, N. Kachi, T. Kawahara, K. Mizoguchi, H. Ishii, T. Miyahara, K. Yoshioka, S. Masubuchi, S. Kazama, T. Matsushita, A. Sekiyama and S. Suga, J. Electr. Spectr. Relat. Phenom. **92**, 159 (1998).

This work was supported by the Russian State Program on Superconductivity, the Russian Science Foundation for Fundamental Research (Projects 00-15-96575 and 99-03-32503), the Swedish National Science Research Council (NFR), the Goran Gustavsson Foundation for Research in Natural Sciences and Medicine, NSF Grants DMR-901 7997 and DMR-9420425, the DOE EPSCOR and the Louisiana Education Quality Special Fund (DOE-LEQSF (1993-95-03)). The ALS, Lawrence Berkeley National Laboratory is supported by the U.S. Department of Energy under Contract No. DE-AC03-76SF 00098.

Principal investigator: Ernst Kurmaev, Institute of Metal Physics, Russian Academy of Sciences-Ural Division, 620219 Yekaterinburg GSP-170, Russia. Email: kurmaev@ifmlrs.uran.ru. Telephone: +7-3432-744183.

# X-ray Absorption and Emission Spectroscopy at the Nitrogen K-Edge in Dilute $GaAs_{1-x}N_x$

M. Adamcyk[1], A. Ballestad[1], A. Moewes[2], E. Nodwell[1], T. Tiedje[1], S. Tixier[1]

[1]Advanced Materials and Process Engineering Laboratory,
Department of Physics and Astronomy, University of British Columbia,
Vancouver, B.C. V6T 1Z4, Canada
[2]Department of Physics and Engineering Physics,
University of Saskatchewan, Saskatoon, Sask. S7N 5E2, Canada

$GaAs_{1-x}N_x$ and $In_yGa_{1-y}As_{1-x}N_x$ alloys containing a few percent nitrogen have attracted attention in recent years due to their potential use in 1.3 micron emitters on GaAs substrates. The incorporation of nitrogen at low concentrations in these III/V materials results in a large band gap bowing parameter and a sharp decrease of the band gap with increasing nitrogen [1]. A wide range of lattice constants can be obtained by varying the N content. For example $In_{0.3}Ga_{0.7}As_{0.98}N_{0.02}$ quantum wells are pseudomorphic to GaAs and emit at 1.3 micron. In the present work, we have studied the density of states in the valence and conduction bands of dilute $GaAs_{1-x}N_x$ using soft x-ray emission and absorption at the nitrogen K-edge. The emission spectrum is compared to a tight binding band structure calculation for the electronic structure of $GaAs_{1-x}N_x$.

The $GaAs_{1-x}N_x$ samples were grown by Molecular Beam Epitaxy (MBE) at a substrate temperature in the 500-600°C range using a RF plasma source for the dissociation of molecular nitrogen. The nitrogen content ranged from 0.02% to 2%. Nitrogen concentrations were obtained using X-ray diffraction and SIMS. The samples were cleaved in two pieces; one piece was annealed at 850° for 1 min. Nitrogen K-edge absorption and emission spectra were measured at beamline 8.0.1. The absorption spectra were obtained in the fluorescence yield mode. The emission spectra were measured using a 600 lines/mm diffraction grating providing an energy resolution of 0.8eV (FWHM) as determined from the scattered primary beam.

Emission and absorption spectra at the nitrogen K-edge are shown in Fig. 1 for a $GaAs_{1-x}N_x$ sample with a 2% N content, together with calculated nitrogen 2p density of states. The emission spectrum (lower spectrum in the figure) was excited at a photon energy of 402.1 eV corresponding to the peak absorption in the upper spectrum in Fig. 1. The small peak at 402.1 eV in the emission spectrum is the elastically scattered excitation radiation which is not completely rejected by the soft x-ray spectrometer. This peak serves as an energy calibration for the emission spectrometer. The emission and absorption spectra show a band gap of about 1 eV in agreement with optical measurements.

Absorption at the nitrogen K-edge probes the unoccupied density of states in the conduction band with p-symmetry at the nitrogen sites. The spectrum shows a strong

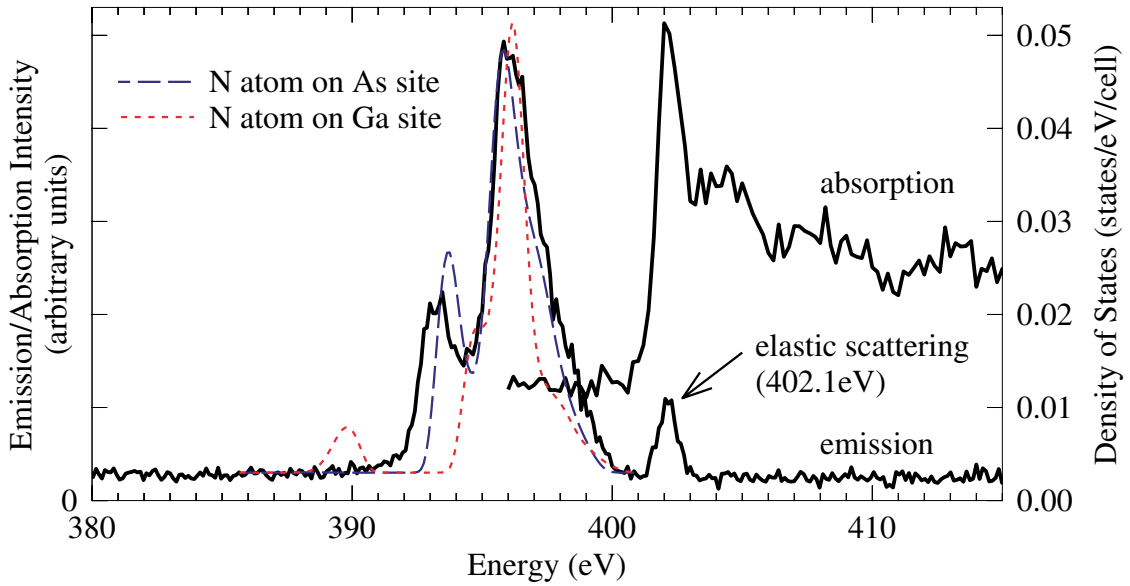


Figure 1: Emission and absorption curves for $GaAs_{1-x}N_x$ with 2% N and calculated local DOS on the Nitrogen 2P state. Orthogonal (random) noise of 0.003 states/eV/cell has been added to the calculated spectra. The origin of the energy scale in the calculations is arbitrary.

excitonic type peak just above the bottom of the conduction band which we attribute to the well known nitrogen resonance in the conduction band. The shape of the absorption spectrum was independent of the nitrogen content.

The emission spectrum in Fig. 1 at the nitrogen K-edge is due to transitions from valence band states on nitrogen sites with p-symmetry to the nitrogen 1s core hole. The spectrum has two peaks located at 393.2 eV and 396.1 eV. No changes in the shape of the spectrum were observed as a function of nitrogen content in the 0.02% - 2% range. Similarly no changes were observed with annealing at 850°C. Annealing is expected to substantially reduce the number of nitrogen interstitials. The absence of a change in the emission spectrum with annealing suggests that the fraction of interstitial nitrogen is low. Emission spectra were measured as a function of excitation energy through the absorption edge and no resonant effects were observed in the soft x-ray emission.

Emission spectra were calculated in a tight binding model in which a single nitrogen atom is located on a Ga or an As site in a 2x2x2 supercell containing 64 atoms. The model spectra are the p-projected densities of states on the nitrogen atom. The energies for the atomic orbitals and interatomic overlap matrix elements for the Ga and As 4s and 4p orbitals were taken from Harrison [2]. The energy level for the nitrogen 2p orbital was taken to be an adjustable parameter and was used to fit the experimental spectrum. The spectra were convolved with a 0.8 eV Gaussian window in accordance with the experimental resolution. The lifetime broadening of the emission band is ignored. A best fit was obtained with the nitrogen 2p orbital energy $\epsilon_p$ equal to -8.5 eV which compares with the -11.47 eV recommended by Harrison. For $\epsilon_p <$ -9.5 eV the nitrogen 2p orbital forms a bound state in the valence band and the shape of the emission spectrum changes. The good agreement with the experimental data in Fig. 1 suggests that there is

no nitrogen p-like bound state in the valence band. When the nitrogen is located on a Ga site a deep bound state is obtained in the model as indicated by the peak in the dotted curve in Fig. 1 at 389.8 eV. The good fit with the calculated spectrum for nitrogen on the As site suggests that most of the nitrogen is on the group V site, as expected. No emission was detected from the lower part of the GaAs valence band, which is dominated by As 4s, in good agreement with the model.

**Acknowledgments**

We thank Tony Van Buuren for his help and the Natural Sciences and Engineering Research Council of Canada (NSERC) for financial support.

# References

[1] S.-H. Wei and A. Zunger, Phys. Rev. Lett. **76**, 664 (1996).

[2] W.A. Harrison, *Electronic Structure and the Properties of Solids* (Dover, New York, 1989).

Principal investigator: E. Nodwell, Advanced Materials and Process Engineering Laboratory, University of British Columbia, Vancouver, B.C. V6T 1Z4, Canada. Email: nodwell@physics.ubc.ca. Telephone: 604-822-5425.

# X-ray emission spectra and electronic structure of charge transfer salts

E. Z. Kurmaev[1], A. Moewes[2], U. Schwingenschlögl[3], R. Claessen[3], M. I. Katsnelson[1], H. Kobayashi[4], S. Kagoshima[5], Y. Misaki[6], D.L. Ederer[7], K. Endo[8], and M. Yanagihara[9]

[1]Institute of Metal Physics, Russian Academy of Sciences-Ural Division, 620219 Yekaterinburg GSP-170, Russia
[2] Department of Physics and Engineering Physics, University of Saskatchewan, 116 Science Place, Saskatoon, Saskatchewan S7N 5E2, Canada
[3] Experimentalphysik II, Universität Augsburg, D-86135 Augsburg, Germany
[4]Institute for Molecular Science, Okazaki 444, Japan
[5] Department of Basic Science, University of Tokyo, Komaba 3-8-1, Meguro, Tokyo 153-8902, Japan
[6]Department of Molecular Engineering, Graduate School of Engineering, Kyoto University Yoshida, Sakyo-ku, Kyoto 606-8501, Japan
[7]Department of Physics, Tulane University, New Orleans, LA 70118, USA
[8]Department of Chemistry, Faculty of Science, Kanazawa University, Kakuma-machi, Kanazawa, 920-1192 Japan
[9]Research Institute for Scientific Measurements, Tohoku University, Sendai 980-77, Japan

Charge transfer salts formed by linear chains of organic molecules BETS (bis(ethylenediteho)tetraselenafulvalene), BEDT-TTF (bis(ethylenediteho)-tetrathiafulvalene) and TMTSF (tetramethyltetraselenafulvalen) display a rich variety of electronic properties from magnetic insulators to superconductors depending on the nature of the donors or acceptors and their location in the crystal structure. Low-dimensionality of charge transfer salts is of special interest due to the theoretical suggestion that the normal state of these systems may be unusual. It has been shown that one-dimensional conductors are not Fermi liquids like normal metals, but Luttinger or Luttinger-Emery liquids with distinct different physical properties. High-resolution angle-resolved photoemission spectra (ARPES) have shown a strong suppression of quasiparticle states near the chemical potential [1]. On the other hand a decrease in photoemission intensity near the Fermi level may result from extrinsic changes in the electronic structure at the surface, reconstruction, off-stoichiometry, or degradation. Additional measurements using bulk sensitive spectral techniques such as X-ray emission spectroscopy are necessary to verify the validity of observations resulting from photoemission experiments.

We report soft x-ray fluorescence measurements for the charge transfer salts $(TMTSF)_2PF_6$, $(BETS)_2FeBr_4$ and (CPDT-STF)(TCNQ), carried out at Beamline 8.0 of the Advanced Light Source. Nonresonant carbon Kα (2p→1s transition) X-ray emission spectra (XES) were recorded employing the soft X-ray fluorescence endstation [2]. Photons with an energy of 300 eV, well above the carbon K-edge, were used for excitation. The carbon Kα spectra were obtained with an energy resolution of 0.3-0.4 eV.

Fig. 1 displays the carbon Kα soft x-ray emission spectra (XES) [3]. A two-peak structure (labeled *a*, *b*) is found for all compounds. The same energy separation of peaks *a* and *b* in C Kα (~2.8 eV) XES is found for all charge transfer salts indicating that the same structure of carbon π-states in the valence band is present in all spectra. Such low-energy subbands have been found in X-ray emission spectra of compounds and are attributed to ns-states of non-metal atoms. Therefore this subband can stem from the hybridization of carbon 2p-states of the BEDT-TTF molecule and 2s states of the oxalate layer $[(H_3O)Fe(C_2O_4)_3]$ or from the nitrogen in benzonitrile

$C_6H_5CN$, which is due to hybridization between carbon π-metal electrons of donor (BEDT-TTF)-molecule and s-states of anion. The presence of an additional subband in carbon Kα XES evidences strong cation-anion interaction in $(BEDT\text{-}TTF)_4[(H_3O)Fe(C_2O_4)_3]C_5H_5N$.

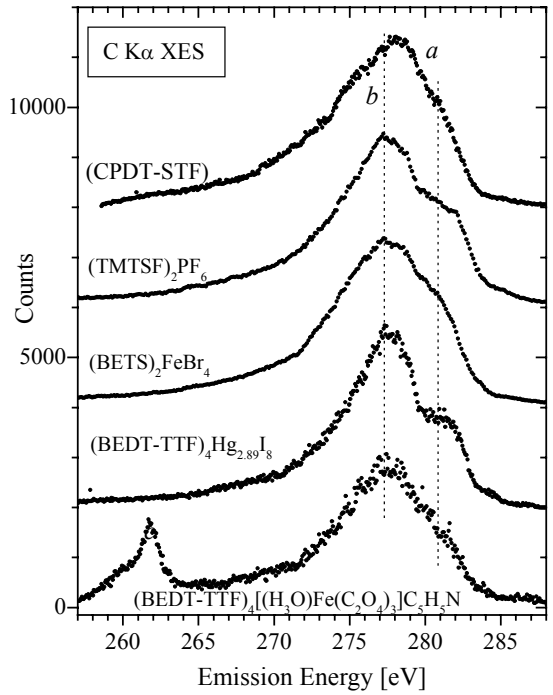


**Fig. 1 C Kα XES of charge transfer salts in the entire valence-band region**

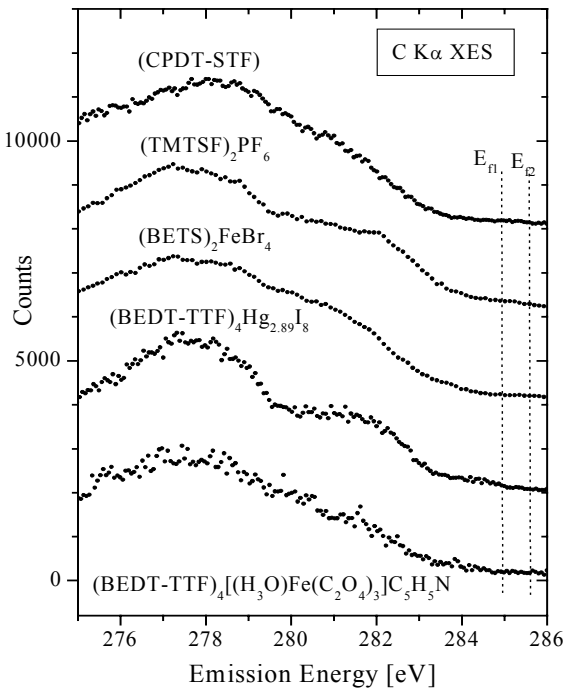


**Fig. 2 C Kα XES in the vicinity of the Fermi level.**

In order to examine the behavior of the carbon emission features near the Fermi level, one would need XPS binding energies of the C 1s core levels. Unfortunately such measurements have been performed, up to now, only for few charge transfer salts [3]. The binding energies vary between 0.2 and 0.7 eV, allowing us to estimate the position of the Fermi level in the carbon Kα spectra displayed. Fig. 2 shows carbon Kα XES in the vicinity of the Fermi level. For carbon C Kα XES two Fermi level positions are indicated ($E_{f1}$ and $E_{f2}$) which correspond to the lower and higher C 1s binding energies, respectively. All spectra show almost linear tails in the vicinity of the Fermi level (extending towards higher emission energies) and a suppression of the spectral weight at $E_f$. This pseudogap as well as the absence of a Fermi edge is incompatible with the usual spectroscopic behavior of normal 3D metals, which display Fermi-edges.

Our observations are in contrast to the conventional Fermi liquid picture of a metal where quasiparticle bands cross the Fermi level. We conclude that non-Fermi liquid features are observed in X-ray emission spectra of charge transfer salts. At the same time we point out that the decrease in spectral weight in the XES spectra stretches over almost 2 eV, which seems unreasonably large for Luttinger liquids. This value is even larger than the conduction bandwidths derived for organic CT salts (0.5 to 1 eV). This problem also exists in the non-Fermi liquid interpretation of the photoemission spectra.

## REFERENCES


1. F. Zwick, M. Grioni, G. Margaritondo, V. Vescoli, L. Degiorgi, B. Alavi, and G. Gruner, Solid State Commun. 113 (2000) 179.
2. J.J. Jia, T.A. Callcott, J. Yurkas, A. W.Ellis, F.J. Himpsel , M.G. Samant, J. Stöhr, D.L. Ederer, J.A. Carlisle, E.A. Hudson, L.J. Terminello, D.K. Shuh, and R.C.C. Perera, *Rev. Sci. Instrum*. 66 (1995) 1394.
3. E. Z. Kurmaev, A. Moewes, U. Schwingenschlögl, R. Claessen, M. I. Katsnelson, H. Kobayashi, S. Kagoshima, Y. Misaki, D.L. Ederer, K. Endo, and M. Yanagihara, Phys. Rev. B 64 (2001) 233107.



The Russian Foundation for Basic Research (Project 00-15-96575) and NATO Collaborative Linkage Grant supported this work. Funding by the Natural Sciences and Engineering Research Council (NSERC) is gratefully acknowledged. The Deutsche Forschungsgemeinschaft (Schwerpunktprogramm 1073) funded the work in Augsburg.



Principal investigator: Ernst Kurmaev, Institute of Metal Physics, Russian Academy of Sciences-Ural Division, 620219 Yekaterinburg GSP-170, Russia. Email: kurmaev@ifmlrs.uran.ru. Telephone: +7-3432-744183.

# X-ray transitions for studying the electronic structure of 5d metals

E.Z. Kurmaev[1], A. Moewes[2], Z. Pchelkina[1], I. Nekrasov[1], T.A. Callcott[3], and D.L. Ederer[4]

[1]Institute of Metal Physics, Russian Academy of Sciences-Ural Division, 620219 Yekaterinburg GSP-170, Russia

[2] Department of Physics and Engineering Physics, University of Saskatchewan, 116 Science Place, Saskatoon, Saskatchewan S7N 5E2, Canada

[3]University of Tennessee, Knoxville, Tennessee 37996, USA

[4]Department of Physics, Tulane University, New Orleans, LA 70118, USA

Transition metals of the 5d-series, their alloys and compounds are used in a wide range of applications. Unfortunately the direct study of their electronic structure by means of soft X-ray emission spectroscopy is limited due to the absence of suitable X-ray transitions. According to XPS measurements [1], the 5d transition elements (from Hf to Au) have $4p_{1/2,3/2}$ ($N_{2,3}$) core levels in the binding energy region of 380-643 eV. The X-ray emission bands of these metals, arising from the electric dipole transitions between the 5d valence electrons and 4p core level vacancies ($5d \rightarrow 4p_{3/2,1/2}$ transition) can be used for studying the occupied density of 5d-states (DOS). Due to the presence of strong competing radiationless transitions, these spectra are not listed in systematic studies of soft X-ray emission bands of 5d-transition metals [2, 3]. Due to the inherently low fluorescence yield of the ultra-soft x-ray emission process, we utilized the high brightness available at Lawrence Berkeley National Laboratory's Advanced Light Source for the measurements of fluorescence $N_{2,3}$ X-ray emission spectra (XES) of 5d metals. The spectra were taken at Beamline 8.0, employing the soft x-ray fluorescence endstation [4]. Photons with an energy of 399-490 eV, were used for excitation. All measurements reported here were made with a 100-micrometer entrance slit for the spectrometer.

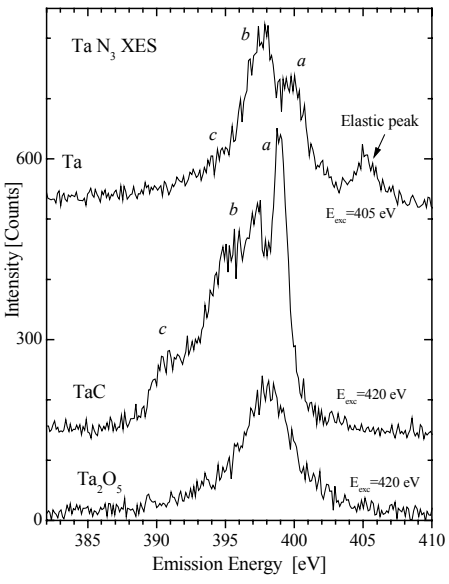


**Fig. 1 (a) Ta $N_3$ XES of Ta, TaC and $Ta_2O_5$.**

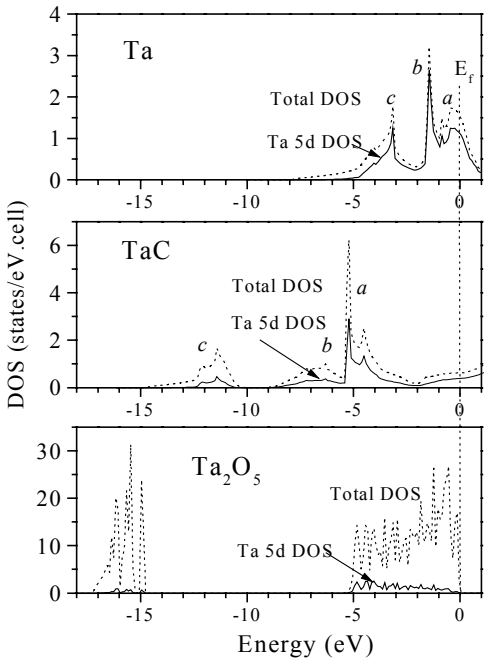


**Fig. 1 (b) Total and Ta 5d DOS**

We succeeded in measuring non-resonant 5d-metal $N_3$ ($5d \rightarrow 4p_{3/2}$ transition) soft X-ray emission spectra for Ta, TaC and $Ta_2O_5$ [5]. The measurements are displayed in Fig. 1(a). X-ray emission is governed by the dipole selection rule, $\Delta l = \pm 1$, which allows only for d- or s-valence electrons to fill the p-type core holes in 5d atoms. The intensity of $N_{2,3}$ non-resonant X-ray emission spectra of 5d elements maps the d-density at the atomic site, or in a band structure picture, the contribution of partial d-type density of states. The measured spectra have a signal to noise ratio of about 10 and show different spectral shape for metal, carbide and oxide evidencing the sensitivity to chemical bonding. According to band structure calculations [5] displayed in Fig. 1b, the main features of Ta 5d DOS are the same as in the total DOS and different in pure metal, carbide and oxide. Ta 5d DOS in pure metal have three subbands (*a*-*c*) and occupy less energy range than that of TaC. Ta 5d DOS in TaC are strongly hybridizing with the C 2p band giving rise to the structures labeled (*a* to *b*). The additional subband labeled *c* is due to hybridization with C 2s-states. The rather complicated band structure of TaC is reflected in Ta $N_3$ XES. The energy position of calculated and experimental peaks is in reasonable agreement though the ratio of peaks is rather different. In the case of tantalum pentoxide ($Ta_2O_5$), the band structure calculations show simpler structure because all Ta 5d electrons occupy the O 2p-band and the d-like band is empty (metal atoms have $d^0$ configuration). Therefore only the O 2p–Ta 5d band and the atomic-like O 2s-band are present in the valence band of $Ta_2O_2$. In good agreement with the calculated spectrum, the Ta $N_3$ emission is of simpler structure for $Ta_2O_5$ than for TaC. O 2s-states are not seen in Ta $N_3$ XES of $Ta_2O_5$ because they are more localized than the C 2s-states and less hybridized with Ta 5d-states.

$5d \rightarrow 4p$ transitions seem to be more favorable for studying the electronic structure of 5d-metals than $5d \rightarrow 5p$ and $5d \rightarrow 4f$ transitions, which are present in the ultra-soft region of 20-90 eV [3]. The reason is that the corresponding metal $N_3$ X-ray emission spectra are less influenced by core-level vacancies due to the higher localization of 4p-levels compared to 5p and 4f-levels. Therefore one can measure the undistorted density of 5d states.

## REFERENCES


1. R. Nyholm, A. Berndtson, and N. Martensson, J. Phys. C 13 (1980) L109.
2. J.A. Beardeen, Rev. Mod. Phys. 39 (1967) 78.
3. V.A. Fomichev, T.M. Zimkina, A.V. Rudnev, and S.A. Nemnonov, in *Band Structure Spectroscopy of Metals and Alloys* (ed. by D.J.Fabian and L.M.Watson), Academic Press, London and New York, 1973, pp. 259-293.
4. J.J. Jia, T.A. Callcott, J. Yurkas, A.W. Ellis, F.J. Himpsel, M.G. Samant, J. Stohr, D.L. Ederer, R.C.C. Perera, Rev. Sci. Inst. 66 (1995) 1394
5. E.Z. Kurmaev, A. Moewes, Z.V. Pchelkina, I.A. Nekrasov, A.A. Rempel and D.L. Ederer, Phys. Rev. B 63 (2001) 73108.



This work was supported by the Russian Foundation for Basic Research (Projects 00-15-96575), the National Sciences and Engineering Research Council (NSERC). The work at the Advanced Light Source at Lawrence Berkeley National Laboratory was supported by U.S. Department of Energy (Contract No. DE-AC03-76SF00098).



Principal investigator: Ernst Kurmaev, Institute of Metal Physics, Russian Academy of Sciences-Ural Division, 620219 Yekaterinburg GSP-170, Russia. Email: kurmaev@ifmlrs.uran.ru. Telephone: +7-3432-744183.